KARPAGAM ACADEMY OF HIGHER EDUCATION

(Deemed to be University)
(Established Under Section 3 of UGC Act 1956)
COIMBATORE-21
(For the candidates admitted from 2016 onwards)

DEPARTMENT OF PHYSICS

SUBJECT: NANOMATERIALS AND APPLICATIONS
SEMESTER: VI
SUB.CODE:16PHU603A **CLASS: III B.Sc PHYSICS**

Objective: The aim of this paper is to give information to students about nano technology, nano materials, their preparation and characterization techniques.

UNIT - I

NANOSCALE SYSTEMS: Length scales in physics, Nanostructures: 1D, 2D and 3D nanostructures (nanodots, thin films, nanowires, nanorods), Band structure and density of states of materials at nanoscale, Size Effects in nano systems, Quantum confinement: Applications of Schrodinger equation-Infinite potential well, potential step, potential box, quantum confinement of carriers in 3D, 2D, 1Dnanostructures and its consequences.

UNIT - II

SYNTHESIS OF NANOSTRUCTURE MATERIALS: Top down and Bottom up approach, Photolithography. Ball milling. Gas phase condensation. Vacuum deposition. Physical vapor deposition (PVD): Thermal evaporation, E-beam evaporation, Pulsed Laser deposition. Chemical vapor deposition (CVD).Sol-Gel. Electro deposition. Spray pyrolysis. Hydrothermal synthesis. Preparation through colloidal methods. MBE growth of quantum dots.

UNIT - III

CHARACTERIZATION: X-Ray Diffraction. Optical Microscopy. Scanning Electron Microscopy. Transmission Electron Microscopy. Atomic Force Microscopy.Scanning Tunneling Microscopy. Fourier Transform Infrared spectroscopy, UV-visible spectroscopy

UNIT – IV

OPTICAL PROPERTIES: Coulomb interaction in nanostructures. Concept of dielectric constant for nanostructures and charging of nanostructure. Quasi-particles and excitons. Excitons in direct and indirect band gap semiconductor nanocrystals. Quantitative treatment of quasi-particles and excitons, charging effects. Radiative processes: General formalization-absorption, emission and luminescence. Optical properties of heterostrctures and nanostructures.

UNIT - V ELECTRON TRANSPORT: Carrier transport in nanostrcutures. Coulomb blockade effect, thermionic emission, tunneling and hoping conductivity. Defects and impurities: Deep level and surface defects.

APPLICATIONS: Applications of nanoparticles, quantum dots, nanowires and thin films for photonic devices (LED, solar cells). Single electron transfer devices (no derivation). CNT based transistors. Nanomaterial Devices: Quantum dots heterostructure lasers, optical switching and optical data storage. Magnetic quantum well; magnetic dots -magnetic data storage. Micro Electro Mechanical Systems (MEMS), Nano Electromechanical Systems (NEMS).

Reference books:

1. C.P.Poole, Jr. Frank J.Owens, Introduction to Nanotechnology (Wiley India Pvt. Ltd.).
2. S.K. Kulkarni, Nanotechnology: Principles & Practices (Capital Publishing Company)
3. K.K. Chattopadhyay and A. N. Banerjee, Introduction to Nanoscience and Technology (PHI Learning Private Limited).
4. Introduction to Nanoelectronics, V.V. Mitin, V.A. Kochelap and M.A. Stroscio, 2011, Cambridge University Press.
5. Richard Booker, Earl Boysen, Nanotechnology (John Wiley and Sons).

KARPAGAM ACADEMY OF HIGHER EDUCATION

(Deemed to be University)

(Established Under Section 3 of UGC Act 1956)

Coimbatore – 641 021

(For the candidates admitted from 2016 onwards)

DEPARTMENT OF PHYSICS

SUBJECT NAME: **NANO MATERIALS AND APPLICATIONS**
SUB.CODE:16PHU603A
SEMESTER: VI CLASS: III B.Sc (PHY)

Serial No.	Lecture Duration Period (hr)	Topics to be covered	Support Material & Page No.
1	1	Length scales in physics	T1- 11,
2	1	Nanostructures: 1D, 2D and 3D nanostructures (nanodots, thin films, nanowires, nanorods)	W1
3	1	Band structure and density of states of materials at nanoscale, Size Effects in nano systems	T2- 22-24 T3- 231
4	1	Quantum confinement: Applications of Schrodinger equation- Infinite potential well, potential step, potential box,	T2-20-23
5	1	quantum confinement of carriers in 3D, 2D	W2
6	1	1D nanostructures and its consequences	
7	1	Revision	
Total No. of Hours planned for Unit-I = 7			
UNIT-II			
1	1	Top down and Bottom up approach, Photolithography	T2-241-244
2	1	Ball milling, Gas phase condensation. Vacuum deposition.	T2-55-57
3	1	Physical vapor deposition (PVD): Thermal evaporation, E-beam evaporation, Pulsed Laser deposition.	T2-61-64
4	1	Chemical vapor deposition (CVD)	T2- 71-73,

5	1	Sol-Gel	T2-103-104
6	1	Electro deposition. Spray pyrolysis. Hydrothermal synthesis. Preparation through colloidal methods. MBE growth of quantum dots.	T2-105, 91-94
7	1	Revision	
Total No. of hours planned for Unit-II – 7			
Unitt-III			
1	1	X-Ray Diffraction	T2-160-166
2	1	Optical Microscopy	T2- 135-140
3	1	Scanning Electron Microscopy. Transmission Electron Microscopy.	T2- 143-147
4	1	Atomic Force Microscopy	T2- 152-155
5	1	Scanning Tunneling Microscopy	T2-149-152
6	1	Fourier Transform Infrared spectroscopy	T2-179-181
7	1	UV-visible spectroscopy	T2-173-176
8	1	Revision	
Total No. of hours planned for Unit-III – 8			
Unit-IV			
1	1	Coulomb interaction in nanostructures. Concept of dielectric constant for nanostructures and charging of nanostructure.	T2-366
2	1	Quasi-particles and excitons. Excitons in direct and indirect band gap semiconductor nanocrystals.	T2-204-206,
3	1	Quantitative treatment of quasi-particles and excitons, charging effects.	
4	1	Radiative processes: General formalization-absorption, emission and luminescence.	T2-184-185
5	1	Continuation	

6	1	Optical properties of heterostrctures and nanostructures	T2-208-213
7	1	Continuation	
8	1	Revision	
Total No. of hours planned for Unit-IV – 8			
Unit-V			
1	1	Carrier transport in nanostrcutures. Coulomb blockade effect, thermionic emission, tunneling and hoping conductivity. Defects and impurities: Deep level and surface defects.	T2-260-263
2	1	Applications of nanoparticles, quantum dots, nanowires and thin films for photonic devices (LED, solar cells).	T4-95, T5-239
3	1	Single electron transfer devices (no derivation). CNT based transistors. Nanomaterial Devices: Quantum dots heterostructure lasers	
4	1	optical switching and optical data storage. Magnetic quantum well; magnetic dots -magnetic data storage.	T5- 241
5	1	Micro Electromechanical Systems (MEMS),	T3-332-339
6	1	Nano Electromechanical Systems (NEMS).	T3-335-339
7	1	Revision	
8	1	Old Question Paper Discussion	
9	1	Old Question Paper Discussion	
10	1	Old Question Paper Discussion	
Total No. of hours planned for Unit-IV – 10			
Total No. of hours planned for this paper = 40			

Suggested Books

T1- Nanotechnology-Richard Booker, Earl Boysen – John Wiley & Sons

T2- Nanotechnology principle practices- Sulabha K Kulkarni, Springer

T3-Introduction to Nanotechnology-Charles P.Poole, Jr Frank J.Owens, John Wiley

T4- Nanotechnology 101 –John Mongillo, Greenwood Press, London

T5- NANOTECHNOLOGIES: Principles, Applications, Implications and Hands-on Activities, European Commission

UNIT-I

NANOSCALE SYSTEMS: Length scales in physics, Nanostructures: 1D, 2D and 3D nanostructures (nanodots, thin films, nanowires, nanorods), Band structure and density of states of materials at nanoscale, Size Effects in nano systems, Quantum confinement: Applications of Schrodinger equation- Infinite potential well, potential step, potential box, quantum confinement of carriers in 3D, 2D, 1Dnanostructures and its consequences.

Nanostructured material

Nanomaterial— condensed material, in whole or in part composed of structural elements (particles, grains, crystallites, fibres, rods, layers) with the characteristic dimensions from several nanometers to several tens of nanometers; the long-range order in the structural elements is highly disturbed and therefore the short-range order determines multiparticle correlations in the arrangement of atoms in these elements; all macroscopic properties of the material are determined by the size and/or mutual arrangement of structural elements.

Description

The main types of nanostructured materials based on the dimensions of their structural elements are: zero-dimensional (0D), one-dimensional (1D), two-dimensional (2D) and three-dimensional (3D) nanomaterials. Zero-dimensional nanomaterials include nanocluster materials and nanodispersions, i.e. materials in which nanoparticles are isolated from each other. One-dimensional nanomaterials are nanofibre (nanorod) and nanotubular materials with fibre (rod, tube) length from 100 nm to tens of microns. Two-dimensional nanomaterials are films (coatings) with nanometer thickness. Structural elements in 0D, 1D and 2D nanomaterials can be distributed in a liquid or solid macroscopic matrix or be applied on a substrate. Three-dimensional nanomaterials include powders, fibrous, multilayer and polycrystalline materials in which the 0D, 1D and 2D structural elements are in close contact with each other and form interfaces. An important type of three-dimensional nanostructured materials is a compact or consolidated (bulk) polycrystal with nanosize grains, whose entire volume is filled with those nanograins, free surface of the grains is practically absent, and there are only grain interfaces. The formation of such interfaces and "disappearance" of the nanoparticle (nanograin) surface is the fundamental difference between three-dimensional compact nanomaterials and nanocrystalline powders with various degrees of agglomeration that consist of particles of the same size as the compact nanostructured materials.

In the past two decades, hundreds of novel NSMs have been obtained; therefore, the need in their classification is ripened. NSMs as a subject of nanotechnology are low dimensional materials comprising of building units of a submicron or nanoscale size at least in one direction and exhibiting size effects. The first classification idea of NSMs was given by Gleiter in 1995 and further was explained by Skorokhod in 2000. However, Gleiter and Skorokhod scheme was

not fully considered because of 0D, 1D, 2D, and 3D structures such as fullerenes, nanotubes, and nanoflowers were not taken into account. Therefore, Pokropivny and Skorokhod reported a modified classification scheme for NSMs, in which 0D, 1D, 2D and 3D NSMs are included. Herein we classified the NSMs based on the scheme of Pokropivny et al. scheme.

0D NSMs

A major feature that discriminates various types of nanostructures is their dimensionality. The word ‘‘nano’’ stems from the Greek word ‘‘nanos’’, which means dwarf. This word ‘‘nano’’ has been assigned to indicate the number 109 , i.e., one billionth of any unit. In the past 10 years, significant progress has been made in the field of 0D NSMs. A rich variety of physical and chemical methods have been developed for fabricating 0D NMSs with well-controlled dimensions. Recently, 0D NSMs such as uniform particles arrays (quantum dots), heterogeneous particles arrays, core–shell quantum dots, onions, hollow spheres and nanolenses have been synthesized by several research groups. Moreover, 0D NSMs, such as quantum dots has been extensively studied in light emitting diodes (LEDs), solar cells, single-electron transistors, and lasers.

1D NSMs

In the last decade, 1D NSMs have stimulated an increasing interest due to their importance in research and developments and have a wide range of potential applications. It is generally accepted that 1D NSMs are ideal systems for exploring a large number of novel phenomena at the nanoscale and investigating the size and dimensionality dependence of functional properties. They are also expected to play an important role as both interconnects and the key units in fabricating electronic, optoelectronic, and EEDs with nanoscale dimensions. The field of 1D NSMs such as nanotubes has attained a significant attention after the pioneering work by Iijima. 1D NSMs have a profound impact in nanoelectronics, nanodevices and systems, nanocomposite materials, alternative energy resources and national security.

2D NSMs

2D nanostructures have two dimensions outside of the nanometric size range. In recent years, a synthesis 2D NSMs have become a focal area in materials research, owing to their many low dimensional characteristics different from the bulk properties. In the quest of 2D NSMs,

considerable research attention has been focused over the past few years on the development of 2D NSMs. 2D NSMs with certain geometries exhibit unique shape-dependent characteristics and subsequent utilization as building blocks for the key components of nanodevices [47–49]. In addition, a 2D NSMs are particularly interesting not only for basic understanding of the mechanism of nanostructure growth, but also for investigation and developing novel applications in sensors, photocatalysts, nanocontainers, nanoreactors, and templates for 2D structures of other materials.

3D NSMs

Owing to the large specific surface area and other superior properties over their bulk counterparts arising from quantum size effect, 3D NSMs have attracted considerable research interest and many 3D NSMs have been synthesized in the past 10 years. It is well known that the behaviors of NSMs strongly depend on the sizes, shapes, dimensionality and morphologies, which are thus the key factors to their ultimate performance and applications. Therefore it is of great interest to synthesize 3D NSMs with a controlled structure and morphology. In addition, 3D nanostructures are an important material due to its wide range of applications in the area of catalysis, magnetic material and electrode material for batteries. Moreover, the 3D NSMs have recently attracted intensive research interests because the nanostructures have higher surface area and supply enough absorption sites for all involved molecules in a small space. On the other hand, such materials with porosity in three dimensions could lead to a better transport of the molecules.

POTENTIAL BOX

Consider a box of length '*a*' such that

Potential V=0 if $0 < x < a$

And V =α if $x < 0$ or $x > a$

as illustrated

Energy states of the particle of mass *m* can be obtained using time independent Schrödinger equation for one dimension as

$$\frac{-\hbar}{2M}+\frac{\partial}{\partial X^2}^2 \varphi(x) + v(x)\varphi(x) = E\varphi(x)$$

Let $\varphi(x)$ have a general form as

$$\varphi(x) = \text{Asin}(2\text{mE}/\hbar)\text{^}1/2 + \text{B cos}(\frac{2\text{mE}}{\_2})\text{^}1/2\ \text{x}$$

As the particle exists only inside the box, wave function should not exist outside

The box and should be zero at the boundaries.

At *x*=0, boundary condition $\varphi(x)$ leads to *B*=0. Therefore,

$$\varphi(x) = \text{Asin}(2\text{mE}/\hbar)\text{^}1/2\text{x}$$

At *x*==*a*, boundary condition

$$\varphi(x) = 0 = \text{Asin}(2\text{mE}/\hbar)\text{^}1/2\text{x}$$

But '*a*' is not zero, therefore

$$\sin(2\text{mE}/\hbar)\text{^}1/2\text{a}=0 \text{ or, } \sin(2\text{mE}/\hbar)\text{^}1/2\text{a}=\text{n}\pi$$

Where *n*D0, 1, 2, 3, : : :

Therefore

$$\text{En}=\frac{n^2h^2\pi^2}{2ma^2}$$

i.e….,En α n2

Putting *En*in Eq

$$\varphi(x) = Asin\left(\frac{n\pi}{a}\right)x$$

Although *n* can take any integer value according to Eq, in practice *n*=0and are not allowed inside the box, because, if allowed, would be $\varphi(x) = 0$ andProbability of finding the particle inside the box would be zero. For the same reasonφ cannot be zero inside the box. Therefore *n* takes the values *n*D1, 2, 3, : : :. This shows that energies of particle in a one dimensional potential box are quantized.

Corresponding wave functions and probabilities of different states of particle in the box would look like those in b, c respectively.

A0 are not allowed inside the box, because, if allowed, $\varphi(x)$ would be 0 andProbability of finding the particle inside the box would be zero. For the same reason$\varphi(x)$Cannot be zero inside the box. Therefore *n* takes the values *n*D1, 2, 3, : : :. This shows that energies of particle in a one dimensional potential box are quantized. Corresponding wave functions and probabilities of different states of particle in the box would look like those in b, c respectively.

a =0 are not allowed inside the box, because, if allowed, $\varphi(x)$ would be 0 andProbability of finding the particle inside the box would be zero. For the same reason$\varphi(x)$Cannot be zero inside

the box. Therefore *n* takes the values *n*D1, 2, 3, : : :. This shows that energies of particle in a one dimensional potential box are quantized.

POTENTIAL STEP

In quantum mechanics, the **particle in a box** model (also known as the **infinite potential well** or the **infinite square well**) describes a particle free to move in a small space surrounded by impenetrable barriers. The model is mainly used as a hypothetical example to illustrate the differences between classical and quantum systems. In classical systems, for example, a ball trapped inside a large box, the particle can move at any speed within the box and it is no more likely to be found at one position than another. However, when the well becomes very narrow (on the scale of a few nanometres), quantum effects become important. The particle may only occupy certain positive energy levels. Likewise, it can never have zero energy, meaning that the particle can never "sit still". Additionally, it is more likely to be found at certain positions than at others, depending on its energy level. The particle may never be detected at certain positions, known as spatial nodes.

The particle in a box model is one of the very few problems in quantum mechanics which can be solved analytically, without approximations. Due to its simplicity, the model allows insight into quantum effects without the need for complicated mathematics. It serves as a simple illustration of how energy quantization (energy levels), which are found in more complicated quantum systems such as atoms and molecules, come about.

APPLICATIONS OF SCHRODINGER EQUATION

Consider one dimensional closed box of width L. A particle of mass ‘m’ is moving in a one-dimensional region along X-axis specified by the limits x=0 and x=L as shown in fig. The potential energy of particle inside the box is zero and infinity elsewhere.

I.e Potential energy V(x) is of the form

V(x) = {o; if o<x<L∞: elsewhere

The one-dimensional time independent Schrodinger wave equation is given by

$$d2\psi/dx2+ 2m/\hbar^2 [E-V] \psi=0 \qquad (1)$$

Here we have changed partial derivatives in to exact because equation now contains only one variablei.e x-Co-ordinate. Inside the box V(x) =0

Therefore the Schrodinger equation in this region becomes

$$d^2/\psi/dx^2 + 2m/\hbar^2 E\psi = 0$$

Or $$d^2\psi/dx^2 + K^2\psi = 0 \qquad (2)$$

Where $$k = 2mE/\hbar^2 \quad (3)$$

K is called the Propagation constant of the wave associated with particle and it has dimensions reciprocal of length.

The general solution of eq (2) is

(i) $$\Psi = A \sin Kx + B \cos K x \qquad (4)$$

Where A and B are arbitrary conditions and these will be determined by the boundary conditions.

(ii) **Boundary Conditions**

The particle will always remain inside the box because of infinite potential barrier at the walls. So the probability of finding the particle outside the box is zero i.e. =0 outside the box. We know that the wave function must be continuous at the boundaries of potential well at x=0 and x=L, i.e.

$$\Psi(x) = 0 \text{ at } x=0 \qquad (5)$$

$$\Psi(x) = 0 \text{ at } x= L \qquad (6)$$

These equations are known as Boundary conditions.

(iii) Determination of Energy of Particle

Apply Boundary condition of eq. (5) to eq. (4)

$$0 = A \sin (X*0) + B \cos (K*0)$$

$$0 = 0 + B*1$$

$$B = 0 \qquad (7)$$

Therefore eq. (4) becomes

$$\Psi(x) = A \sin Kx \qquad (8)$$

Applying the boundary condition of eq. (6) to eq. (8), we have

$$0 = A \sin KL$$

$$\text{Sin } KL = 0$$

$$KL = n\pi$$

$$K = n\pi/L \qquad \ldots\ldots (9)$$

Where $n = 1, 2, 3 - - -$

A Cannot be zero in eq. (9) because then both A and B would be zero. This will give a zero wave function everywhere which means particle is not inside the box.

QUANTUM CONFINEMENTS OF CARRIERS IN 2D AND 3D

The most popular term in the nano world is *quantum confinement effect* which is essentially due to changes in the atomic structure as a result of direct influence of ultra-small length scale on the energy band structure (Takagahara and Takeda 1992a, Wise 2000, Zhao et al. 2004). The length scale corresponds to the regime of quantum confinement ranges from 1 to 25 nm for typical semiconductor groups of IV, III-V and II-VI. In which the spatial extent of the electronic wave function is comparable with the particle size. As a result of these "geometrical" constraints, electrons "feel" the presence of the particle boundaries and respond to changes in particle size by adjusting their energy. This phenomenon is known as the quantum-size effect. Quantization effects become most important when the particle dimension of a semiconductor near to and below the bulk semiconductor Bohr exciton radius which makes materials properties size dependent. In general, the Bohr radius of a particle is defined as (Yoffe 1993),

$$a_B = \varepsilon \frac{m}{m^*} a_o$$

where ε is the dielectric constant of the material, m* is the mass of the particle, m is the rest mass of the electron, and ao is the Bohr radius of the hydrogen atom. When the particle size approaches Bohr exciton radius, the quantum confinement effect causes increasing of the excitonic transition energy and blue shift in the absorption and luminescence band gap energy (Yoffe 1993). For example, 4.8 nm diameter PbSe NCs show an effective band gap of approximately 0.82 eV, exhibiting a strong confinement induced blue shift of >500 meV compared to the bulk PbSe band gap of 0.28 eV (the Bohr exciton radius in PbSe is 46 nm) (Wise 2000). In addition, quantum confinement leads to a collapse of the continuous energy bands of a bulk material into discrete, atomic like energy levels.

A schematic of the discrete energy level of a semiconductor.

Energy states leads to a discrete absorption spectrum, which is in contrast to the continuous absorption spectrum of a bulk semiconductor as shown in Fig. 1.1. A quantum confined structure is one in which the motion of the carriers (electron and hole) are confined in one or more directions by potential barriers (Miller et al. 1984). Based on the confinement

direction, a quantum confined structure will be classified into three categories as quantum well, quantum wire and quantum dots or nanocrystals.

Classification of quantum confined structures.

In QDs, the charge carriers are confined in all three dimensions which the electrons exhibit a discrete atomic-like energy spectrum. Quantum wires are formed when two dimensions of the system are confined. In quantum well, charge carriers (electrons and holes) are confined to move in a plane and are free to move in a two-dimensional. Also the energy level of one of the quantum numbers changes from continuous to discrete. Compared with bulk semiconductors, the quantum well has a higher density of electronic states near the edges of the conduction and valence bands, and therefore a higher concentration of carriers can contribute to the band-edge emission (Chen et al. 2012). As more number of the dimension is confined, more discrete energy levels can be found, in other words, carrier movement is strongly confined in a given dimension. Density of electron states in bulk, 2D, 1D and 0D semiconductor structure. 0D structures has very well defined and quantized energy levels. The quantum confinement effect corresponding to the size of the nanostructure can be estimated via a simple effective-mass approximation model

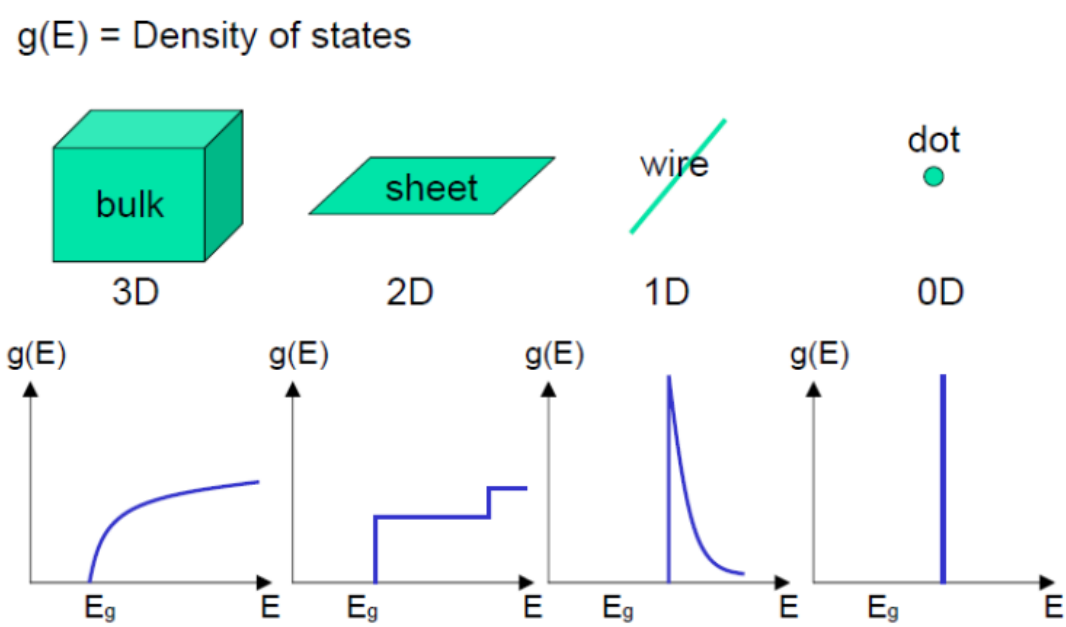

Density of electron states of a semiconductor as a function of dimension. The optical absorption spectrum is roughly proportional to the density of states.

This method can predict the confined energy levels of nanostructures by solving Schrodinger equation assuming the barriers have an infinite confining potential. The "effective mass" solutions of the Schrödinger equation for electrons confined in a quantum dot or NCs, quantum wire and quantum well are,

Quantum dot or Nanocrystals:

$$E_{n,m,l} = \frac{\pi^2\hbar^2}{2m^*}\left(\frac{n^2}{L_z^{\,2}} + \frac{m^2}{L_y^{\,2}} + \frac{l^2}{L_x^{\,2}}\right), \psi = \phi(z)\phi(y)\phi(x) \text{ ---------- } (2)$$

Quantum wire:

$$E_{n,m}(k_x) = \frac{\pi^2\hbar^2}{2m^*}\left(\frac{n^2}{L_z^{\,2}} + \frac{m^2}{L_y^{\,2}}\right) + \frac{\hbar^2 k_x^{\,2}}{2m^*}, \psi = \phi(z)\phi(y)\exp(ik_x x) \text{ ---------- } (3)$$

Quantum well:

$$E_n(k_x k_y) = \frac{\pi^2\hbar^2 n^2}{2m^* L_z^{\,2}} + \frac{\hbar^2}{2m^*}\left(k_x^{\,2} + k_y^{\,2}\right), \psi = \phi(z)\exp\left(ik_x x + ik_y y\right) \text{ ---------- } (4)$$

where *n, m, l* = 1, 2 … the quantum confinement numbers, Lx, Ly and Lz are the confining dimensions, is the wave function describing the electronic motion in *x* and *y* direction, similar to free electron wave functions. A brief reference to quantum wells and its properties follows in the next section.

1D NANOSTRUCTURE AND THEIR CONSEQUENCES

One-dimensional (1D) nanostructures, including nanowires, nanotubes and quantum wires, have been regarded as the most promising building blocks for nanoscale electronic and optoelectronic devices. Worldwide efforts in both the theory and the experimental investigation of growth, characterization and applications of 1D nanostructures have resulted in a mature, multidisciplinary field. In this book, a wealth of state-of-the-art information offers the opportunity to uncover the underlying science from diverse perspectives. Leading researchers elucidate the synthesis and properties of 1D nanostructures for various morphologies and compositions (semiconductor, metal, carbon, etc.) as well as their considerable impact on spintronics, information storage, and the design of field-effect transistors.

The smallest possible crystalline wires with cross-section as small as a single atom can be engineered in cylindrical confinement. Carbon nanotubes, a natural semi-1D nanostructure, can be used as a template for synthesis. Confinement provides mechanical stabilization and prevents linear atomic chains from disintegration; other structures of 1D nanowires are predicted to be mechanically stable even upon isolation from the templates.

Nano materials are used in a variety of, manufacturing processes, products and healthcare including paints, filters, and insulation and lubricant additives. In healthcare Nanozymes are nanomaterials with enzyme-like characteristics. They are an emerging type of artificial enzyme, which have been used for wide applications in such as bio sensing, bio imaging, tumour diagnosis,antibiofouling and more. In paints nanomaterials are used to improve UV protection and improve ease of cleaning. High quality filters may be produced using nanostructures, these filters are capable of removing particulate as small as a virus as seen in a water filter created by Seldom Technologies. In the air purification field, Nano technology was used to combat the spread of MERS in Saudi Arabian hospitals in 2012. Nanomaterials are being used in modern and human-safe insulation technologies, in the past they were found in Asbestos-based insulation. As a lubricant additive, Nano materials have the ability to reduce friction in moving parts. Worn and corroded parts can also be repaired with self-assembling anisotropic nanoparticles called TriboTEX.Nanomaterials can also be used in three-way-catalyst (TWC) applications. TWC converters have the advantage of controlling the emission of nitrogen oxides (NOx), which are precursors to acid rain and smog. In core-shell structure, nanomaterials form shell as the catalyst support to protect the noble metals such as palladium and rhodium. The primary function is that the supports can be used for carrying catalysts active components, making them highly dispersed, reducing the use of noble metals, enhancing catalysts activity, and improving the mechanical strength.

KARPAGAM ACADEMY OF HIGHER EDUCATION

Coimbatore-641021.

(For the candidates admitted from 2016 onwards)

DEPARTMENT OF PHYSICS

UNIT I (Objective Type/Multiple choice Questions each Questions carry one Mark)

NANOMATERIALS AND APPLICATIONS

PART –A(Online Examination)

S.No.	QUESTIONS	opt1	opt2	opt3	opt4	ANSWER
1	Nanotechnology was brought into day light by delivering lectures by:	Feymann	Einstein	Newton	Max Planck	Feymann
2	The prefix "nano" comes from a	French word meaning billion	Greek word meaning dwarf	Spanish word meaning particle	Latin word meaning invisible	Greek word meaning dwarf
3	Who first used the term nanotechnology and when?	Richard Feynman, 1959	Norio Taniguchi, 1974	Eric Drexler, 1986	Sumio Iijima, 1991	Norio Taniguchi, 1974
4	What is a buckyball?	A carbon molecule (C60)	Nickname for Mercedes-Benz's futuristic concept car (C111)	Plastic explosives nanoparticle (C4)	Concrete nanoparticle with a compressive strength of 20 nanonewtons (C20)	A carbon molecule (C60)
5	Richard Feynman is often credited with predicting the potential of nanotechnology. What was the title of his famous speech given on December 29, 1959?	There is a tiny room at the bottom	Things get nanoscopic at the bottom	Bottom? What bottom?	There is plenty of room at the bottom	There is plenty of room at the bottom
6	Which of these consumer products is already being made using nanotechnology methods?	Fishing lure	Golf ball	Sunscreen lotion	All of the above	All of the above

7	What is graphene?	A new material made from carbon nanotubes	A one-atom thick sheet of carbon	Thin film made from fullerenes	A software tool to measure and graphically represent nanoparticles	A one-atom thick sheet of carbon
8	What is the 2017 budget for the U.S. National Nanotechnology Initiative?	$587 million	$917 million	$1.4 billion	$2.1 billion	$1.4 billion
9	In which of the following the atoms do not move from each other?	Shape memory alloys	Nano materials	Dielectrics	Static materials	Nano materials
10	10 nm = _____ m	10^{-8}	10^{-7}	10-9	10-10	10^{-8}
11	The diameter of hydrogen atom is...	1	10	0.1	0.01	0.1
12	Carbon atoms make ____ type of bond with other carbon atoms.	covalent	ionic	metallic	hydrogen	covalent
13	Fullerene or bucky ball is made up of ____ carbon atoms.	100	20	75	60	60
14	1 m = _____ nm.	10^{-9}	10-8	109	108	109
15	"There is plenty of room at the bottom." This was stated by _____.	Eric Drexler	Richard Feynmann	Sumio Tijima	Richard Smalley	Richard Feynmann
16	Who coined the word 'nanotechnology'?	Eric Drexler	Richard Feynmann	Sumio Tijima	Richard Smalley	Eric Drexler
17	According to the definition by CRN, nanotechnology is...	mechanical engineering	atomic engineering	Newtonian mechanics	micro-electronics	atomic engineering
18	Nanoscience can be studied with the help of…	quantum mechanics	Newtonian mechanics	macro-dynamics	geophysics	quantum mechanics
19	Greeks and Romans had used nanoparticles in the manufacture of...	cosmetics for eyes	medicines	metal articles	hair-dye	hair-dye
20	Egyptians were using ____ to prepare make-up for eyes.	nanoaluminium	nanocopper	nanosteel	nanolead	nanolead
21	The sword of Tipu Sultan was made of...	nanolead	nanoaluminium	Damascus steel	Pure iron	Damascus steel
22	_____ contains nanoparticles prepared by using biologically processed metal ores.	Homeopathic medicines	Modern antibiotics	Ayurvedic 'Bhasmas'	Modern cosmetics	Ayurvedic 'Bhasmas'
23	The diameter of human hair is ____ nm.	50,000	75,000	90,000	1,00,000	50,000

24	The diameter of human hair is ____ m.	5×10^{-8}	5 x 10-7	5 x 10-6	5 x 10-5	5 x 10-5
25	The cut-off limit of human eye is ____ nm.	2,000	5,000	10,000	50,000	10,000
26	The size of E.Coli bacteria is ____ nm.	2,000	5,000	50	90	2,000
27	The size of RBC is ____ nm.	50	90	2,000	5,000	5,000
28	The thickness of a transistor is ____ nm.	50	90	2,000	5,000	90
29	The size of a virus is ____ nm.	2	20	50	2000	50
30	The diameter of a bucky ball is ____ nm.	1,000	100	10	1	1
31	The width of a typical DNA molecule is ____ nm.	1	2	5	10	2
32	1 micrometer (micron) = _____ m.	10-9	10-8	10-7	10-6	10-6
33	1 micrometer (micron) = _____ nm.	1,000	100	10	0.01	1,000
34	The surface area to volume ratio of a sphere with radius 1 cm is R_1 and that of a sphere with radius 5 cm is R_2. Then R_1 = ____ R_2.	3	0.3	5	1/5	5
35	The surface area to volume ratio of a cube with side 1 unit is R_1 and that of a cube with side 10 units is R_2. Then R_2 = ____ R_1.	0.1	10	1/100	100	0.1
36	The two important properties of nanosubstances are...	pressure and friction	sticking and friction	sticking and temperature	temperature and friction	sticking and friction
37	With the help of _____, Robert F. Curl and others discovered fullerene.	electron microscope	magnetic resonance	condensation technique	mass spectrograph	mass spectrograph
38	In the structure of fullerene each carbon atom forms covalent bonds with ____ other carbon atoms.	one	two	three	four	three
39	Who had invented the famous 'Geodesic' dome structure?	Eric Drexler	Buckminster Fuller	Richard Smalley	Faraday	Buckminster Fuller
40	The largest cluster of carbon atoms in Bucky balls known till today consists of ____ carbon atoms.	60	75	180	540	540
41	The smallest cluster of carbon atoms in	75	60	20	15	20

	Bucky balls known till today consists of ____ carbon atoms.					
42	The tensile strength of an MWNT is ____ Pa.	63 x 10^6	63 x 107	63 x 108	63 x 109	63 x 109
43	The compressive strength of a nanotube _____ its tensile strength.	is less than	is greater than	is equal to	may be greater than	is less than
44	The hardness of a standard SWNT is ____ Pa.	63 x 10^6	25 x 106	25 x 109	25 x 10-9	25 x 109
45	The bulk modulus of a standard SWNT is _____ that of diamond.	less than	greater than	equal to	less than or equal to	greater than
46	How much current can be passed through 1 cm^2 cross-section of a metal nanotube?	10^{-9} A	109 A	1000 A	0.001 A	109 A
47	The size of a quantum dot is _____ nm.	5	10	50	100	5
48	The capacity of a normal human eye to see the smallest object is _____ µm.	10000	1000	100	10	10
49	Nanoparticles of which substance were found on the surface of the sword of Tipu Sultan?	Gold	Lead	Carbon	Silicon	Carbon
50	Quantum dots are _____particles	semiconductor	conductor	insulator	optical	semiconductor
51	Larger QDs emit longer wavelengths resulting in emission colors such as _____	yellow	orange or red	brown	black	orange or red
52	Smaller QDs emit shorter wavelengths resulting in colors like	brown	red and orange	blue and green	green and yellow	blue and green
53	Nanotechnology, in other words, is	Carbon engineering	Atomic engineering	Small technology	Microphysics	Atomic engineering
54	The diameter of the nano wire is about _____	10-6m	10-3m	10-8m	10-9m	10-9m
55	A suspended nano wire is a wire that is produced in the _____	Air medium	Vaccum	Low vaccum chamber	High vaccum chamber	High vaccum chamber
56	Nano wires are used in_____	Transistors	Resistors	Capacitors	Transducers	Transistors
57	Nano cones are the predominant structures made with_____	Carbon	Nitrogen	Hydrogen	Silicon	Carbon

UNIT-II

SYNTHESIS OF NANOSTRUCTURE MATERIALS: Top down and Bottom up approach, Photolithography. Ball milling. Gas phase condensation. Vacuum deposition. Physical vapor deposition (PVD): Thermal evaporation, E-beam evaporation, Pulsed Laser deposition. Chemical vapor deposition (CVD).Sol-Gel. Electro deposition. Spray pyrolysis. Hydrothermal synthesis. Preparation through colloidal methods. MBE growth of quantum dots.

Top-down approach

The most common top-down approach to fabrication involves lithographic patterning techniques using short-wavelength optical sources. A key advantage of the top-down approach—as developed in the fabrication of integrated circuits—is that the parts are both patterned and built in place, so that no assembly step is needed. Optical lithography is a relatively mature field because of the high degree of refinement in microelectronic chip manufacturing, with current short-wavelength optical lithography techniques reaching dimensions just below 100 nanometres (the traditional threshold definition of the nanoscale). Shorter-wavelength sources, such as extreme ultraviolet and X-ray, are being developed to allow lithographic printing techniques to reach dimensions from 10 to 100 nanometres. Scanning beam techniques such as electron-beam lithography provide patterns down to about 20 nanometres. Here the pattern is written by sweeping a finely focused electron beam across the surface. Focused ion beams are also used for direct processing and patterning of wafers, although with somewhat less resolution than in electron-beam lithography. Still-smaller features are obtained by using scanning probes to deposit or remove thin layers.

Mechanical printing techniques—nanoscale imprinting, stamping, and molding—have been extended to the surprisingly small dimensions of about 20 to 40 nanometres. The details of these techniques vary, but they are all based on making a master "stamp" by a high-resolution technique such as electron-beam lithography and then applying this stamp, or subsequent generations of it, to a surface to create the pattern. In one variation a stamp's surface is coated with a very thin layer of material (the "ink") that can then be deposited ("inked") directly onto the surface to reproduce the stamp's pattern. For example, the controlled patterning of a molecular monolayer on a surface can be achieved by stamping an ink of thiol functionalized organic molecules directly onto a gold-coated surface (molecules that contain a sulfur end group, called a thiol, bond strongly to gold). In another approach the stamp is used mechanically to press the pattern into a thin layer of material. This surface layer is typically a polymeric material that has been made pliable for the molding process by being heated during the stamping procedure. Plasma etching can then be used to remove the thin layer of the masking material under the stamped regions; any residual polymeris thus removed, and a nanoscale lithographic pattern is left on the surface. Still another variation is to make the relief pattern out of photoresist on a silicon wafer by optical or electron-beam lithography and then pour a liquid precursor—for example, polydimethylsiloxane, a form of silicone—over the pattern and then cure it. The result is a rubbery solid that can be peeled

off and used as a stamp. These stamps can be inked and printed as described above, or they can be pressed to the surface and a liquid polymer allowed to flow into the raised regions of the mask by capillary action and cured in place. A distinction for this latter approach is that the stamp is flexible and can thus be used to print nanoscale features on curved surfaces.

These nanoscale printing techniques offer several advantages beyond the ability to use a wider variety of materials with curved surfaces. In particular, such approaches can be carried out in ordinary laboratories with far-less-expensive equipment than that needed for conventional submicron lithography. The challenge for all top-down techniques is that, while they work well at the microscale (at millionths of a metre), it becomes increasingly difficult to apply them at nanoscale dimensions. A second disadvantage is that they involve planar techniques, which means that structures are created by the addition and subtraction of patterned layers (deposition and etching), so arbitrary three-dimensional objects are difficult to construct.

Bottom-up approach

Bottom-up, or self-assembly, approaches to nanofabrication use chemical or physical forces operating at the nanoscale to assemble basic units into larger structures. As component size decreases in nanofabrication, bottom-up approaches provide an increasingly important complement to top-down techniques. Inspiration for bottom-up approaches comes from biological systems, where nature has harnessed chemical forces to create essentially all the structures needed by life. Researchers hope to replicate nature's ability to produce small clusters of specific atoms, which can then self-assemble into more-elaborate structures.

A number of bottom-up approaches have been developed for producing nanoparticles, ranging from condensation of atomic vapours on surfaces to coalescence of atoms in liquids. For example, liquid-phase techniques based on inverse micelles (globules of lipid molecules floating in a nonaqueous solution in which their polar, or hydrophilic, ends point inward to form a hollow core, as shown in the figure) have been developed to produce size-selected nanoparticles of semiconductor, magnetic, and other materials. An example of self-assembly that achieves a limited degree of control over both formation and organization is the growth of quantum dots. Indium gallium arsenide (InGaAs) dots can be formed by growing thin layers of InGaAs on GaAs in such a manner that repulsive forces caused by compressive strain in the InGaAs layer results in the formation of isolated quantum dots. After the growth of multiple layer pairs, a fairly uniform spacing of the dots can be achieved. Another example

of self-assembly of an intricate structure is the formation of carbon nanotubes under the right set of chemical and temperature conditions.

Lithography

Lithography is the key technology to realize very small feature size for nano components. Optical lithography, the main technology used today is predicted to be applicable beyond 100nm and 70nm with the use of respectively 193nm wavelength and 157nm wavelength tools. The reduction of feature sizes down to 50nm and below will require more advanced lithography tools. As the candidate for the next generation for the microelectronics industry, *Extreme Ultraviolet Lithography* is being strongly supported. EUV lithography, at the wavelength of 13nm, will achieve feature size at 45nm and below.

Photolithography

Photolithography is the selective process that allows the patterning of a desired design onto the material we want to fabricate with (the wafer in the semiconductor industry). Photo resist is applied as the first step in applying a pattern in a uniform film. The mask is a metal sheet that holds the actual pattern that will be etched into the photo resist. The mask is cut so that when a UV light is shined from behind the exposed parts of the photo resist will be the actual pattern. These exposed parts can then be cleaned away (positive resist) or will stay on to the fabricated device (negative resist). As a result of photolithography being the number one limiting factor on the size of wafer production this is the field where most of the research has gone. Contact printing was the very first form of photolithography. In this form the mask was placed directly on top of the photo resist during the exposure process. This process gave a good resolution but sometimes resulted in slight damage to the wafer and the mask. In order to defeat the problems the next innovation, projection printing, separated the mask from the photo resist.

High Energy Ball Milling

It is one of the simplest ways of making nanoparticles of some metals and alloys in the form of powder. There are many types of mills such as planetary, vibratory, rod, tumbler etc. Usually one or more containers are used at a time to make large quantities of fine particles. Size of container, of course, depends upon the quantity of interest. Hardened steel or tungsten carbide balls are put in containers along with powder or flakes be of arbitrary size and shape. Container is closed with tight lids. Usually 2:1 mass ratio of balls to material is advisable. If the container is more than half filled, the efficiency of milling is reduced. Heavy milling balls increase the impact energy on collision. Larger balls used for milling produce

smaller grain size but larger defects in the particles. The process, however, may add some impurities from balls. The container may be filled with air or inert gas. However this can be an additional source of impurity, if proper precaution to use high purity gases is not taken. A temperature rise in the range of 100–1,100 ıC is expected to take place during the collisions. Lower temperatures favour amorphous particle formation. The gases like O2, N2 etc. can be the source of impurities as constantly new, active surfaces are generated. Cryo-cooling is used sometimes to dissipate the heat generated. During the milling, liquids also can be used. The containers are rotated at high speed (a few hundreds of rpm) around their own axis. Additionally they may rotate around some central axis and are therefore called as 'planetary ball mill'.

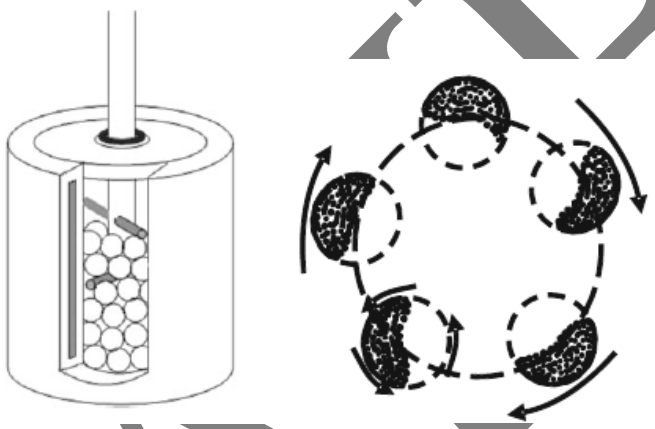

When the containers are rotating around the central axis as well as their own axis, the material is forced to the walls and is pressed against the walls as illustrated in Fig. 3.2. By controlling the speed of rotation of the central axis and container as well as duration of milling it is possible to ground the material to fine powder (few nm to few tens of nm) whose size can be quite uniform. Some of the materials like Co, Cr, W, Ni-Ti, Al-Fe and Ag-Fe are made nanocrystalline using ball mill. Few milligrams to several kilograms of nanoparticles can be synthesized in a short time of a few minutes to a few hours.

Chemical Vapour Deposition (CVD)

Chemical vapour deposition, a hybrid method using chemicals in vapour phase isconventionally used to obtain coatings of a variety of inorganic or organic materials.It is widely used in industry because of relatively simple instrumentation, ease ofrocessing, possibility of depositing different types of materials and economical viability.Under certain deposition conditions nanocrystalline films or single crystallinefilms are possible. There are many variants of CVD like Metallo Organic CVD(MOCVD), Atomic Layer Epitaxy (ALE), Vapour Phase Epitaxy (VPE), PlasmaEnhanced CVD (PECVD). They differ in source gas

pressure, geometrical layoutand temperature used. Basic CVD process, however, can be considered as a transportof reactant vapour or reactant gas towards the substrate kept at some high temperature where the reactant cracks into different products which diffuse onthe surface, undergo some chemical reaction at appropriate site, nucleate and growto form the desired material film. The by-products created on the substrate have tobe transported back to the gaseous phase removing them from substrate.Vapours of desired material may be often pumped into reaction chamber usingsome carrier gas. In some cases the reactions may occur through aerosol formationin gas phase. There are various processes such as reduction of gas, chemical reactionbetween different source gases, oxidation or some disproportionate reaction bywhich CVD can proceed. However it is preferable that the reaction occurs at thesubstrate rather than in the gas phase. Usually _300–1,200 ıC temperature is used atthe substrate. There are two ways viz. 'hot wall' and 'cold wall' by which substratesare heated.In hot wall set up the deposition can take place even on reactor walls. This isavoided in cold wall design. Besides this, the reactions can take place in gas phasewith hot wall design which is suppressed in cold wall set up. Further, coupling ofplasma with chemical reaction in cold wall set up is feasible.

Usually gas pressures in the range of 100–105 Pa are used. Growth rate andfilm quality depend upon the gas pressure and the substrate temperature. Whenthe growth takes place at low temperature, it is limited by the kinetics of surfacereaction. At intermediate temperature it is limited by mass transport i.e. supply ofreacting gases to the substrate. Here the reaction is faster and supply of reactantsis slower. At high temperature, growth rate reduces due to desorption of precursorsfrom the substrate.

When two types of atoms or molecules say *P* and *Q* are involved in the desiredfilm, there are two ways in which growth can take place. In what is known asLangmuir-Hinshelwood mechanism, both *P* and *Q* type of atoms/molecules are adsorbed on the substrate surface and interact there to produce the product *PQ*.When one species is adsorbed in excess of the other, the growth depends on theavailability of adsorption sites for both *P* and *Q*.

However it is also possible to have another way in which reaction can occuri.e. one species say *P* adsorbs on the substrate and the species *Q* from gas phaseinteracts with *P*. Thus there is no sharing of sites. This type of mechanism is knownas Elay–Riedel mechanism.

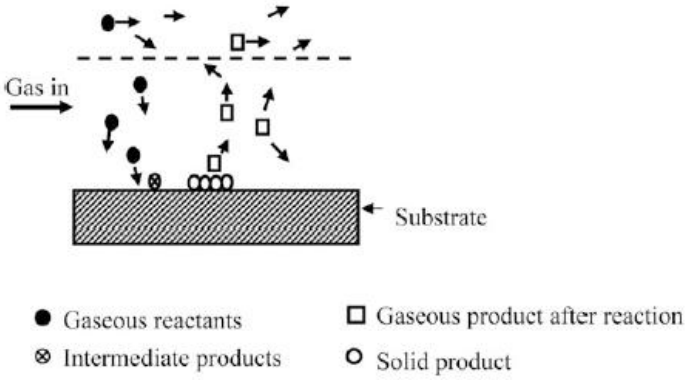

Basic concept of Chemical Vapour Deposition (CVD) process

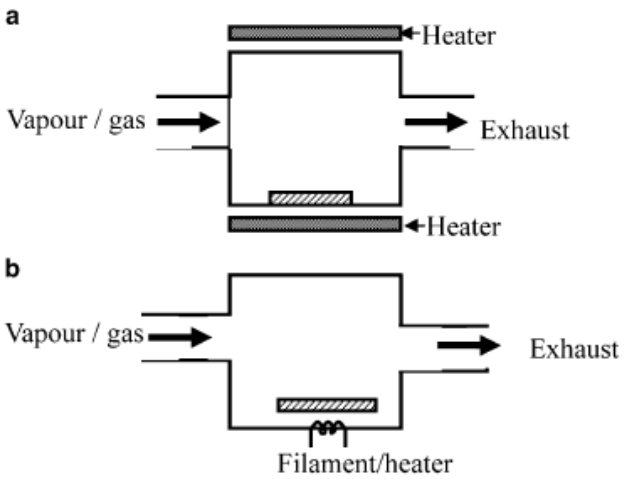

(**a**) Hot wall and (**b**) cold wall CVD

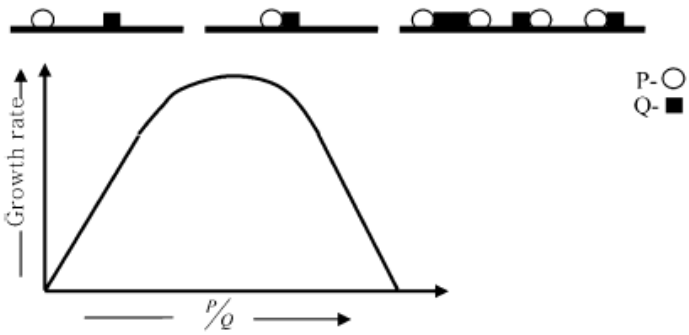

Langmuir-Hinshelwood mechanism of growth

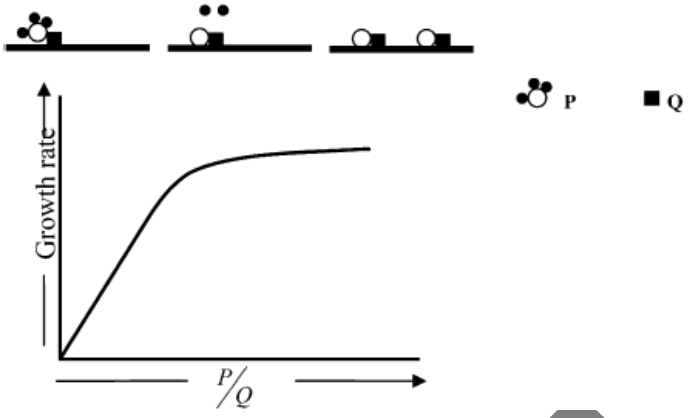

Elay–Riedel mechanism

Colloids and Colloids in Solutions

Colloids are known since very long time. A class of materials, in which two ormore phases (solid, liquid or gas) of same or different materials co-exist with thedimensions of at least one of the phases less than a micrometre is known as colloids.Colloids may be particles, plates or fibres. Nanomaterials are a subclassof colloids, in which one of the dimensions of colloids is in nanometre range.There are several examples around us, having different combinations of phases,in the form of colloids like liquid in gas (fog), liquid in liquid (fat droplets in milk),solid in liquid (tooth paste), solid in solid (tinted glass), gas in liquid (foam). Therecan be multiple existing colloids like water and oil bubbles in porous mineral rocks.Organic and inorganic materials can be dispersed into each other to form colloids.Several examples exist even of bio-colloids. Blood and bones are good examplesof bio-colloids. Blood has corpuscles dispersed in serum and bone has colloids ofcalcium phosphate embedded in collagen.Colloids may even form networks. For example aerogels are a network of silica colloidal particles, pores of which arefilled with air.

Interactions of Colloids and Medium

Colloids are particles with large surface to volume ratio. Correspondingly thereare large number of atoms/molecules on the surface of a colloidal particle, do not have as many neighbours as those for an atom/molecule inside the interior.Therefore atoms on the surface are in a highly reactive state, which easily interactto form bigger particles or tend to coagulate. It is thus necessary to understandthe stability of colloids i.e. how the colloids dispersed in a medium can remainas separated particles. In general there are a number of interactions involved. Forthe sake of understanding these interactions, we consider the inorganic spherical

colloids of equal size, dispersed in a liquid medium. When fine particles aredispersed in a liquid medium, it is known that they undergo *Brownian motion*. If we are able to tag a

particle in the solution, it would appear as if it is making a random motion. All other particles also executerandom motion, hitting each other and changing direction of motion in solution.Distance travelled between successive collisions is random too. However an averagedistance travelled by a colloidal particle can be found as

_R2 D_kT3 r˜__t (4.1)

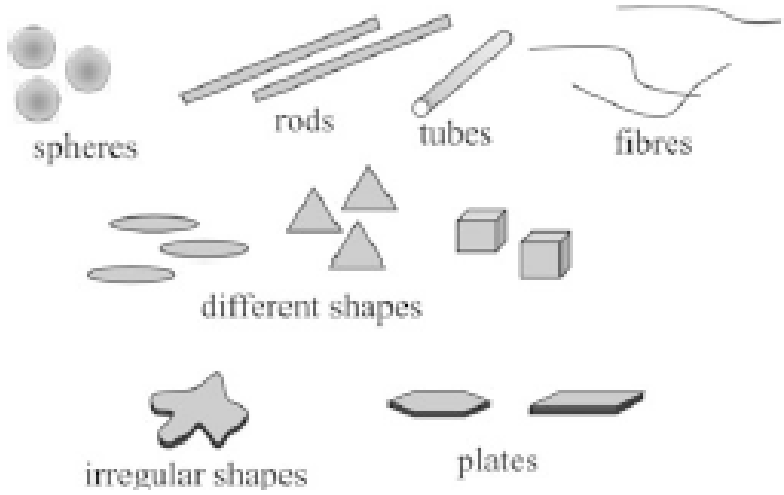

Different shapesof colloids

where _R is distance travelled by a particle from its original position in time _*t*,*k* – Boltzmann's constant, *T* – temperature of liquid, *r* – particle radius and ˜ isviscosity of the liquid.

Interactions of such constantly and randomly moving particles with each otherand with liquid in general would be quite complex. Consider for example the vander Waals interaction (see Chap. 2) between two atoms or molecules. There are twoparts in the interaction viz. attractive and repulsive parts,irrespective of whether there exist permanent dipoles or not. The interaction isgiven as

where*dG1* is the interaction energy, *A* and *B* are constants and *R* is the distance between two particles.

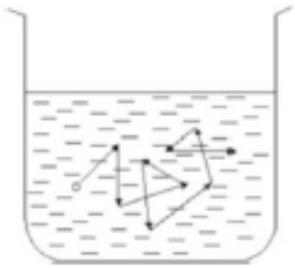

Brownian motionof colloidal particles

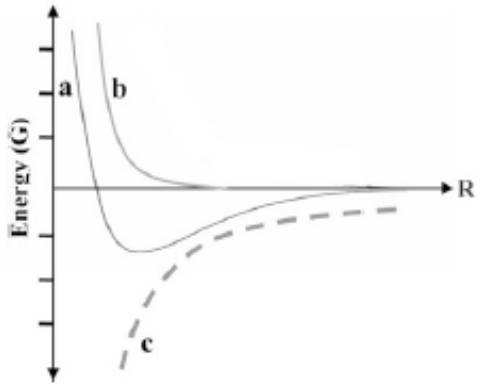

Van der Waalsinteraction: (*a*) Resultingenergy,

(*b*) Repulsive energyand (*c*) Attractive energy

Here the first term is repulsive interaction (Born repulsive interaction) effectiveonly at short distance and second term represents long range attractive interaction(van der Waals attraction). Repulsive part arises due to repulsion between electronclouds in each atom and attractive part is due to interaction between fluctuatingor permanent dipoles of atoms/molecules. Equation is known as Lennard-Jones equation

Colloids in Vacuum

Lennard-Jones equation is sufficient to describe an interaction between twoatoms or molecules. When we consider colloids with large number of atoms, weneed to take into account all the atoms and their interactions with each other. This isquite a complex situation. To describe the interaction betweencolloidal particles Derjaguin, Landau, Verwey and Overbeek proposed a theoryknown as DLVO theory. In order to reduce the complexity of the problem, theyassumed two interacting spherical particles of equal size. Let the radius of each particle be '*r*' and let two particles be separated by a distance '*R*'.It was shown that for two similar spherical particles in vacuum the attractiveinteraction is given by

where*AH* is known as Hamaker constant and is given by

$A_H = A_0^2 n^2$

where*A*0 is a constant related to *A* in the Lennard-Jones equation and *n* is thenumber of atoms/molecules per unit volume in a colloid.

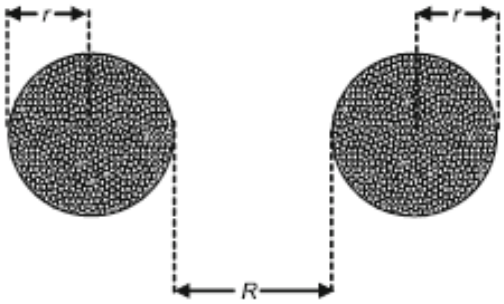

Interaction evenbetween two sphericalparticles of same material andsame size is complex due topresence of large number ofatoms in each particle

Colloids in a Medium

Consider now a situation, inwhich inorganic spherical colloids are immersed in a liquid (and do not dissolve).The attractive interactions between the colloids get modified through the change ofHamaker constant as *A*H, which can be written now as

AH D_pA1*v* _pA2*v*

where*A*1*v* is the Hamaker constant for particle of inorganic solid under consideration,in vacuum and *A*2*v* is Hamaker constant of colloid of medium in vacuum. It canbe seen from above equation that in general the effect of liquid medium is to reducethe Hamaker constant of colloid particle. Hence the attractive force between colloidparticles will in general reduce.

Molecular Beam Epitaxy (MBE)

This technique can be used to deposit elemental or compound quantum dots,quantum wells as well as quantum wires in a very controlled manner. High degree of purity is achievable using ultra highvacuum (better than 10_8 Pa). Special sources of deposition known as Knudsen cell (K-cell) or effusion cell are employed to obtain molecular beams of the constituentelements. The rate of deposition is kept very low and substrate temperature is ratherhigh in order to achieve sufficient mobility of the elements on the substrate and layerby layer growth to obtain nanostructures or high purity thin films. Technique likeReflected High Energy Electron Diffraction (RHEED) is incorporated to monitorthe high crystallinity of the growing film.

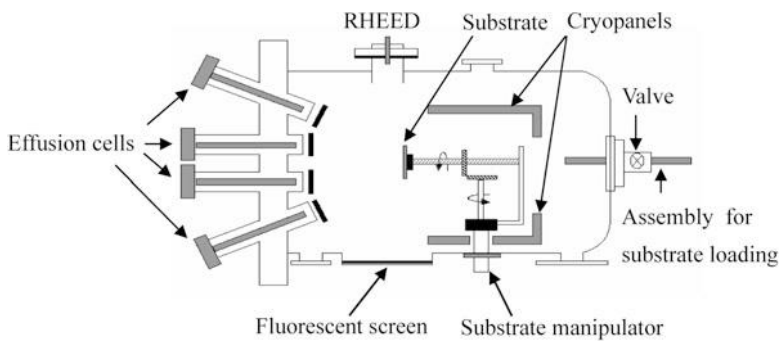

Schematic diagram of molecular beam epitaxy

Synthesis of Metal Nanoparticles by Colloidal Route

Colloidal metal nanoparticles are often synthesized by reduction of some metalsalt or acid. For example highly stable gold particles can be obtained by reducingchloroauric acid (HAuCl4) with tri sodium citrate (Na3C6H5O7).

The reaction can be carried out in water.Metal gold nanoparticles exhibit intense red, magenta and other colours, dependingupon the particle size. Gold nanoparticles discussed above are stabilized byrepulsive Coulombic interactions. It is also possible to stabilize gold nanoparticlesusing thiol or some other capping molecules.

In a similar manner, silver, palladium, copper and other metal nanoparticles canbe synthesized using appropriate precursors, temperature, pH, duration of synthesisetc. Particle size, size distribution and shape strongly depend on the reactionparameters and can be controlled to achieve desired results. It is also possible tosynthesize alloy nanoparticles using appropriate precursors.

Sol-Gel Method

As the name suggests sol gel involves two types of materials or components, ‘sol’and ‘gel’. Sol gels are known since the time when M. Ebelman synthesized themin 1845. However it is only since the last one or two decades that considerableinterest in it, both in scientific and industrial field, has generated due to realizationof the several advantages one gets as compared to some other techniques. First ofall sol gel formation is usually a low temperature process. This means less energyconsumption and less pollution too. It is therefore not surprising that in the nuclearfuel synthesis it is a desired process. Although sol-gel process generates highly pure,well controlled ceramics it competes with other processes like CVD or metalloorganicvapours derived ceramics. The choice of course depends upon the product ofinterest, its size, instrumentation available and ease of processing. In some cases solgelcan be an economical route, provided precursors are not very expensive. Someof the benefits like

getting unique materials such as aerogels, zeolites, and orderedporous solids by organic-inorganic hybridization are unique to sol-gel process. Itis also possible to synthesize nanoparticles, nanorods or nanotubes using sol-geltechnique.

Sols are solid particles in a liquid. They are thus a subclass ofcolloids. Gels are nothing but a continuous network of particles with pores filledwith liquid (or polymers containing liquid). A sol gel process involves formationof 'sols' in a liquid and then connecting the sol particles (or some subunits capableof forming a porous network) to form a network. By evaporating the liquid, it ispossible to obtain powders, thin films or even monolithic solid. Sol gel methodis particularly useful to synthesize ceramics or metal oxides although sulphides,borides and nitrides also are possible.

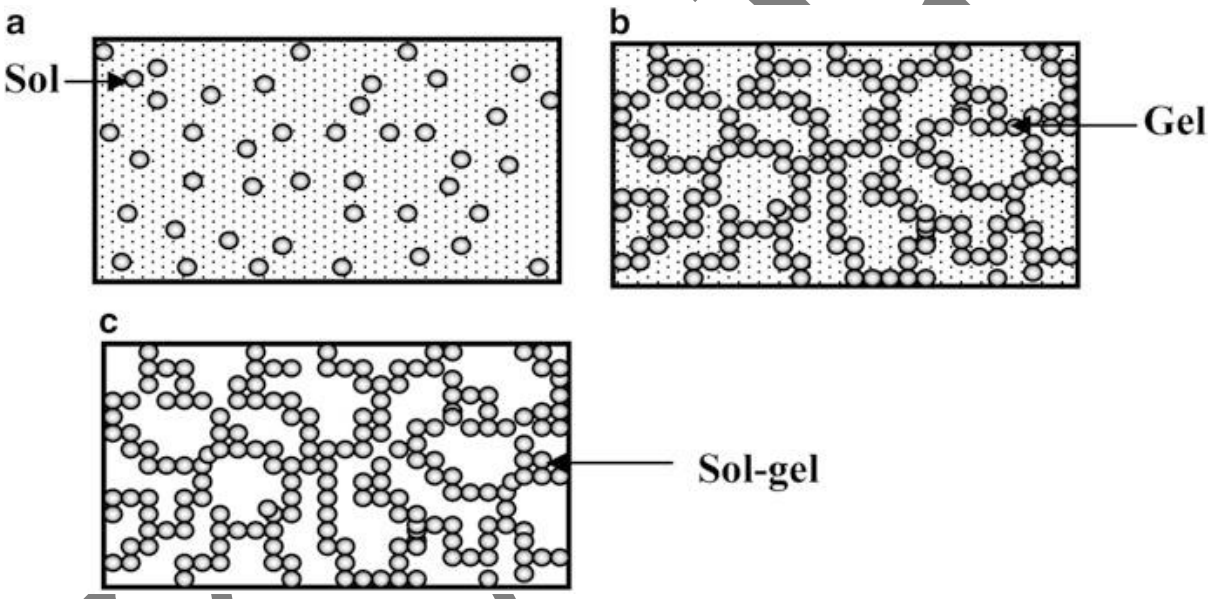

Sol (**a**), gel (**b**) and sol-gel (**c**) monolithic solid

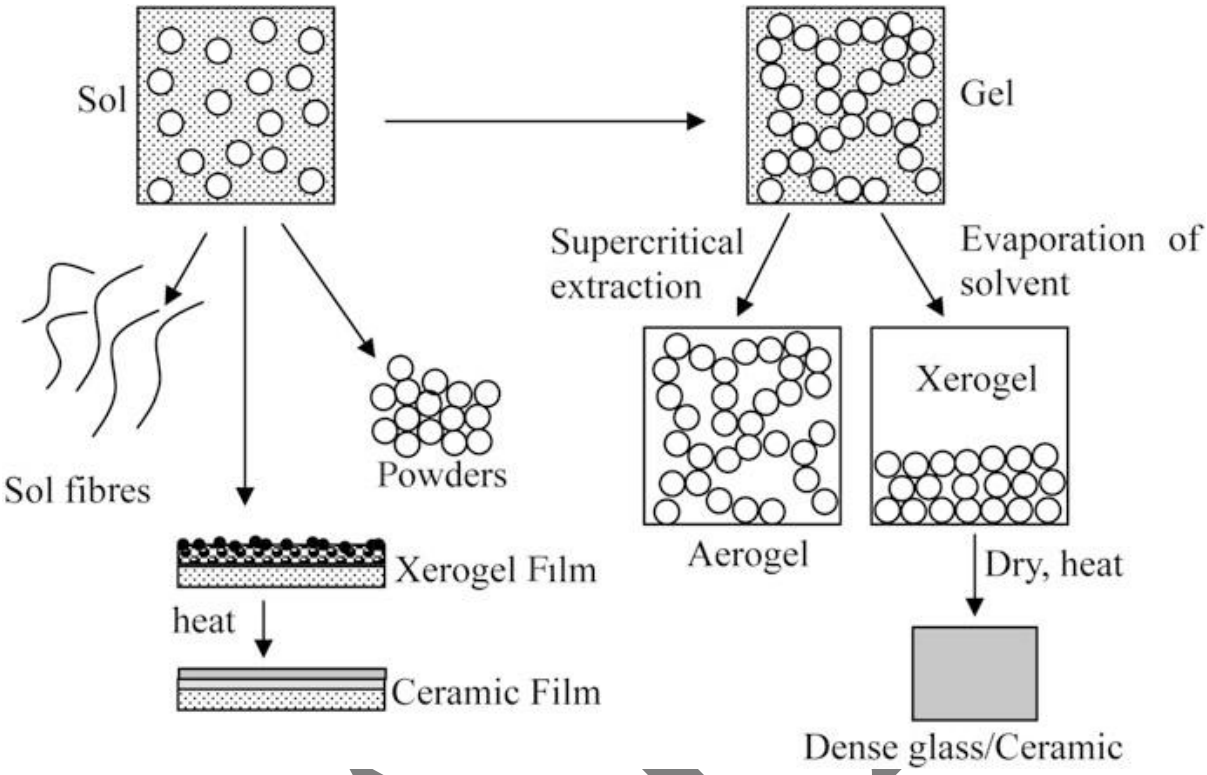

Synthesis of sol-gel in general involves hydrolysis of precursors, condensationfollowed by polycondensation to form particles, gelation and drying process by various routes. Precursors (starting chemicals) are to be chosenso that they have a tendency to form gels. Bothalkoxides or metal salts can be used.Alkoxides have a general formulaM(ROH)n, whereMis a cation and R is an alcoholgroup, *n* is the number of (ROH) groups with each cation. For example (ROH) canbe methanol (CH3OH), ethanol (C2H5OH), propanol (C3H7OH) etc. bonded to acation like Al or Si. Salts are denoted as MX, in which M is a cation and X is an

anion like in CdCl2, CdCis a cation and Cl_ is an anion.Although it is not mandatory that only oxides be formed by a sol-gel process,often oxide ceramics are best synthesized by a sol-gel route. For example insilica, SiO4 group with Si at the centre and four oxygen atoms at the apexesof tetrahedron are very ideal for forming sols with interconnectivity through thecorners of tetrahedrons, creating some cavities or pores.

Due to its higher electronegativity as compared to metal cations, Si is lesssusceptible to nucleophilic attacks.By polycondensation process (i.e. many hydrolyzed units coming together byremoval of some atoms from small molecules like OH), sols are nucleated andultimately sol-gel is formed.

Hydrothermal Synthesis

This synthesis method is useful to make a large scale production of nano to microsize particles. In this technique adequate chemical precursors are dissolved in waterand placed in vessel made of steel or any other suitable metal which can withstandhigh temperature typically upto 300°C and high pressure above 100 bars. Thevessel, known as *autoclave*, is usually provided with temperature and pressurecontrol as well as measuring gauges.It is a very old technique, probably first used by the German scientist RobertBunsen, way back in 1839 to synthesize crystals of strontium and barium carbonates.He used a thick glass tube and used temperature above 200°C and pressuremore than 100 bars. The technique was later used mostly by geologists and hasbecome popular amongst nanotechnologists due to the advantages like large yieldand novel shapes and sizes that can be obtained using this technique.The technique becomes useful when it is difficult to dissolve the precursors atlow temperatures or room temperature. It is also advantageous to use the techniqueto grow nanoparticles if the material has a high vapour pressure near its meltingpoint or crystalline phases are not stable at melting point. The uniformity of shapesand sizes of the nanoparticles also can be achieved by this technique. Variousoxide, sulphide, carbonate and tungstate nanoparticles have been synthesized bythe hydrothermal synthesis.Another variation of hydrothermal synthesis technique is known as *forcedhydrolysis*. In this case usually dilute solutions (10_2 to 10_4 M) of inorganic metalsalts are used and hydrolysis is carried out at rather higher temperatures than 150°C.

Physical Vapour Deposition with Consolidation

This technique basically involves use of materials of interest as sources of evaporation,an inert gas or reactive gas for collisions with material vapour, a cold finger onwhich clusters or nanoparticles can condense, a scraper to scrape the nanoparticles and piston-anvil (an arrangement in which nanoparticle powder can be compacted).All the processes are carried out in a vacuum chamber so that the desired purityof the end product can be obtained. Figure schematically illustrates a set upfor carrying out physical vapour deposition and compressing the powder in a pelletform.

Usually metals or high vapour pressure metal oxides are evaporated or sublimatedfrom filaments or boats of refractory metals like W, Ta and Mo in which thematerials to be evaporated are held. The density of the evaporated material closeto the source is quite high and particle size is small (<5 nm). Such particles wouldprefer to acquire a stable lower surface energy state. Due to small particle or cluster interaction bigger particles

get formed. Therefore, they should be removedaway as fast as possible from the source. This is done by forcing an inert gas nearthe source, which removes the particles from the vicinity of the source. In general

the rate of evaporation and the pressure of gases inside the chamber determine theparticle size and their distribution. Distance of the source from the cold finger isalso important. Evaporated atoms and clusters tend to collide with gas moleculesand make bigger particles, which condense on cold finger. While moving awayfrom the source to cold finger the clusters grow. If clusters have been formed oninert gas molecules or atoms, on reaching the cold finger, gas atoms or moleculesmay leave the particles there and then escape to the gas phase. If reactive gases likeO2, H2 and NH3 are used in the system, evaporated material can interact with these

gases forming oxide, nitride or hydride particles. Alternatively one can first makemetal nanoparticles and later make appropriate post-treatment to achieve desiredmetal compound etc. Size, shape and even the phase of the evaporated material can depend upon the gas pressure in deposition chamber. For example using gaspressure of H2 more than 500 kPa, TiH2 particles of _12 nm size were produced.By annealing them in O2 atmosphere, they could be converted into titania (TiO2)having rutile phase. However if titanium nanoparticles were produced in H2 gaspressure less than 500 kPa, they could not be converted into any crystalline oxidephase of titanium but always remained amorphous.

Clusters or nanoparticles condensed on the cold finger (water or liquid nitrogencooled) can be scraped off inside the vacuum system. The process of evaporationand condensation can be repeated several times until enough quantity of the materialfalls through a funnel in which a piston-anvil arrangement has been provided. Onecan even have separate low and high pressure presses. A pressure of few mega pascal(MPa) to gigapascal (GPa) is usually applied depending upon the material. Lowporosity pellets are easily obtained. Density of the material thus can be _70 to 90 %of the bulk material.

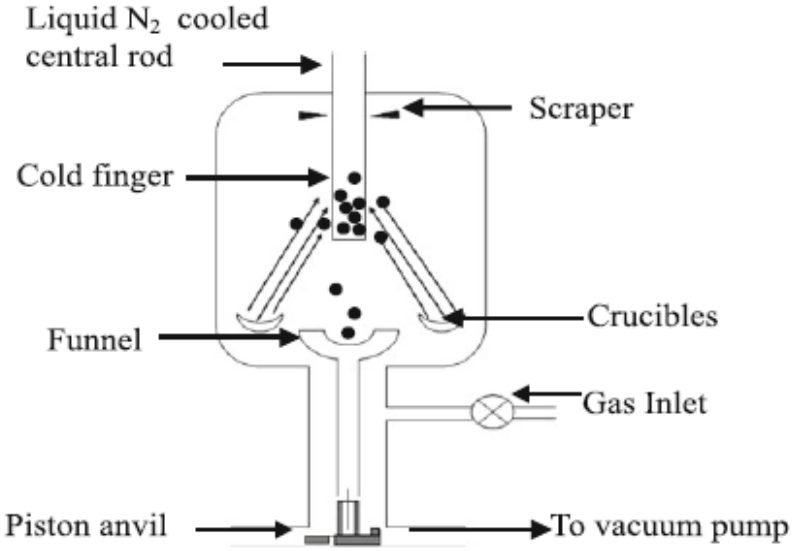

Ionized Cluster Beam Deposition

This method was first developed by Takagi and Yamada around 1985 and is alsouseful to obtain adherent and high quality single crystalline thin films. The set upconsists of a source of evaporation, a nozzle through which material can expand intothe chamber, an electron beam to ionize the clusters, an arrangement to acceleratethe clusters and a substrate on which nanoparticle film can be deposited, all housedin a suitable vacuum chamber. Small clusters from molten material are expanded through the fine nozzle. Thevapour pressure _1 Pa to 1 kPa needs to be created in the source and the nozzleneeds to have a diameter larger than the mean free path of atoms or molecules. vapour form in the source to form the clusters. On collision with electron beam,clusters get ionized. Due to applied accelerating voltage, the clusters are directedtowards the substrate. By controlling the accelerating voltage, it is possible tocontrol the energy with which the clusters hit the substrate. Stable clusters of somematerials would require considerable energy to break their bonds and would ratherprefer to remain as small clusters of particles. Thus it is possible to obtain the filmsof nanocrystalline material using ionized cluster beam. However it is not unlikelythat some neutral atoms also get incorporated in the film. Besides, the clusters arenot mass selected. Therefore they can have wide distribution of particle sizes. In factanything that can cross the accelerating voltage can get incorporated in the film.

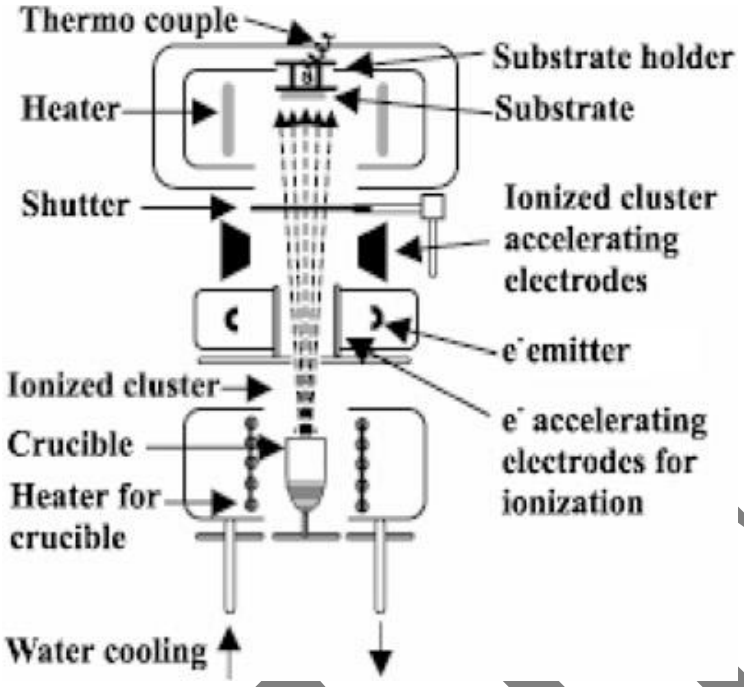

Laser Vapourization (Ablation)

In this method, vapourization of the material is effected using pulses of laser beamof high power. The set up is an Ultra High Vacuum (UHV) or high vacuum system equippedwith inert or reactive gas introduction facility, laser beam, solid target and cooledsubstrate. Clusters of any material of which solid target can be made are possibleto synthesize. Usually laser operating in the UV range such as excimer (excitedmonomers) laser is necessary because other wavelengths like IR orisible are often reflected by surfaces of some metals.

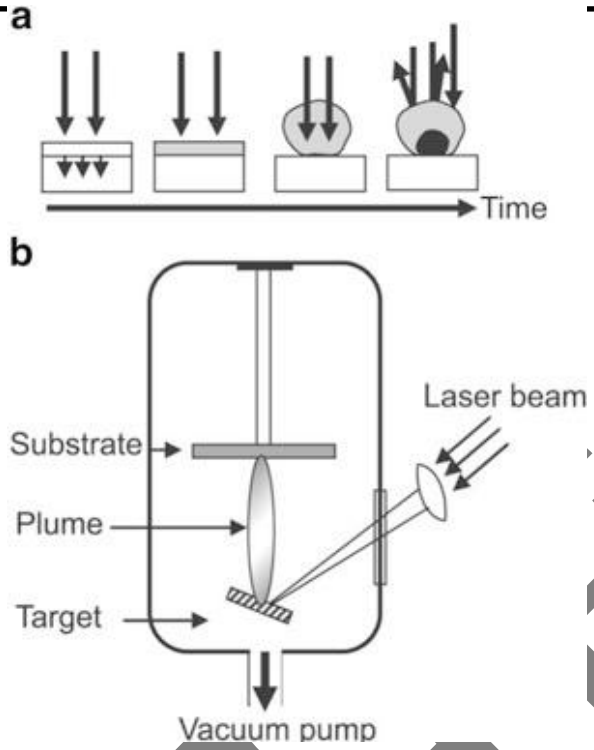

A powerful beam of laser evaporates the atoms from a solid source an atomscollide with inert gas atoms (or reactive gases) and cool on them forming clusters.They condense on the cooled substrate. The method is often known as laser ablation.Gas pressure is very critical in determining the particle size and distribution.Simultaneous evaporation of another material and mixing the two evaporatedmaterials in inert gas leads to the formation of alloys or compounds. This methodcan produce some novel phases of the materials which are not normally formed. Forexample Single Wall Carbon Nanotubes (SWNT) are mostly synthesized by thismethod.

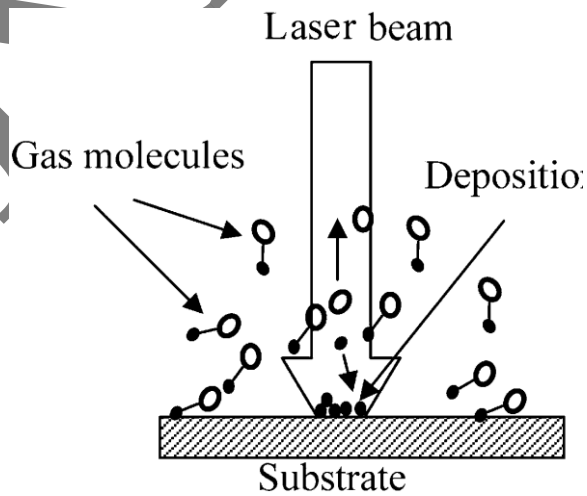

KARPAGAM ACADEMY OF HIGHER EDUCATION

Coimbatore-641021.

(For the candidates admitted from 2016 onwards)

DEPARTMENT OF PHYSICS

UNIT II (Objective Type/Multiple choice Questions each Questions carry one Mark)

NANOMATERIALS AND APPLICATIONS

PART –A(Online Examination)

S.No.	QUESTIONS	opt1	opt2	opt3	opt4	ANSWER
1	Which of the following uses radio frequency to produce nano-particles?	Plasma arching	Chemical vapour deposition	Sol-gel technique	Electro deposition	Plasma arching
2	Which of the following methods can be used to produce nano-powders of oxides?	Plasma arching	Sol-gel technique	Chemical vapour deposition	Mechanical crushing	Chemical vapour deposition
3	Which of the following is used to make both nano-particles and nano-powders?	Chemical vapour deposition	Sol-gel technique	Plasma arching	Electro deposition	Sol-gel technique
4	Which method can be used to prepare iron nitriles nano-crystals using ammonia gas?	Pulsed laser deposition	Sol-gel technique	Electro-deposition	Mechanical crushing	Mechanical crushing
5	Which of the following is used to modify the optical properties of a material system?	Electricity	Magnetic field	Pressure	Light	Light
6	Which of the following is used in electro optic modulators?	Lithium tantalite	Barium sodium niobate	Lithium niobate	Lithium sodium niobate	Lithium niobate
7	Sol-gel method is _____ approach	Bottom up	Up bottom	Top down	Down top	Bottom up
8	Sol-gel method is known since	1970	1960	1980	1990	1980
9	Which ratio decides the efficiency of nanosubstances?	Weight/volume	Surface area/volume	Volume/weight	Pressure/volume	Surface area/volume

10	While synthesizing the nano cones the plasma temperature is above_____	1000oC	1500oC	2000oC	2500oC	2000oC
11	The sol-gel is a _____ of solid particle.	Sublimation	Melting	Colloidal suspension	Cool down	Colloidal suspension
12	The gel is a _____ mass.	Heavy molecular	Semi regid	Regid	Light molecular	Semi regid
13	Sol-gel method is _____ chemical process.	Dry	Wet	Semi liquid	Semi solid	Wet
14	_____ undergo hydrolysis and poly condensation reactions.	Metal ions	Metal carbonates	Metal nitrates	Metal oxides	Metal oxides
15	The solvent evolves towards the formation of an inorganic continuous network containing a	Gaseous phase	Gel	Solid phase	Semi solid phase	Gel
16	Formation of an inorganic continuous network containing the metal centres with _____	Azo	Oxo	Nitro	Hydro	Oxo
17	After drying process the liquid phase is removed from the gel and _____ is performed.	Calcination	De-oxygenation	Oxygenation	Hydrogenation	Calcination
18	One of the advantages of sol-gel method is able to get uniform and _____ powder.	Micro size	Large size	Nano size	Small size	Small size
19	Sol-gel method can produce _____ systems.	Uniform multi component	Non uniform multi component	Multi component	Non uniform multi component	Uniform multi component
20	Metal nano particles particularly _____ nano particles are prepared by the chemical reduction method.	Silver	Gold	Platinum	Tungsten	Silver
21	The _____ and citrate solution are used as reducing agents in chemical reduction method.	Hydrazine hydrate	Hydrazine	Hydrazone	Semi carbazene	Hydrazine hydrate
22	What is range of temperature at Hydro thermal reservoirs?	350oC	210oC	50oC	1900oC	350oC
23	When do hydrothermal resources arise?	When the movement of tectonic plates	When the area is prone to volcanic eruptions	When water has access to high	When temperature on earth surface is	When water has access to high temperature

		occurs		temperature	very high	
24	Fabrics are extensively made out of nano materials like _____	Carbon nano tubes	Fullerenes	Mega tubes	Polymers	Fullerenes
25	The power required for electro-deposition is	DC and very low voltage	DC and high voltage	AC and very low voltage	AC and high voltage	C and very low voltage
26	The energy required for refining of gold in kWh / tone is about	100 to 150	250 to 350	300 to 350	350 to 400	300 to 350
27	On industrial scale sodium metal is prepared by electrolysis of fused	NaOH	NaCl	NaO	NH_3	NaCl
28	Electrolyte used for tin plating is	sulphide ore	stannous sulphate	hydrogen sulphate	sodium chloride	stannous sulphate
29	When zinc is plated on steel, anode is made up of	steel	oxygen	zinc	carbon	zinc
30	If the containerof ball mill is more than half filled, the efficiency of milling is	increased	reduced	same	zero	reduced
31	_____ mass ratio of balls to material is advisable	3:01	4:01	2:01	1:01	2:01
32	If surface area of liquid is large then evaporation will be	small	large	moderate	none of above	large
33	Changing of a liquid into vapours from surface of liquid without heating it is called	expansion	contraction	evaporation	fusion	evaporation
34	Evaporation from surface of any liquid depends on	temperature	wind	nature of liquid	all of above	all of above
35	Evaporation causes	cooling	heating effect	increase in weight	increase in density	cooling

36	Evaporation takes place at	freezing point	boiling point	In between freezing point and boiling point	at all temperatures	at all temperatures
37	Lithography was invented by _____ in 1798.	Alois Senefelder	John Denver	Manuel Neuer	Billy Armstrong	Alois Senefelder
38	The surface is treated with a _____ that is soaked into the image area, but avoided the H2O treated, non-image area.	Polar ink	Non-polar ink	Silk screen	Pressure screen	Non-polar ink
39	Lithography is:	Process used to transfer a pattern to a layer on the chip	Process used to develop an oxidation layer on the chip	Process used to develop a metal layer on the chip	Process used to produce the chip	Process used to transfer a pattern to a layer on the chip
40	The system utilised to apply the H2O solution to the plate surface is called the _____	Dissociating system	Dampening system	H2O hating system	Littering	H2O hating system
41	Dot gain in the mid tones is said to be about _____ lower than with conventional lithography.	10%	20%	30%	40%	10%
42	Silicon oxide is patterned on a substrate using:	Physical lithography	Photolithography	Chemical lithography	Mechanical lithography	Photolithography
43	The chemical used for shielding the active areas to achieve selective oxide growth is:	Silver Nitride	Silicon Nitride	Hydrofluoric acid	Polysilicon	Silicon Nitride
44	An _____ is a sol with the continuous phase a gas. Fog is an _____ of water droplets.	Aerosol	Emulsion	Agglomerate	Electrophoresis	Aerosol
45	An _____ is a sol in which the suspended particles are liquid droplets and the continuous phase is also a liquid. The 2 phases are	Aerosol	Emulsion	Agglomerate	Electrophoresis	Emulsion

	immiscible, otherwise a solution would form.					
46	A _____ is a sol of solid particles scattered in a liquid. Foam is a colloidal system in which gas bubbles dispersed in a liquid or solid.	Colloidal suspension	Streaming potential	Sedimentation potential	Electrophoresis	Colloidal suspension
47	The _____ of colloids are of maximum importance since the interaction of the particles with each other and the principal phase is of primary concern.	Magnitude	Shape	Surface	Size	Surface
48	As the concentration increases to the critical micelle concentration(C.M.C.) soap particles abruptly collected into spherical structures called _____	Ball	Sphere of ions	Micelles	Dirt particle	Micelles
49	_____ is the charged field generated by charged particles moving in a stationary liquid.	Colloidal suspension	Emulsion	Sedimentation potential	Electrophoresis	Sedimentation potential
50	When tiny particles of a substance are dispersed through medium then mixture is called	alloys	amalgams	suspension	colloid	colloid
51	Particle size in suspension is	less than 10^3 nm	10^2 nm	greater than 10^3	10 nm	less than 10^3 nm
52	What is the best description of blood?	sol	foam	solution	aerosol	sol
53	Which of the following is a characteristic of a horizontal tube evaporator?	Agitation is provided only by bubbles leaving the evaporator as vapor	The tube bundle is arranged vertically, with the solution inside the tubes condensing outside	To handle viscous solution a pump is used to force liquid upwards	Also called short vertical tube evaporator	Agitation is provided only by bubbles leaving the evaporator as vapor
54	Which of the following is not an assumption in the evaporator model?	The feed has only one volatile	Only the latent heat of vaporization is	Boiling action in heat exchanger	Overall temperature driving force is	Overall temperature driving force is the temperature that of

		components	available for heating the solution	ensures perfect mixing	the temperature that of saturated steam	saturated steam

UNIT-III

CHARACTERIZATION: X-Ray Diffraction. Optical Microscopy. Scanning Electron Microscopy. Transmission Electron Microscopy. Atomic Force Microscopy.Scanning Tunneling Microscopy. Fourier Transform Infrared spectroscopy, UV-visible spectroscopy

X-Ray Diffraction

X-ray diffraction (XRD) is an effective method for determining the crystal structure of materials. It detects crystalline materials having crystal domains greater than 3-5 nm. It is used to characterize bulk crystal structure and chemical phase composition.

Crystalline & Amorphous materials

Materials can be classified as

- Crystalline material: Crystalline material can be single crystal or polycrystalline
- Amorphous material

Crystalline material

Crystalline materials are composed of atoms arranged in a regular ordered pattern in three dimensions. This periodic arrangement is known as crystal structure. It extends over distance much larger than the inter atomic separations. In single crystal this order extends through out the entire volume of the material. There are seven crystal system: cubic, tetragonal, orthorhombic, rhombohedral, hexagonal, monoclinic and triclinic. Different crystal structures are based on framework of one of the 14 Bravais lattice.

Parallel planes of atoms intersecting the unit cell are used to define directions and distances in the crystal. The '*d* spacing' is defined as the distance between adjacent planes. The orientation and interplaner spacing (d) of these lattice planes are defined by three integers *h,k,l* called Miller Indices. The (hkl) designate a crystal face or family planes throughout a crystal lattice.

Polycrystalline materials consist of many small single crystal regions called grains. Grains are separated by grain boundaries. The grains can have different shape and size and are disoriented with respect to each other.

Amorphous materials: When the atoms are not arranged in a regular periodic manner the material is called amorphous. Such material posses only short range order, distance less than a nanometer.

X-Ray Diffraction:

X-ray is a form of electromagnetic radiation having range of wavelength from 0.01-0.7 nm which is comparable with the pacings between lattice planes in the crystal. Spacing between atoms in metals ranges from 0.2-0.3 nm. When an incident beam of X-rays interacts with the

target atom, X-ray photons are scattered in different directions. Scattering is elastic when there is no change in energy between the incident photon and the scattered photon. In inelastic scattering the scattered photon loses energy. These scattered waves may super impose and when the waves are in phase then the interference is constructive and if out of phase then destructive interference occurs. Atoms in crystal planes form a periodic array of coherent scatterers. Diffraction from different planes of atoms produces a diffraction pattern, which contains information about the atomic arrangement within the crystal.

Bragg's law

The X-ray beams incident on a crystalline solid will be diffracted by the crystallographic planes. Bragg's law is a simple model explaining the conditions required for diffraction. It is given as $n\lambda = 2d \sin\theta$, where n is an integer and $\lambda$is wavelength. For parallel planes of atoms, with a spacing d_{hkl} between the planes, constructive interference occurs only when Bragg's law is satisfied. In diffractometers, the X-ray wavelength is fixed. Consequently, a family of planes produces a diffraction peak only at a specific angle θ. The spacing between diffracting planes of the atoms determinses the peak positions. The peak intensity is determined by the atoms are in the diffracting plane. The Fig. 1 explains the Bragg's law. Two in-phase incident waves, beam 1 and beam 2, are deflected by two crystal planes (Z *and* Z_1). The diffracted waves will be in phase when the Bragg's Law, $n\lambda = 2d \sin\theta$, is satisfied. In order to keep these beams in phase, their path difference (SQ + QT) has to equal one or multiple X-ray wavelengths ($n\lambda$) i.e $SQ + QT = n\lambda$ or $SQ + QT = 2PQ \sin\theta = 2d \sin\theta = n\lambda$. Hence the path difference depends on the incident angle (θ) and spacing between the parallel crystal planes (d).

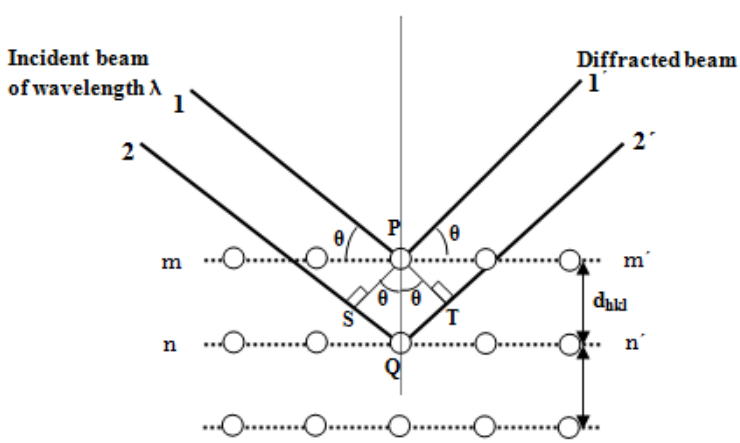

Fig. 1. Braggs analysis for X-ray diffraction by crystal planes

Working principle and Instrumentation

The instrument is called an X-ray diffractometer. In the diffractometer, an X-ray beam of a single wavelength is used to examine the specimens. By continuously changing the incident angle of the X-ray beam, a spectrum of diffraction intensity versus the angle between incident and diffraction beam is recorded.

The main components of diffractometer are

- X-ray Tube: the source of X Rays.
- Incident-beam optics: to condition the X-ray beam before it hits the sample
- Goniometer: the platform that holds and moves the sample, optics, detector, and/or tube
- Sample holder
- Receiving-side optics: to condition the X-ray beam after it has encountered the sample
- Detector: to count the number of X Rays scattered by the sample

The 'θ' is the angle between the X-ray source and the sample. whereas 2θ is the angle between the incident beam and the detector. The incident angle θ is always half of the detector angle 2θ. The basic function of a diffractometer is to detect X-ray diffraction from materials and to record the diffraction intensity as a function of the diffraction angle *(2θ)*. The X-ray radiation generated by an X-ray tube passes through Soller slits which collimate the X-ray beam. The X-ray beam passing through the slits strikes the specimen. X-rays are diffracted by the specimen and form a convergent beam at the receiving slits before they enter a detector.

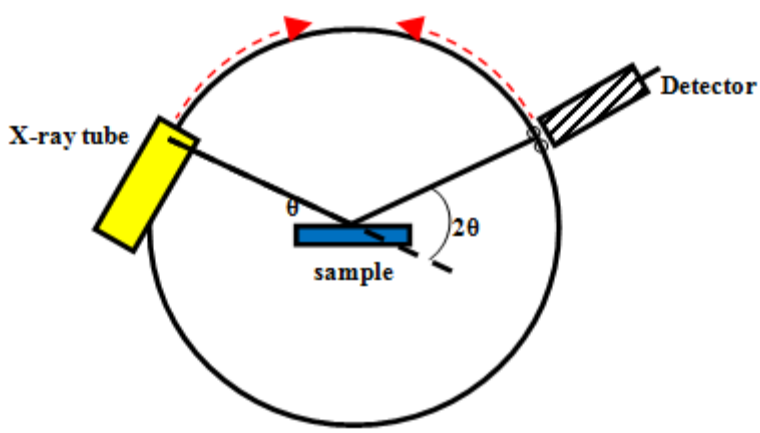

Fig. 2. Basic components of X-ray diffractometers

The diffracted X-ray beam passes through a monochromatic filter to suppress wavelengths other than K_a radiation and decrease any background radiation, before being received by the detector. The K_a radiation is generated by bombarding of target surface (Cu, Fe,

Cr) by accelerated electrons. Most commonly a copper target is used generating K_a wave length of 0.154 nm.

Relative movements among the X-ray tube, specimen and the detector ensure the recording of diffraction intensity in a range of 2θ.

An instrument can be operated in two ways:

- tube is fixed, the sample and the detector rotates
- sample is fixed and the tube and the detector rotates

Powder diffraction

A single crystal produces only one family of peaks in the diffraction pattern. A polycrystalline sample contains thousands of crystallites. Therefore, all possible diffraction peaks are observed. Powder diffraction is used for characterization of polycrystalline materials. The basic assumption of powder diffraction is that for every set of planes, there are statistically relevant number of crystallites that are properly oriented to diffract the incident beam. The diffraction pattern is the fingerprint of any crystalline phase. The position, intensity, shape and width of the diffraction lines give s information on the samples. Powder diffraction data consists of a record of photon intensity versus detector angle 2Θ. Diffraction data can be reduced to a list of peak positions and intensities. Each d_{hkl}corresponds to a family of atomic planes (*hkl*). However, individual planes cannot be resolved by this method; this is a limitation of powder diffraction versus single crystal diffraction

Applications

Catalysts are extensively characterized by XRD technique. The major applications of XRD are discussed below.

1. Phase Identification

The catalysts are generally composed of mixture of several phases. The diffraction pattern for each phase is as unique as a fingerprint. Phases with the same chemical composition can have drastically different diffraction patterns. Phase identification is based on the comparison of the diffraction pattern of the specimen with that of pure reference phases or with a database. Databases such as the Powder Diffraction File (PDF) contain lists for thousands of crystalline phases. The PDF contains over 200,000 diffraction patterns. Modern computer programs can determine the phases present in a sample by quickly comparing the diffraction data to all of the patterns in the database. Various crystalline phases can be quantified based on the

fact that each phase of the mixture gives its characteristic diffractogram independently of the others and the intensity depends on the amount present in the mixture.

Determination of average crystallite size

Ideally, a Bragg diffraction peak is a line without width. In reality, diffraction from a crystal specimen produces a peak with a certain width. This is known as peak broadening. The peak width depends on the size of the crystals. Peak width is inversely related to crystal size; that is, peak width increases with decreasing crystal particle size.

The average crystallite size can be determined by Scherrer formula using elementary line broadening analysis. The Scherrer formula assumes that the breadth of the diffraction peak of crystallites (small single crystals) mainly depends on the characteristics of crystallites (size and the defect in the lattice). Elementary analysis of the broadening assumes that lattice deformation is negligible. According to Scherrer, the thickness of crystallite, L, can be determined by

$$L = \frac{k\lambda}{\beta \cos\theta}$$

k = constant ; λ = wavelength of X-ray source ;
β = breadth of diffraction profile = Full width at half maxima
θ = half of the diffraction angle/Bragg angle

The diffraction corresponding to the most intense peak is selected to calculate the average crystallite size using Scherrer relation. The Scherrer formula assumes that crystallite size is the major source leading to line broadening effects of the diffractions peaks, but there is always a broadening can also be due to instrumental factors such as slit width, sample size, imperfect focusing or misalignment of diffractometers.

3. Spacing between atomic planes of a crystal

Based on Bragg's Law, information on spacing between atomic planes can be obtained when constructive interference occurs. Knowing the spacing of crystallographic planes by diffraction methods, the crystal structure of materials can be determined. The plane spacing of cubic crystal is related to the lattice parameter (*a)* by the following equation.

$d_{hkl}=a/\sqrt{(h^2+k^2+l^2)}$

Optical Microscopes

Human eye perceives an object when visible light reflected from an object enters the eye. Size of an object observed by an eye depends upon the arc subtended by the object at the lens and image on the retina of the eye. smaller the distance from the eye, bigger is the image of the object in the eye. There are, however, two limitations. An object kept at a distance smaller than _25 cm (this

distance is known as the distance of distinct vision) from the eye cannot produce a sharp image of the object and other is that a human eye cannot detect an object smaller than_100 _mas a distinct object if placed close to another object. However, by placing a convex lens close to an eye, a magnified virtual image can be formed at a larger distance so as to form an image with larger angle. Such a magnifying lens forms the simplest kind of microscope. where 25 in the numerator is the distance of distinct vision in cm and '*f* ' is the focal length of magnifying lens in cm.

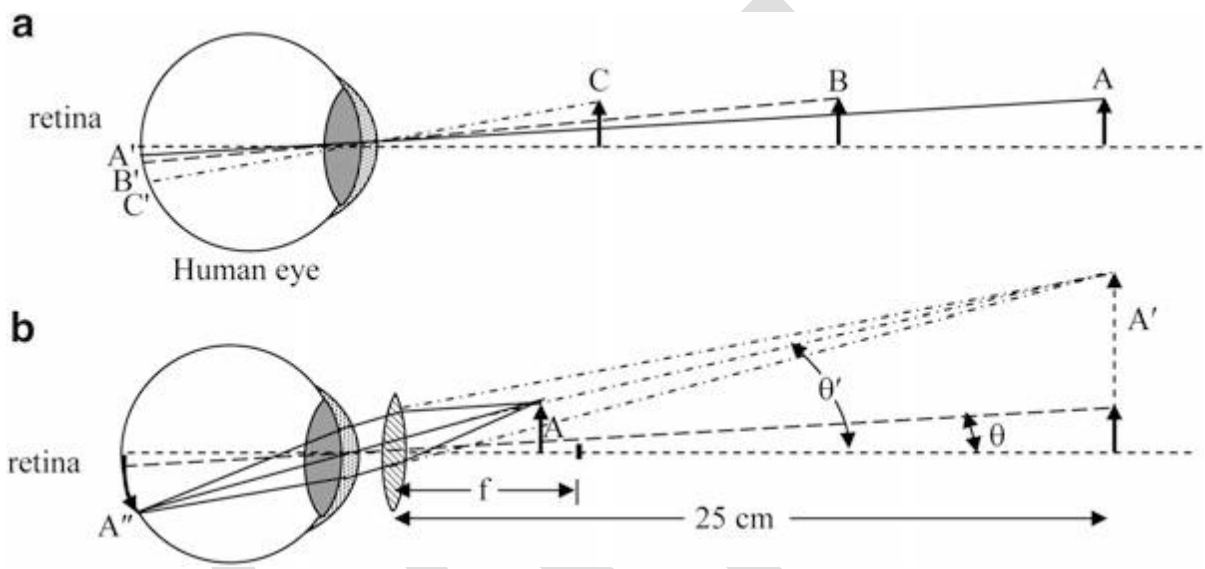

(**a**) Size of the image depends on the distance from the eye. (**b**) By keeping a convex lens close to the eye, image of an object can be magnified

An object would appear ten times larger with lens having *f* =2.5 cm (*M*=25/2.5) and is written as '10_'. When an image is 100 times bigger than the object, it is written as '100_' and so on.

With the magnifying ability of lenses in mind, Galileo invented in the year 1610 the simplest optical microscope. Currently used microscopes make use of at least two lenses viz. objective and eyepiece. Objective lens is the lens close to the object and eyepiece is close to the eye The objective lens (from a distance larger than its focal distance) forms the real image of an object, which in turn gets magnified as a virtual image due to eyepiece.

Overall magnification M = -x/f1 . 25/f2

where _*x*/*f*1 is magnification due to objective lens and 25/f2 is the magnification due to eyepiece. Here '*x*' is the distance of image from the focal point of the lens. Negative sign indicates that the image is inverted In a commercial optical microscope more than two lenses, apertures, sample

stage and light source are present in order to improve the quality of the observed image (lenses produce various defects in images like distortion, astigmatism etc. which can be partially corrected). Magnification of an optical microscope cannot be increased indefinitely as all the microscopes are limited by their ability to resolve the images to some limit. This is limited by the diffraction of the scattered light from an object. Two close-by areas on a sample can be considered as two apertures, the light passing through which can interfere to form a combined image. The closest distance between two points (or two areas), which can be seen as separate or resolved $NA=n \sin\theta$ is the numerical aperture of a lens with n as the refractive index of the lens. Approximating $NA=1$, $R=\lambda/2$ which is often referred to as $\lambda/2$ limit or diffraction limited resolution. $\lambda/2$ limit is common to all microscopes based on the principle of scattering of waves, may be electromagnetic or those associated with particles.

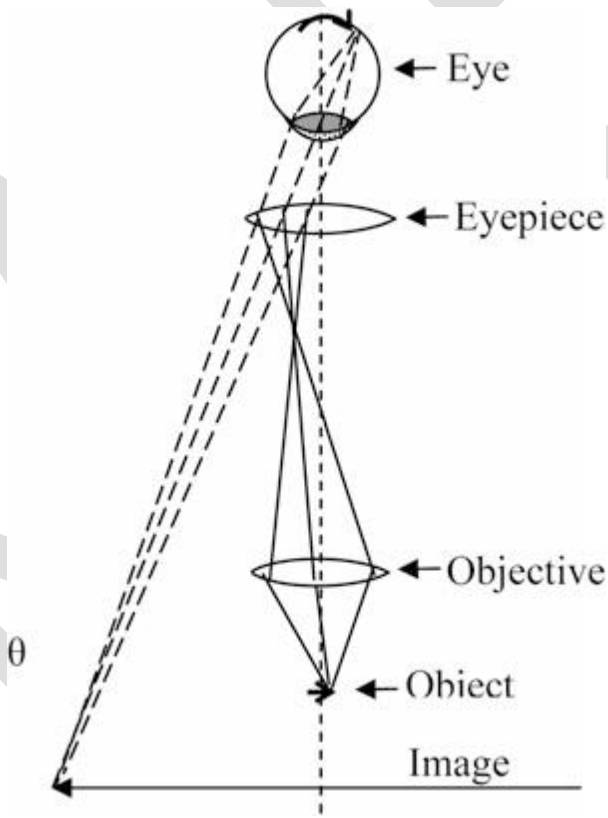

Ray diagram of the simplest kind of an optical microscope using just two convex lenses

Optical microscopes in general can resolve up to ~0.2 mm as visible light ranges from 400 to 700 nm and the smallest wavelength, which can be used is 400 nm. In order to observe the images of objects, additionally, it is necessary to obtain sufficient contrast between the image of interest and its surrounding. This depends upon the method of illumination, absorption of light

due to sample and some other factors like polarization of light etc. When a beam of light is incident on a perfectly flat solid surface, it is known, following Snell's law, that it can get partly reflected and partly refracted. However, if we consider a beam of light falling on a rough surface, then depending upon the surface roughness or morphology the intensity of the reflected beam can vary in different directions (Snell's law is obeyed but one needs to consider local normal to the surface) or the reflected beam would diverge. This would mean that there would be an intensity variation from the sample surface. If the sample is having some grains or different optical properties (refractive index or reflecting power) for different parts of the sample surface, then intensity variations would occur and can be detected. The optical microscopes in the current use are equipped with a set of lenses to improve the sample illumination, sample movement stage, lenses with different magnification, camera with various apertures and other facilities to obtain high quality images as well as ease of operation.

Scanning Electron Microscope

The scanning electron microscope (SEM) uses a focused beam of high-energy electrons to generate a variety of signals at the surface of solid specimens. The signals that derive from electron-sample interactions reveal information about the sample including external morphology (texture), chemical composition, and crystalline structure and orientation of materials making up the sample. In most applications, data are collected over a selected area of the surface of the sample, and a 2-dimensional image is generated that displays spatial variations in these properties. Areas ranging from approximately 1 cm to 5 microns in width can be imaged in a scanning mode using conventional SEM techniques (magnification ranging from 20X to approximately 30,000X, spatial resolution of 50 to 100 nm). The SEM is also capable of performing analyses of selected point locations on the sample; this approach is especially useful in qualitatively or semi-quantitatively determining chemical compositions, crystalline structure, and crystal orientations. The design and function of the SEM is very similar to the and considerable overlap in capabilities exists between the two instruments.

Principles of Scanning Electron Microscopy (SEM)

Accelerated electrons in an SEM carry significant amounts of kinetic energy, and this energy is dissipated as a variety of signals produced by electron-sample interactions when the incident electrons are decelerated in the solid sample. These signals include secondary electrons (that produce SEM images), backscattered electrons (BSE), diffracted backscattered electrons

(EBSD that are used to determine crystal structures and orientations of minerals), photons (characteristic X-rays that are used for elemental analysis and continuum X-rays), visible light (cathodoluminescence--CL), and heat. Secondary electrons and backscattered electrons are commonly used for imaging samples: secondary electrons are most valuable for showing morphology and topography on samples and backscattered electrons are most valuable for illustrating contrasts in composition in multiphase samples (i.e. for rapid phase discrimination). X-ray generation is produced by inelastic collisions of the incident electrons with electrons in discrete ortitals (shells) of atoms in the sample. As the excited electrons return to lower energy states, they yield X-rays that are of a fixed wavelength (that is related to the difference in energy levels of electrons in different shells for a given element). Thus, characteristic X-rays are produced for each element in a mineral that is "excited" by the electron beam. SEM analysis is considered to be "non-destructive"; that is, x-rays generated by electron interactions do not lead to volume loss of the sample, so it is possible to analyze the same materials repeatedly.

Essential components of all SEMs include the following:

- Electron Source ("Gun")
- Electron Lenses
- Sample Stage
- Detectors for all signals of interest
- Display / Data output devices
- Infrastructure Requirements:
  - Power Supply
  - Vacuum System
  - Cooling system
  - Vibration-free floor
  - Room free of ambient magnetic and electric fields

SEMs always have at least one detector (usually a secondary electron detector), and most have additional detectors. The specific capabilities of a particular instrument are critically dependent on which detectors it accommodates.

In an electron microscope, electrons emitted from a hot filament are usually used. However, sometimes cold cathode (a cathode that emits electrons without heating it) is also used.

A cold cathode emits electrons under the application of a very high electric field. It is also known as a field emitter. Such SEMs are known as FE-SEM and are able to give better images than hot filament SEM. However, such FE-SEM is less common than hot cathode SEM. In a scanning electron microscope, backscattered electrons or secondary electrons are detected

Due to interaction of focussed beam with solid, the backscattered electrons are somewhat defocussed resulting into lowered resolution than one would expect. In an electron microscope, the electron beam can be focussed to a very small spot size using electrostatic or magnetic lenses. Usually the electrostatic lenses are used for a SEM. The fine beam is scanned or rastered on the sample surface using a scan generator and back scattered electrons are collected by an appropriate detector. Signal from scan generator along with amplified signal from the electron collector generates the image of sample surface. In order to avoid the oxidation and contamination of filament as well as reduce the collisions between air molecules and electrons, filament and sample have to be housed in a vacuum chamber. Usually vacuum 102–103 Pa or better is necessary for a normal operation of scanning electron microscope. This makes electron microscopes rather inconvenient. However some manufacturers have been successful in marketing electron microscopes known as environmental microscopes, in which samples can be at rather high pressure of few hundreds of Pa (100–500 Pa). Sample preparation is therefore minimized and sample in biological conditions can be investigated. For this the electrons are accelerated as usual in a high vacuum system but they enter the sample chamber through a thin foil or aperture so that a large pressure difference can be maintained One disadvantage of electron microscopes is that insulating samples cannot be analyzed directly as they get charged due to incident electrons and images become blurred/faulty. Therefore insulating solids are coated with a very thin metal film like gold or platinum making them conducting without altering any essential details of the sample. The metal film is usually sputter coated on the sample to be investigated prior to the introduction into the electron microscope. This enables even biological samples to be analyzed using an electron microscope. Additionally, some microscopes provide with a low energy electron flood gun to reduce the sample charging effect by providing more electrons to an insulating sample.

Electron microscopes can also be used to obtain the composition of sample using a technique known as Energy Dispersive Analysis of X-rays (EDAX). The high energy electrons striking the sample produce characteristic X-rays of atoms with which they interact. When

analysis of the energies and intensities of such characteristic X-rays are compared one can obtain the composition analysis of the sample under investigation.

Transmission Electron Microscope (TEM)

Transmission electron microscope is ideal for investigating the nanomaterials, as very high resolution is possible (better than 0.5 nm) using it. As the name suggests the electrons are transmitted through the specimen in this microscope. Electrons of very high energy (typically >50 keV) are used which pass through a series of magnetic lenses, as in an optical or SEM discussed earlier. The basic components of TEM are electron source, condenser lens, specimen, objective lens, diffraction lens, intermediate lens, projector lens and a fluorescent screen in the given order. There may be some additional lenses in different microscopes in order to improve the image quality and resolution. The lenses are electromagnetic whose focal lengths are varied to obtain optimized images rather than moving the lenses themselves as is done in an optical microscope. Similar to SEM, the components (and specimen) of a TEM also have to be housed in a chamber having high vacuum 103–104 Pa for its proper functioning. As illustrated in Fig. 7.8, TEM has the advantage that one can not only obtain the images of the specimen but also diffraction patterns, which enable to understand the detailed crystal structure analysis of the sample. Using diffraction analysis one can find out size dependent changes in the lattice parameters as well as defects in the sample. Moreover it is also possible to analyze single particles of very small (nanometre) dimension. In some microscopes, it is possible to vary the sample temperature. This enables to investigate the problems such as size dependent melting point variation of nanoparticles

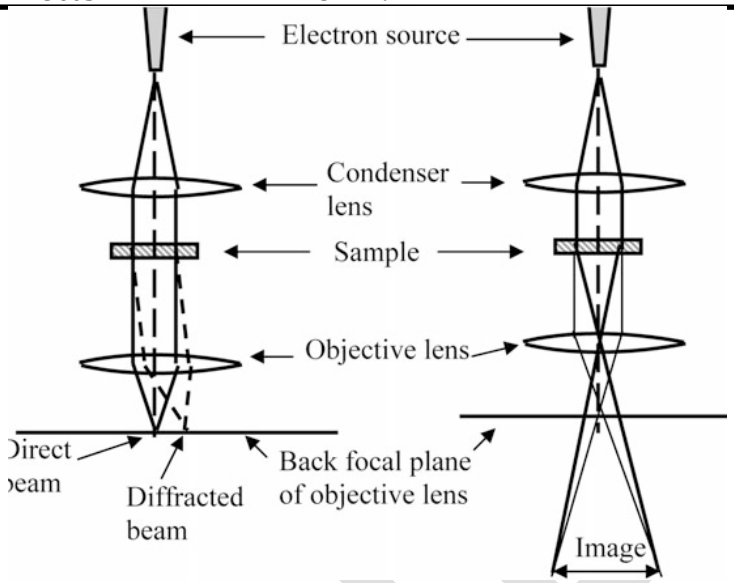

Scanning Tunnelling Microscope

The scanning tunnelling microscope is based on the tunneling principle. When two metals say M1 and M2 are brought at small distance (but larger than 10 nm) as even though their Fermi levels do not coincide, transfer of electrons from one metal to the other is not possible. To transfer electrons from one metal to the other, it is necessary for the electrons in the vicinity of the Fermi level to overcome the potential barrier known as the work function of the material. Typically, the work functions of metals are few electron volts (2–5 eV) and transfer of electrons at room temperature is forbidden. However, the metals brought in extremely close distance of the order of a few nanometres (usually less than 10 nm) behave differently. Electrons can be transferred from one metal to the other to establish a common Fermi level without going over the potential barrier, set by the work function. At short distance of few nanometres, the wavefunctions of electrons from either side decay into the other metal. In other words, electrons can 'tunnel' from one metal to the other to occupy state of lower energy. This causes Fermi levels of the two metals to coincide with a small 'contact potential'. This reduces the barrier heights but changes are still small and barriers are sufficiently large for electrons to overcome them. Once the Fermi levels coincide, the electrons cannot flow from one metal to the other. However, by raising the Fermi level of one metal with respect to the other, electrons can tunnel from one metal to the other.

The energy required by electrons to overcome the energy barrier is still very high and not obtained by applying the potential, but electrons can tunnel. The tunneling probability or current

depends upon the availability of the empty states in metal in which electrons flow (density of empty states) and distance between the two metals. Fermi level positions can be altered by applying a small voltage between the two metals. The metal (M1) which is connected to the negative terminal of the power supply has raised Fermi level with respect to the other metal (M2) whose Fermi level is lowered. The tip potential is made negative, therefore its Fermi level is raised and current flows from tip to the sample. Indeed it is possible to raise Fermi level of sample higher than the tip, so that electrons flow from sample to the tip. It is then quite obvious that by lowering the sample with respect to the tip and measuring the current flowing towards the sample, we are able to probe unoccupied states or empty energy levels of the sample. If the sample Fermi level is at higher level, electrons below Fermi level flow to the tip. Therefore, one can know about occupied states in the sample. Thus, STM is capable of performing even spectroscopy of occupied and unoccupied levels.

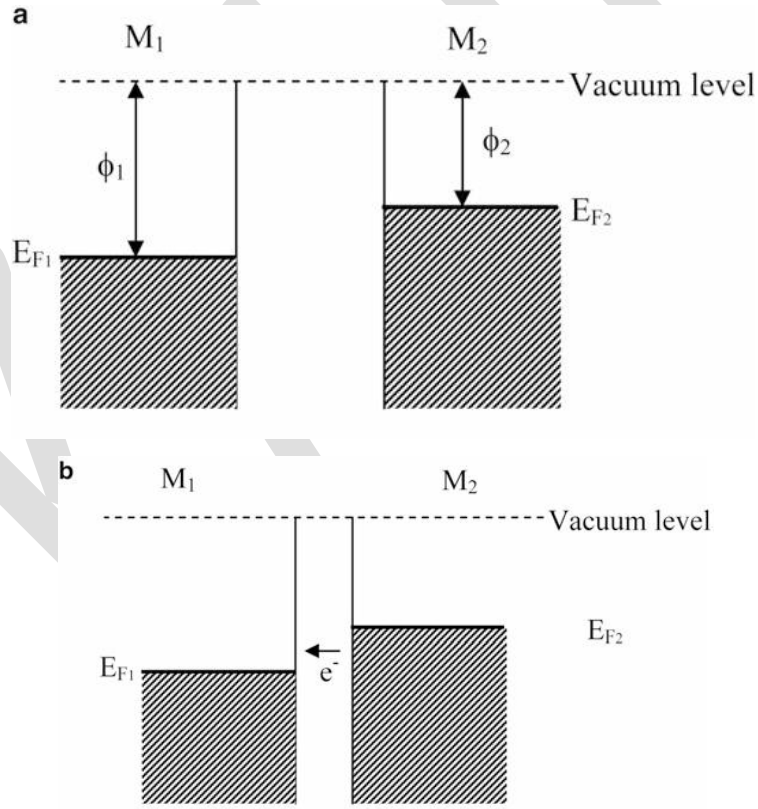

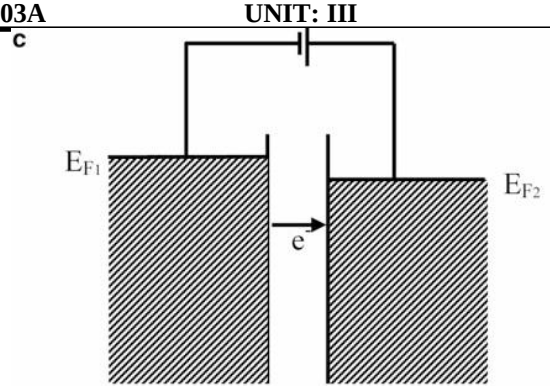

Fig. Tunnelling of electrons from one metal to other. (**a**) Metals are at small distance, but not less than 10 nm. (**b**) Metals are in close contact with each other, at a distance less than 10 nm. (**c**) Potential is applied between two metals

An STM can be operated in two different modes viz.

1. Constant current mode
2. Constant height mode

Constant current mode: Probe in the form of a sharp metal tip is moved slowly on the sample surface so that the current between the tip and the sample remains constant. In order to maintain the constant current between the tip and the sample, distance between the tip and the atomic corrugations also needs to be kept constant. Thus the tip will have to follow the atom contours.

By successively scanning the desired sample area in a raster mode, profile of surface atoms can be generated as an image, which is really the movement of the tip or the probe in an attempt to keep constant current between the sample and the tip, controlled by a proper feed-back loop. This is known as constant current mode.

Constant height mode: Alternatively, the tip can be moved on the sample surface at a constant height (typically >0.5 nm), between current and the distance, a surface profile can be generated from the variations observed in the tunnel current. Thus the image is the replica of the variation of current as the tip scans the desired area of the sample surface. Advantage of the constant height mode as compared to the constant current mode is that the tip can be moved faster on the sample surface, as there is no necessity of the feed-back circuit. Besides it is dangerous to move the tip close to the sample in constant current mode, as that can occasionally hit some rough hillocks of the sample and get destroyed. This is avoided in the constant height

mode and tip can be moved faster. However this would be at the cost of better sensitivity in the constant current mode.

Major limitation of STM is that the tunnelling current has to flow between the sample and the probe. Although the current is very small (of pico ampere order), it can be detected. However, in case of insulating samples, even this much current is not possible.

Atomic force microscopy

Atomic force microscopy is arguably the most versatile and powerful microscopy technology for studying samples at nanoscale. It is versatile because an atomic force microscope can not only image in three-dimensional topography, but it also provides various types of surface measurements to the needs of scientists and engineers. It is powerful because an AFM can generate images at atomic resolution with angstrom scale resolution height information, with minimum sample preparation.

Surface Sensing

An AFM uses a cantilever with a very sharp tip to scan over a sample surface. As the tip approaches the surface, the close-range, attractive force between the surface and the tip cause the cantilever to deflect towards the surface. However, as the cantilever is brought even closer to the surface, such that the tip makes contact with it, increasingly repulsive force takes over and causes the cantilever to deflect away from the surface.

Detection Method

A laser beam is used to detect cantilever deflections towards or away from the surface. By reflecting an incident beam off the flat top of the cantilever, any cantilever deflection will cause slight changes in the direction of the reflected beam. A position-sensitive photo diode (PSPD) can be used to track these changes. Thus, if an AFM tip passes over a raised surface

feature, the resulting cantilever deflection (and the subsequent change in direction of reflected beam) is recorded by the PSPD.

Imaging

An AFM images the topography of a sample surface by scanning the cantilever over a region of interest. The raised and lowered features on the sample surface influence the deflection of the cantilever, which is monitored by the PSPD. By using a feedback loop to control the

height of the tip above the surface—thus maintaining constant laser position—the AFM can generate an accurate topographic map of the surface features.

An AFM can be operated in three different modes viz. (1) Contact mode, (2) Noncontact mode and (3) Tapping mode.

Contact mode: In this case, the tip is in contact with the sample surface and is almost forced into it. However due to repulsive interaction between electron charge cloud of the tip atom and that of the surface atom, the tip is repelled back which bends the cantilever and deviates athe direction of the laser beam. In this mode the interaction due to the first term on right hand side of Eq. (7.7) is dominant due to very small value of '*R*', the distance between two atoms. The main disadvantage of this mode is that the tip or sample can get damaged due to forcing of the tip into sample, especially, polymers or other organic materials like biological samples which can get damaged by this method.

Non-contact mode: In non-contact mode, the tip or the probe moves at some small distance away from the sample surface. Therefore, it cannot damage the sample. This term arises due to polarization of interacting atoms and is due to dipole-dipole.

Tapping mode: Tapping mode is a combination of contact and non-contact modes. The resolution in contact mode is higher than that due to non-contact mode, because in contact mode the interaction between tip and surface atoms is much more sensitive to the distance as compared to that in non-contact mode. With tapping mode, high resolution advantage of contact mode and non-destructiveness of noncontact mode are achieved. The tip is oscillated in the vicinity of the surface at a distance of _50 nm in such a way that it nearly touches the sample during its cycle of oscillation. Tapping mode is simple and robust to use.

Fourier Transform Infra Red Spectrometer

Fourier Transform Infra Red (FTIR) spectrometer makes use of the Michelson interferometer for recording the spectra. Infra red rays falls on the beam splitter BS.

IR source and detector are similar to those used in dispersive type IR spectrometer. Part of the beam falls on a movable (0–1 cm) mirror M1 and a fixed mirror M2.

The rays are reflected back from both the mirrors along the same path and interfere at BS. A part of this combined beam falls on the sample and the detector. Constructive and destructive interference occurring at BS depends upon the path length of the rays. A white beam i.e. the

beam containing a broad continuous spectrum of wavelengths produces constructive and destructive interference pattern of every wavelength with all others.

The recombined beam passing through the sample produces absorption spectrum in which certain characteristic frequencies are absorbed by molecules present in the sample. With modern computers, it is quite an easy job to carry out a Fourier Transform. Detector collects, for example, signal from sample every millisecond and stores each spectrum in different locations. Spectra are then Fourier transformed and resultant spectra are obtained as an output. Thus, spectra can be generated very fast and Fourier Transform also is very fast. Thus better and fast data acquisition is possible using an FTIR spectrometer. Hence most of the modern commercial infrared spectrometers are FTIR spectrometers.

Sample Preparation

Sample preparation is a difficult task in IR range as there is no transparent material for cuvettes. Alkali halides (such as NaCl, KBr) are usually used which are transparent even at longer wavelengths. Powder samples are mixed with alkali halides and pressed in the sample holder. For liquid samples, there are single crystals of KBr or NaCl and liquid is sandwiched between the two. But in this case one cannot use aqueous solutions because alkali halides are soluble in water. For such samples silver chloride is used. One can use Teflon also but it shows absorption bands for C-C and C-F. For frequencies less than 600 cm^{-1} one can use polyethylene cell also.

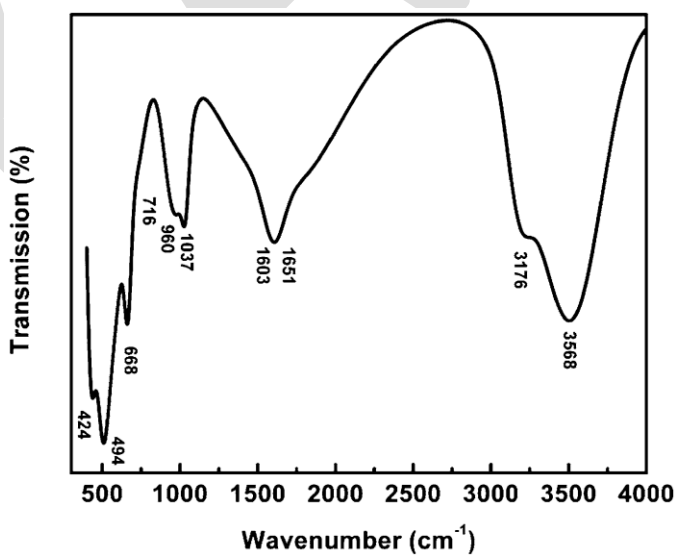

FTIR of TiO_2, suggesting vibrations due to TiO_6 octahedron and adsorbed hydroxyl group (3,568 cm^{-1})

KARPAGAM ACADEMY OF HIGHER EDUCATION

Coimbatore-641021.

(For the candidates admitted from 2016 onwards)

DEPARTMENT OF PHYSICS

UNIT III (Objective Type/Multiple choice Questions each Questions carry one Mark)

NANOMATERIALS AND APPLICATIONS

PART –A(Online Examination)

S.No.	QUESTIONS	opt1	opt2	opt3	opt4	ANSWER
1	The full form of STM is...	Scanning Tunneling Microscope	Scientific Technical Microscope	Systematic Technical Microscope	Super Tensile Microscope	Scanning Tunneling Microscope
2	What does 'F' stand for in AFM?	Fine	Front	Force	Flux	Force
3	X-rays have larger wavelengths than which of the following?	Gamma rays	Beta rays	Microwave	Visible light	Gamma rays
4	X-ray diffraction patterns are used for studying crystal structure of solids because	They have very high energy, hence they can penetrate through solids	They are electromagnetic radiation, and hence do not interact with matter (crystals)	Their wavelengths are comparable to inter-atomic distances	Their high frequency enables rapid analysis	Their wavelengths are comparable to inter-atomic distances
5	For destructive interference to take place, the path difference between the two waves should be:	$n\lambda$	$2n\lambda$	$(n + 1/2)\lambda$	$(2n + 1)\lambda$	$n\lambda$
6	Minimum interplanar spacing required for Bragg's diffraction is:	$\lambda/4$	$\lambda/2$	λ	2λ	$\lambda/2$
7	In Bragg's equation [$n\lambda = 2.d.\sin\theta$], θ is the angle between:	specimen surface and incident rays	normal to specimen surface and incident rays	parallel lattice surfaces d distance apart	normal to parallel lattice surfaces d	parallel lattice surfaces d distance apart

				and incident rays	distance apart and incident rays	and incident rays
8	In the powder method of XRD, the intensities of various bright lines are compared to determine the crystal structure. For simple cubic lattice the ratio of intensities at first two maxima are:	1⁄2	3⁄4	1⁄4	1	1⁄2
9	X-ray diffractometers are not used to identify the physical properties of which of the following?	Metals	Liquids	Polymeric materials	Solids	Liquids
10	X-ray diffractometers provide _____ information about the compounds present in a solid sample.	Quantitative	Qualitative	Quantitative and qualitative	Either quantitative or qualitative	Quantitative and qualitative
11	Using powder method of diffractometers, which of the following can be determined?	Percentage of K+	Percentage of Na+ and Cl-	Percentage of KBr and NaCl	Percentage of Br-	Percentage of KBr and NaCl
12	In powder method, the powder sample is contained in which of the following?	Thin walled glass capillary tubes	Thin walled test tube	Thin walled curvettes	Thin walled flask	Thin walled glass capillary tubes
13	Which of the following is the most common instrument for photographic recording of diffraction patterns?	Debye-Scherrer powder camera	Gamma camera	Geiger tube	Scintillation counter	Debye-Scherrer powder camera
14	With the help of which of the following equations is the distance calculated from known wavelength of the source and measured angle?	Coolidge equation	Bragg's equation	Debye equation	Scherrer equation	Bragg's equation
15	In Diffractometer, the identification of a component of the sample from its powder diffraction pattern is based upon the _____ of lines and their relative _____.	Number, length	Number, intensity	Position, length	Position, intensity	Position, intensity
16	Diffractometers are similar to which of the following?	Optical grating spectrometer	Prism spectrometer	Photo multiplier	Photovoltaic cell	Optical grating spectrometer
17	In Diffractometers, line intensities depend on _____ and kind of atomic reflection centres in each set of plates.	Number	Position	Length	Distance between lines	Number
18	In powder diffractometer, the sharpness of the lines is greatly determined by which of the	Quality of the sample, size of the	Quality of the slit, size of the sample	Thickness of the slit, amount of	Number of slits,	Quality of the slit, size of the

	following?	slit		the sample	composition of the sample	sample
19	X-Rays are	magnetic radiation	electric radiation	electromagnetic radiations	chemical radiations	electromagnetic radiations
20	Kind of electron microscope which is used to study internal structure of cells is	scanning electron microscope	transmission electron microscope	light microscope	compound microscope	transmission electron microscope
21	Electrons of Scanning Electron Microscope are reflected through	glass funnel	specimen	metal-coated surfaces	vacuum chamber	metal-coated surfaces
22	Magnification of light microscope is	1500X	2000X	1000X	2500X	1500X
23	Photograph which is taken from microscope is known as	macrograph	monograph	micrograph	pictograph	micrograph
24	Object can be magnified under electron microscope about	350, 000 times	250, 000 times	300, 000 times	450, 000 times	300, 000 times
25	Which of the following is used in electron microscope?	electron beams	magnetic fields	light waves	electron beams and magnetic fields	electron beams and magnetic fields
26	Electron Microscope can give a magnification up to _____	400,000X	100,000X	15000X	100X	400,000X
27	Which of the following are true for electron microscopy?	specimen should be thin and dry	image is obtained on a phosphorescent screen	electron beam must pass through evacuated chamber	specimen should be thin and dry, image is obtained on a phosphorescent screen and electron beam must pass through evacuated chamber	specimen should be thin and dry, image is obtained on a phosphorescent screen and electron beam must pass through evacuated chamber
28	Degree of scattering in transmission electron microscope is a function of _____	wavelength of electron beam used	number of atoms that lie in the	number and mass of atoms	mass of atoms that lie in the	number and mass of atoms

			electron path	that lie in the electron path	electron path	that lie in the electron path
29	Which among the following helps us in getting a three-dimensional picture of the specimen?	Transmission Electron Microscope	Scanning Electron Microscope	Compound Microscope	Simple Microscope	Scanning Electron Microscope
30	The secondary electrons radiated back in scanning microscope is collected by?	specimen	anode	vacuum chamber	cathode	anode
31	On what factors do the intensity of secondary electrons depends upon?	shape of the irradiated object	chemical composition of the irradiated object	number of electrons ejected	size and chemical composition of the irradiated object, number of electrons ejected and on the number of electrons reabsorbed by surrounding	size and chemical composition of the irradiated object, number of electrons ejected and on the number of electrons reabsorbed by surrounding
32	Where do we obtain the magnified image of the specimen in SEM?	cathode ray tube	phosphorescent screen	anode	scanning generator	cathode ray tube
33	Which of the following techniques are used in Transmission Electron Microscopy (TEM) for examining cellular structure?	Negative-Staining	Shadow Casting	Ultrathin Sectioning	Negative-Staining, Shadow Casting, Ultrathin Sectioning, Freeze-Etching	Negative-Staining, Shadow Casting, Ultrathin Sectioning, Freeze-Etching
34	In Electron microscope, light source is replaced by a beam of very fast moving	electron	neutron	proton	photon	electron
35	Electrons are sub-atomic particles that rule outer part of the	photon	particle	atom	molecule	atom
36	When maintaining the microscope what is used to clean the lenses?	Oil	Water	Alcohol	Detergent	Alcohol
37	What device is used to test the optics of the high	Stage magnometer	Stage micrometer		Glass slide	Stage

	power lens			Haemocytometer		micrometer
38	When maintaining the microscope, which is NOT an essential step?	Clean off grease and spills	Blow away dust	Oil the mechanics and moving parts	Wash the base and arm	Wash the base and arm
39	Which of the following components on a light microscope should be focused first?	The two eye pieces	Objective lenses	Condenser	Revolving nosepiece	The two eye pieces
40	Which of these objectives should be used to first view the specimen?	X10	X40	X4	X100	X4
41	What is the correct name for the main microscope lens that focuses the image?	Ocular	Binocular	Objective	Condenser	Objective
42	What is the correct name for the microscope lens located in the eyepiece?	Ocular	Binocular	Objective	Condenser	Ocular
43	If the eyepiece magnification on light microscope is x10 and the objective is x40, what is the overall magnification?	x10	x40	x400	x4	x400
44	Kind of electron microscope which is used to study internal structure of cells is	scanning electron microscope	transmission electron microscope	light microscope	compound microscope	transmission electron microscope
45	Electrons of Scanning Electron Microscope are reflected through	glass funnel	specimen	metal-coated surfaces	vacuum chamber	metal-coated surfaces
46	Object can be magnified under electron microscope about	350, 000 times	250, 000 times	300, 000 times	450, 000 times	300, 000 times
47	How is the wavelength controlled in an FTIR spectrometer?	By a Michelson Interferometer	By a computer	By a laser	By calibration with a standard sample	By a laser
48	What type of technique is FTIR spectroscopy?	A dispersive technique?	An emission technique	An absorbance technique	A UV-Vis technique	An absorbance technique
49	What does the spectrum of Nitrogen(N2) look like?	The same as that of air	It has only p- and r-branches	The same as that of carbon monoxide	It doesn't have one!	It doesn't have one!
50	What occurs when the moving mirror in an FTIR spectrometer is the same distance from the beamsplitter as the static mirror?	Constructive interference	Destructive interference	Radio interference	The spectrum is measured	Constructive interference

51	In what region of the spectrum does infrared radiation occur?	At the low-energy end	Between the visible and ultraviolet regions	Between the visible and microwave regions	Between the visible and x-ray regions	Between the visible and microwave regions
52	What occurs when a molecule absorbs infrared radiation?	It warms up	It flies around	It spins faster	It vibrates faster	It vibrates faster
53	Which of the following is not true about Fourier Transform Infrared (FTIR) spectrometer?	It is of non-dispersive type	It is useful where repetitive analysis is required	Size has been reduced over the years	Size has increased over the years	Size has increased over the years
54	Which of the following is not the advantage of Fourier Transform Spectrometers?	Signal to noise ratio is high	Information could be obtained on all frequencies	Retrieval of data is possible	Easy to maintain	Easy to maintain
55	In which region of the electromagnetic spectrum does an absorption at 600 nm come?	Vacuum-UV	Visible	near UV	infrared	Visible
56	What is a red shift?	The shifting of an absorption towards the blue end of the spectrum	The shifting of an absorption to higher energy.	The shifting of an absorption to lower energy	The shifting of an absorption to shorter wavelength	The shifting of an absorption to lower energy
57	Why is the computer necessary in Fourier Transform Spectrometer?	To display the detector output	To process the detector output	To determine the amplitude	To determine the frequency	To process the detector output
58	What is the wavelength range for UV spectrum of light?	400 nm – 700 nm	700 nm to 1 mm	0.01 nm to 10 nm	10 nm to 400 nm	10 nm to 400 nm
59	Which of the following has to be computed to determine transmittance and absorbance at various frequencies?	Ratio of signal and noise	Ratio of sample and reference spectra	Sample spectra	Reference spectra	Ratio of sample and reference spectra

UNIT-IV

Optical Properties: Coulomb interaction in nanostructures. Concept of dielectric constant for nanostructures and charging of nanostructure. Quasi-particles and excitons. Excitons in direct and indirect band gap semiconductor nanocrystals. Quantitative treatment of quasi-particles and excitons, charging effects. Radiative processes: General formalization-absorption, emission and luminescence. Optical properties of heterostrctures and nanostructures.

COULOMB INTERACTION IN NANOSTRUCTURES

Coulomb Interactions in a Dielectric Quantum Well

Consider A charge q is at point O, at a distance z from the planar interface between two dielectrics 1 and 2, with relative dielectric constants ε_1 and ε_2, respectively. The charge q is in region 1. The discontinuity of the dielectric constant induces polarization charges at the interface.

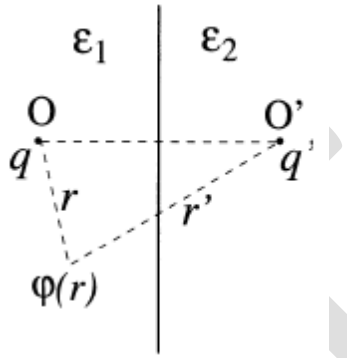

Fig 1: Charge q at distance z from the interface between two dielectrics

Following a well-known approach, the potential in region 1 can be written as the potential created by two charges in an homogeneous medium of dielectric constant ε_1 the charge q, and a fictitious charge q' sitting at the point O', the image of the point O with respect to the interface. Thus, we have

$$\varphi_1(\boldsymbol{r}) = \frac{q}{4\pi\epsilon_1\epsilon_0 r} + \frac{q'}{4\pi\epsilon_1\epsilon_0 r'} \text{ ---------- (1)}$$

where r and r' are the respective distances from the points O and O'. The potential in region 2 is written as the potential due to a fictitious charge q'' at the point O, in an homogeneous medium of dielectric constant ε_2:

$$\varphi_2(\boldsymbol{r}) = \frac{q''}{4\pi\epsilon_2\epsilon_0 r} \text{ ---------- (2)}$$

Using the boundary conditions on the electric field at the interface, we have

$$q' = q\frac{\epsilon_1 - \epsilon_2}{\epsilon_1 + \epsilon_2}$$
$$q'' = q\frac{2\epsilon_2}{\epsilon_1 + \epsilon_2} \text{ ---------- (3)}$$

From these expressions and the electrostatic self-energy of the charge q is:

$$\Sigma(z) = \frac{qq'}{16\pi\epsilon_1\epsilon_0 z} = \frac{q^2}{4z}\,\frac{\epsilon_1 - \epsilon_2}{4\pi\epsilon_1\epsilon_0(\epsilon_1 + \epsilon_2)} \text{ ---------- (4)}$$

Figure 2 shows the self-energy of an electron as function of the distance z, in the case $\varepsilon_1 = 10$ and $\varepsilon_2 = 1$. The self-energy is quite substantial at distances in the nanometre range. The electrostatic self-energy of particles cannot be neglected in nanostructures with large dielectric mismatch.

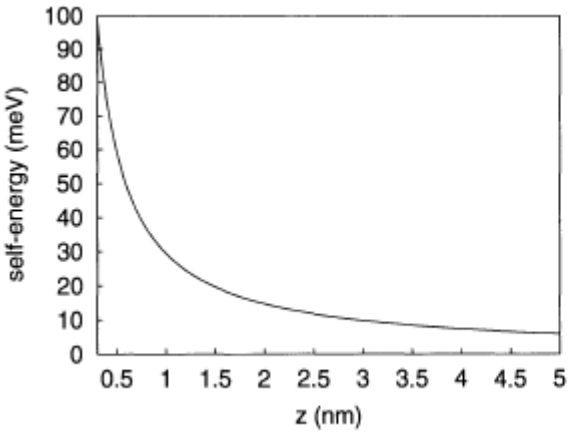

Fig. 2. Electrostatic self-energy of an electron or a hole in a material of dielectric constant $\epsilon_1 = 10$ at a distance z from the interface with a material of dielectric constant $\epsilon_2 = 1$

Image Charge Method for a Dielectric Quantum Well

Consider the problem of a charge q located at the point (r_{ll} = 0, z_o), in a semiconductor quantum well. L is the thickness of the well, and the z axis is perpendicular to the interfaces. A schematic structure is shown in Fig 3. The well, with a dielectric constant ε_1, is sandwiched by barrier layers having a different dielectric constant ε_2. The potential is calculated using the image charge method, following closely. Due to the presence of the two interfaces, there is an infinite series of image charges. The potential in the well is given by regarding the whole structure as having a common dielectric constant ε_1, and by placing image charges q_n at the positions:

$$z_n = nL + (-1)^n z_0, \; n = \pm 1, \pm 2 \ldots \; . \quad \text{---------- (5)}$$

The potential in the left-hand-side barrier layer is given by placing image charges q_n' at Z_n , n = 0, 1, 2 ... and the potential in the right-hand-side barrier layer by placing image charges q_n'' at Zn, n = 0, -1, -2 .... In both cases, the whole structure is seen as having a common dielectric constant ε_2. Using the boundary conditions on the electric field at the interfaces, we have:

$$q_n = q\gamma^{|n|} \; , \quad \gamma = \left(\frac{\epsilon_1 - \epsilon_2}{\epsilon_1 + \epsilon_2}\right)$$

$$q_n' = q_n'' = q_n \frac{2\epsilon_2}{\epsilon_1 + \epsilon_2} \; . \quad \text{---------- (6)}$$

Thus, the potential in the well, at a position (r_{ll}, z), is given by:

$$\varphi(\boldsymbol{r}_{\parallel}, z) = \sum_{n=-\infty}^{\infty} \frac{q\gamma^{|n|}}{4\pi\epsilon_0\epsilon_1\{r_{\parallel}^2 + [z - (-1)^n z_0 - nL]^2\}^{1/2}} \quad \text{---------- (7)}$$

A physically interesting limit is obtained when $r_{\parallel} \gg (\varepsilon_1/\varepsilon_2)L$:

$$\varphi(\boldsymbol{r}_{\parallel}, z) \approx \frac{q}{4\pi\epsilon_0\epsilon_2 r_{\parallel}} \quad \text{---------- (8)}$$

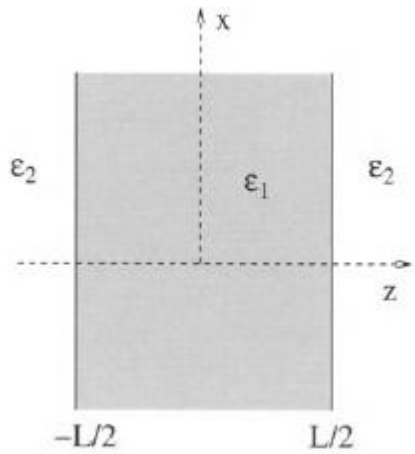

Schematic structure of dielectric quantum well

Thus, if the semiconductor quantum well is sandwiched between insulators or semiconductors with a small dielectric constant ε_2, the long-range Coulomb interactions are strongly enhanced compared to the bulk case. This effect, first pointed out by Keldysh, is due to the penetration of the electric field into the barrier with a small dielectric constant. This effect has important consequences, such as the enhancement of the exciton binding energy of the excitonic oscillator strength, and of the electron-electron interactions.

The self-energy of a charge q located at the point ($r_{\parallel}$, z) does not depend on $r_{\parallel}$:

$$\Sigma(z) = \frac{1}{2} \sum_{n=\pm1,\pm2\ldots} \frac{q^2\gamma^{|n|}}{4\pi\epsilon_0\epsilon_1|z - (-1)^n z - nL|} \quad \text{---------- (9)}$$

This self-energy diverges at the interface. To remedy this divergence, shifted mirror faces are sometimes employed for the lowest order (n = ±1) image charges.

Coulomb Interactions in Dielectric Quantum Dots

We consider Coulomb interactions in a spherical semiconductor quantum dot, where simple analytical results can be obtained. A schematic structure is shown in Fig. 4. The dot, of radius R and dielectric constant ε_{in}, is surrounded by a medium of dielectric constant ε_{out}. The potential energy V(r, r') of a charge q located at r induced by a charge q' at r' is given by

$$V(\boldsymbol{r},\boldsymbol{r}') = V_{\mathrm{b}}(\boldsymbol{r},\boldsymbol{r}') + \delta V(\boldsymbol{r},\boldsymbol{r}') \text{ ---------- (10)}$$

Where

$$V_{\mathrm{b}}(\boldsymbol{r},\boldsymbol{r}') = \frac{qq'}{4\pi\epsilon_{\mathrm{in}}\epsilon_0|\boldsymbol{r}-\boldsymbol{r}'|},$$

$$\delta V(\boldsymbol{r},\boldsymbol{r}') = qq'\sum_{n=0}^{\infty}\frac{(\epsilon_{\mathrm{in}}-\epsilon_{\mathrm{out}})(n+1)r^n r'^n P_n(\cos(\theta))}{4\pi\epsilon_0\epsilon_{\mathrm{in}}[\epsilon_{\mathrm{out}}+n(\epsilon_{\mathrm{in}}+\epsilon_{\mathrm{out}})]R^{2n+1}} \text{ ---------- (11)}$$

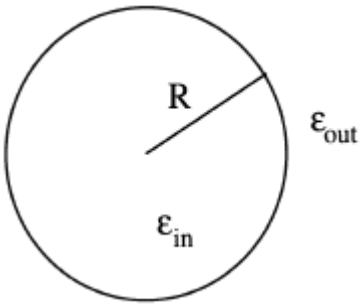

Fig 4: Schematic structure of dielectric quantum dot

θ is the angle between the two vectors r and r ' , and P_n the nth Legendre polynomial. In the particular case where a charge q is at the center of the dot, the electrostatic potential in the dot is given by

$$\varphi(\boldsymbol{r}) = \frac{q}{4\pi\epsilon_0}\left[\frac{1}{\epsilon_{\mathrm{in}}r} - \frac{1}{R}\left(\frac{1}{\epsilon_{\mathrm{in}}} - \frac{1}{\epsilon_{\mathrm{out}}}\right)\right] \text{ ---------- (12)}$$

The second term in the bracket is due to the polarization charge at the surface of the quantum dot. When ε_{out} «ε_{in} , this constant term becomes the main contribution of the potential in a large part of the dot. We know that it explains the large binding energy of donor and acceptor impurities in quantum dots.

The self-energy of a charge q in the dot is given by

$$\Sigma(\boldsymbol{r}) = \frac{1}{2}\delta V(\boldsymbol{r},\boldsymbol{r}) \text{ ---------- (13)}$$

with q' = q.

At the end of the chapter, we will use this formula to calculate the charging energy of an electron or a hole in a quantum dot.

CONCEPT OF DIELECTRIC CONSTANT FOR NANOSTRUCTURES:

The dielectric properties of a system are described by $\varepsilon^{-1}(r,r')$. From this, in a bulk semiconductor, we can deduce directly the macroscopic dielectric constant $\varepsilon_M(q)$ which contains most of the useful information on the dielectric screening. We can wonder if this macroscopic treatment is possible in semiconductor nanostructures and if it remains meaningful. This important question was addressed in different works. In this section, we explain why macroscopic quantities for nanostructures cannot be deduced from $\varepsilon^{-1}(r,r')$ as simply as in the bulk case. We show that a physically meaningful macroscopic dielectric constant must be derived taking into account explicitly the polarization charges at the surfaces or interfaces. Using this prescription, we demonstrate that the macroscopic response is the bulk one a few Fermi wavelengths away from the surface and that the bulk response function $\varepsilon_M(q)$ provides most of the needed information even for very small nanostructures. We also show that the average dielectric constant ε_{ave}in spherical clusters decreases when going to small radius R and we discuss the origin of this size dependence. At the end of this section, we prove that all these conclusions mostly based on microscopic tight binding calculations of the dielectric response in Si quantum wells and dots are in fact completely general for semiconductor nanostructures.

General Arguments on the Dielectric Response in Nanostructures:

An important issue is to know how the previous results can be generalized. We have seen that the dielectric response is the bulk one at typically a few interatomic distance from boundaries. This seems to contradict the general belief that screening becomes less effective in nanocrystals due to the opening of the gap. Indeed, the independent particle polarization χ^0 and is given by a sum of terms which behave like $1/(\varepsilon_i - \varepsilon_j)$where $\varepsilon_i$and ε_j are the energies of the unoccupied and occupied states, respectively. Thus, we have calculated the matrix element χ^0_{nm} of the polarization between two firstnearest neighbour atoms at the center of Si nanocrystals. We plot in Fig. χ^0_{nm}/χ^0_{nm} (bulk) and E_g/E_g(bulk) versus size,,E_g(bulk) and χ^0_{nm} (bulk) being the bulk values. The main result is that the polarization is almost independent of the size, and is not at alI related to the variation of the gap E_g. Similar results are obtained for InAs nanocrystals and for Si quantum welIs as shown on the same figure. χ^0_{nm} is not sensitive to the shift of the band edges induced by the confinement but to the average distance in energy between filled and empty states which remains constant versus size.

Therefore bulk parameters are still pertinent even for very small nanostructures. The decrease of $\varepsilon_{ave}$with size is due to a surface contribution, i.e. to the breaking of polarizable

bonds at the surface. Thus we can now generalize the results by applying the important theorem due to von Laue. This one states that the electron density recovers its bulk value at distances from boundaries of the order of a few Fermi wave-lengths λ_Fi.e. typicalIy the inter-atomic distance. This means that the response function is the bulk one inside a nanocrystal as long as its characteristic size exceeds a

fewλ_F.

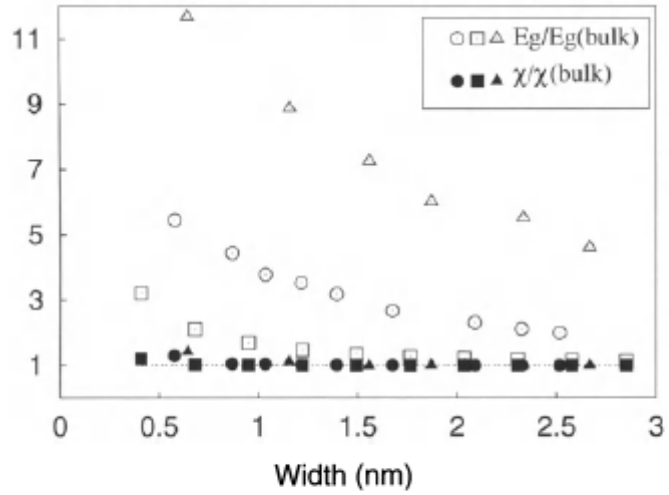

Fig. Ratio of the nearest neighbor inter-atomic polarization χ^0_{nm} and of the bulk value χ^0_{nm}(bulk) at the center of Si layers (*square*), Si spheres (*circle*) and InAs spheres (*triangle*) versus size compared to the ratio of the nanostructure gap and the bulk value

The previous results also apply to the electronic part of the dielectric screening in nanostructures of polar materials (e.g. III- V and II- VI semiconductors). For example, the same kind of calculations have been performed on InAs nanocrystals. Because InAs is a slightly ionic material, the dielectric constant is the sum of two contributions, electronic and ionic:

$$\varepsilon_{ave} = \varepsilon^{el}_{ave} + \varepsilon^{ion}_{ave}$$

Since the ionic contribution comes from the displacement of the ions with respect to their equilibrium position under the application of an external field, it is assumed to be weakly dependent on the crystallite size. The size dependence of the average ε^{el}_{ave} in InAs nanocrystals is shown in Fig.

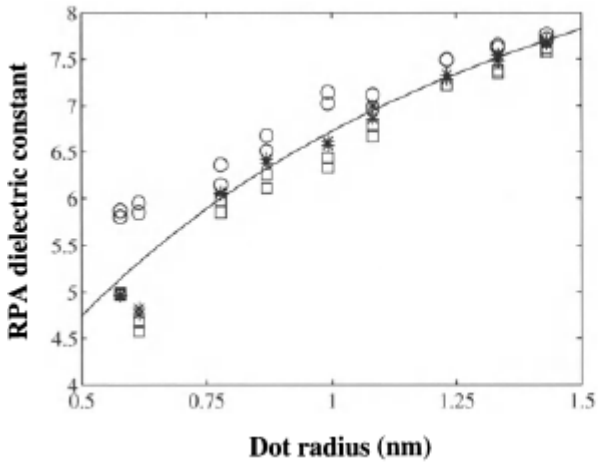

Fig. Electronic contribution to the average dielectric constant in InAs quantum dots. Fit (*straight line*) of these values ($\epsilon^{el}_{ave} = 1 + \frac{\epsilon^{el}_M - 1}{1+(0.79/R)^{1.15}}$) where ϵ^{el}_M is the bulk value and R is the radius in nanometer

The screening properties of semiconductor nanostructures:

- a physically meaningful definition of the local macroscopic dielectric constant in a nanostructure must incorporate the effect of the polarization charges at the boundaries
- the macroscopic dielectric response is the bulk one a few Fermi wavelengths away from the boundaries
- the dielectric response of a semiconductor nanostructure can be fairly well described using the macroscopic wave-vector dependent dielectric constant $E_M(q)$
- the local dielectric constant decreases near the boundaries due to the breaking of polarizable bonds
- the average dielectric constant decreases with decreasing size of the nanostructure due to the increasing contribution of the surfaces
- the opening of the bandgap due to the quantum confinement plays no role in these problems.

CHARING OF A NANOSTRUCTURE:

Case of a Quantum Dot

The level structure of crystallites has been obtained from semi-empirical calculations. Thus, we need to determine the corrections brought by the dielectric effects, due to the finite size of the system. We do this within a macroscopic electrostatic formulation. The self-energy of particles and Coulomb charging effects can be measured experimentally using tunnelling spectroscopy experiments, corresponding to the so-called Coulomb blockade effects.

Consider a spherical quantum dot of radius R and of macroscopic dielectric constant ,we will argue that the best value for ε_{in} is the bulk macroscopic dielectric constant ε_M in that case.

In the case of a strong confinement, we can obtain a fairly good estimationof the self-energy $\sum$ of an electron or a hole (q = ±e) injected in the quantum dot, using in a first-order perturbation theory. In the limit of an infinite potential barrier, the one-particle state is well-given by the effective mass solution:

$$\phi(\boldsymbol{r}) = \frac{1}{\sqrt{2\pi R}} \frac{\sin(\pi r/R)}{r} \quad \text{---------- (1)}$$

The self-energy $\sum$ is calculated .We show that a good approximation of $\sum$ is given by

$$\Sigma \approx \frac{e^2}{8\pi\epsilon_0 R} \frac{\epsilon_{\text{in}} - \epsilon_{\text{out}}}{\epsilon_{\text{in}}\left[\epsilon_{\text{in}} + \epsilon_{\text{out}}\right]} \left(\frac{1}{\eta} + 0.933 - 0.376\eta\right) \quad \text{---------- (2)}$$

Where $\eta = \varepsilon_{out}/(\varepsilon_{in} + \varepsilon_{out})$.When $\eta \ll 1$, which is the usual situation when the quantum dot is embedded in an oxide matrix or in a semiconductor with a large gap, the self-energy becomes

$$\Sigma = \frac{1}{2}\left(\frac{1}{\epsilon_{\text{out}}} - \frac{1}{\epsilon_{\text{in}}}\right) \frac{e^2}{4\pi\epsilon_0 R} + \delta\Sigma \quad \text{---------- (3)}$$

Where

$$\delta\Sigma \approx 0.466 \frac{e^2}{4\pi\epsilon_0 \epsilon_{\text{in}} R} \left(\frac{\epsilon_{\text{in}} - \epsilon_{\text{out}}}{\epsilon_{\text{in}} + \epsilon_{\text{out}}}\right) \quad \text{---------- (4)}$$

Where $\sum$ isgives the shift in energy of the extra electron (hole) in the lowest conduction (highest valence) state (Fig 1). The injection of a second electron (hole) leads to an additional upwards (downwards) shift U given by the screened repulsion with the other electron (hole) (Fig 1). With the same approximations as for $\sum$, U is given by

$$U = \int \phi(\boldsymbol{r})^2 \phi(\boldsymbol{r}')^2 V(\boldsymbol{r}, \boldsymbol{r}') \mathrm{d}\boldsymbol{r}\mathrm{d}\boldsymbol{r}' \quad \text{---------- (5)}$$

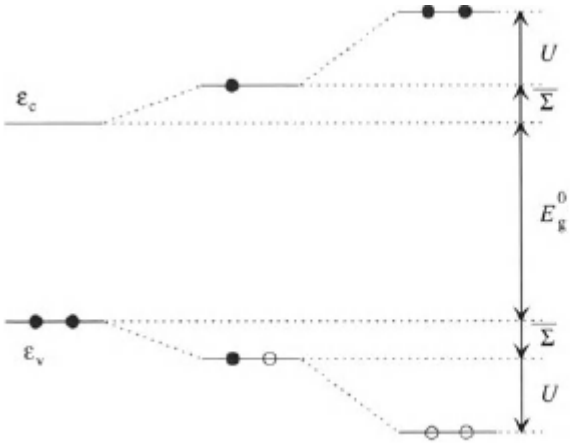

Fig. 1. Top: shift of the lowest conduction level due to the injection of one electron (Σ) or two electrons ($\Sigma + U$). Bottom: the situation for holes is symmetrical

Using the expression of V(r, r') with q = q' = e, U is the sum of two terms. The first one is given by the average repulsion with the other particle

$$e^2 \int \frac{\phi(\boldsymbol{r})^2 \phi(\boldsymbol{r}')^2}{4\pi\epsilon_{\text{in}}\epsilon_0 |\boldsymbol{r} - \boldsymbol{r}'|} \mathrm{d}\boldsymbol{r}\mathrm{d}\boldsymbol{r}' \approx 1.79 \frac{e^2}{4\pi\epsilon_0\epsilon_{\text{in}} R} \quad \text{---------- (6)}$$

and the second one by the average repulsion with the surface polarization charge induced by the other particle:

$$\int \phi(\boldsymbol{r})^2 \phi(\boldsymbol{r}')^2 \delta V(\boldsymbol{r}, \boldsymbol{r}') \mathrm{d}\boldsymbol{r}\mathrm{d}\boldsymbol{r}' \quad \text{---------- (7)}$$

The coefficient 1.79 in (6) was obtained numerically . In (7), only the term η = 0 in the expression of δV given and makes a nonzero contribution to the integral. Thus, we obtain:

$$U = \left(\frac{1}{\epsilon_{\text{out}}} + \frac{0.79}{\epsilon_{\text{in}}} \right) \frac{e^2}{4\pi\epsilon_0 R} \quad \text{---------- (8)}$$

In many situations, the surrounding of the quantum dots is not an homogeneous dielectric medium. Then, Poisson's and Schrodinger equations must be solved self-consistently to calculate the charging energy U. However, U must be necessarily between two bounds, corresponding to $\varepsilon_{out} = 1$ and $\varepsilon_{out} \rightarrow \infty$ in (8).

$$\frac{0.79}{\epsilon_{\text{in}}} \frac{e^2}{4\pi\epsilon_0 R} < U < \left(1 + \frac{0.79}{\epsilon_{\text{in}}} \right) \frac{e^2}{4\pi\epsilon_0 R} \quad \text{---------- (9)}$$

These relations are very useful, for example to interpret the I(V) characteristics of devices based on semiconductor quantum dots. Figure 2 shows the evolution of these two bounds for U in a Si nanocrystal, as function of its diameter. We see that the values of U can be very large when $\varepsilon_{out} = 1$, such that the injection of more than one carrier becomes difficult.

Each time another electron is injected in the nanocrystal, the conduction states exhibit an energy shift U which can be calculated according to (5), using the corresponding wave function. When ε_{out} « ε_{in} U does not depend too much on the details of the wave function because the dominant term in U

is the Coulomb interaction between the electron and its polarization charge at the surface. In that case, (8) remains a good approximation for a wide range of charge states.

In the case of a metallic nanostructure ($\varepsilon_{in} \rightarrow \infty$),(3),(4) and (7) give U = e^e/C and $\sum$ = U/2 as it must be for the charging of a metallic sphere of self-capacitance C = $4\pi\varepsilon_0\varepsilon_{out}$ R. Note that this capacitive model is often extended to the case of semiconductor quantum dots, even if it is not perfectly justified.

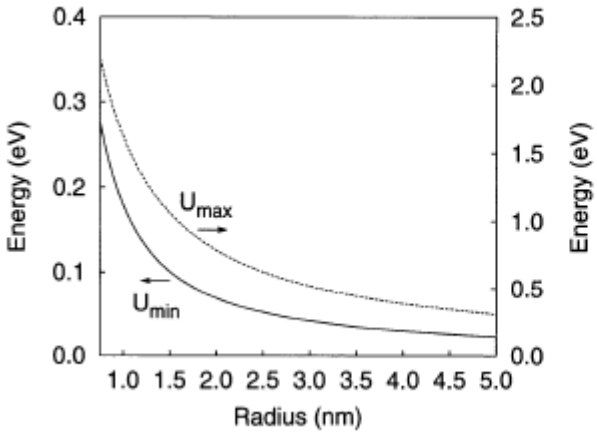

Fig. 2. Minimum and maximum value for the charging energy U in Si nanocrystals

Case of a Quantum Well

In the case of quantum wells, the charging energy U is vanishingly small, due to the infinite size of the system. Thus it remains to calculate the self-energy, following the same method as for the dots. For a quantum well of thickness L, the effective mass solution for the one-particle state is:

$$\phi(\boldsymbol{r}) = \sqrt{\frac{2}{L}}\cos(\pi z/L) \text{ for } -L/2 \leq z \leq L/2 \quad \text{---------- (1)}$$

$$\Sigma \approx \frac{q^2}{4\pi\epsilon_0\epsilon_1 L}\left[\sum_{n=2}^{\infty}\frac{\gamma^n}{n} + \gamma\int_{-1}^{1}\frac{\cos^2(\pi u/2)}{1-u^2}\mathrm{d}u\right] \quad \text{---------- (2)}$$

Where γ is defined and we have replaced $|z - (-1)^n z - nL|$ by $|n|L$ when $|n| \geq 3$, which is justified numerically. Calculating the integral numerically, we obtain:

$$\Sigma \approx \frac{q^2}{4\pi\epsilon_0\epsilon_1 L}\left[0.219\,\gamma - \ln(1-\gamma)\right] \quad \text{---------- (3)}$$

EXCITONS IN DIRECT BAND GAP SEMICONDUCTOR NANOCRYSTALS

Size-selective spectroscopic techniques such as resonant photoluminescence and photoluminescence excitation allow to get extremely detailed information on the lowest excitonic states of quantum dots or nanocrystals. This fine electronic structure is governed by the relative importance of different terms which constitute the Hamiltonian: confinement potential, spin orbit interaction, Coulomb and exchange interactions. Each of these termsdepends on quantum dot size in a different way. Two limiting situations can be considered: the weak confinement regime, when the dot size is larger than a few exciton radii and the strong confinement regime, when the quantum dot size is smaller than the exciton Bohr radius. Inthe latter regime, the confinement energy is much larger than the Coulomb interaction and both carriers are independently confined. However, even in this case, the Coulomb interaction exists since the electron and the hole are in a finite volume.

Tight binding configuration interaction calculations have been applied to the electronic structure of the lowest excitonic states in CdS nanocrystals with cubic lattice. Here, the nature of the predictions will be analysed in a simplified effective mass picture in order to identify clearly the evolution from bulk to quantum dots. Figure 1 summarizes this simple descriptionof excitons in CdS quantum dots. Apart from the confinement effect, there are two terms in the Hamiltonian of a quantum dot which mainly determine the size dependence of its excitonic structure: the spin--orbit interaction and the electron-hole exchange interaction. Matrix elements of the spin-orbit interaction are constant. However the matrix elements of the electron-hole exchange interaction increase as the nanocrystal radius decreases. To understand the size dependence of the splitting's between lowest exciton levels, one first considers two opposite limits: large and small dots.

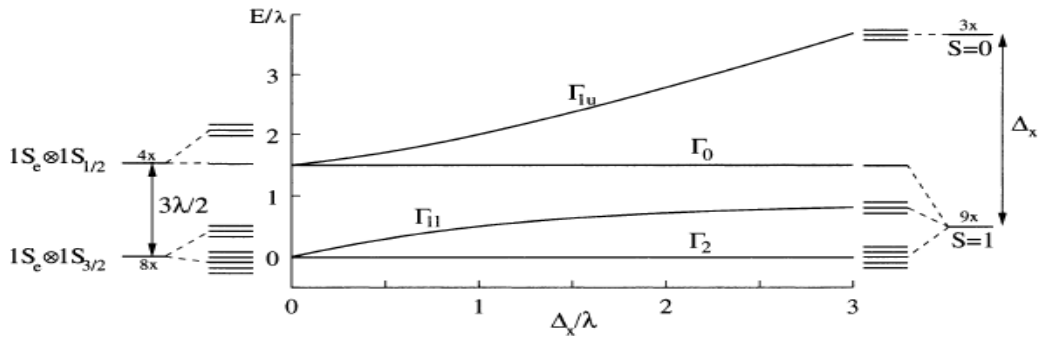

Fig. 1 Right and left: energy level diagrams describing the fine structure of the excitonic spectrum; middle: splitting between lowest energy levels of the exciton as a function of the electron–hole exchange interaction Δ_x which itself depends on quantum dot size. All the energies are in units of the spin–orbit coupling parameter λ

For large dots, the lowest states converge to the classical situation of the bulk CdS, namely light and heavy-hole excitons and the spin-orbit split exciton. In this situation, the electron-hole exchange interaction is negligible with respect to the spin-orbit interaction. In this limit, the effective mass approximation becomes a powerful tool to calculate the electronic structure of spherical nanocrystals. The first electron level is the lS_e state with twofold spin degeneracy and the first level of holes is the $lS_{3/2}$ state which is fourfold degenerate with respect to the hole angular momentum. The next hole level is $lS_{1/2}$ and its distance in energy from the $lS_{3/2}$ level is equal to $3\lambda/2$ where λ is the spin-orbit coupling parameter. Thus the lowest exciton state $lS_e \otimes 1S_3$ is eightfold degenerate and the next higher state $lS_e \otimes lS_{1/2}$ is fourfold degenerate. The introduction in a perturbation scheme of the electron-hole exchange interaction splits the $lS_e \otimes lS_{3/2}$ level into two groups of states. Since the total angular momentum J remains a good quantum number, the lowest exciton state, fivefold degenerate, is characterized by a momentum J = 2 and will be denoted hereafter Γ2 . The upper exciton state, threefold degenerate, corresponds to a momentum J = 1 and will be denoted Γ_{11}. In the effective mass approximation, the value of the splitting is related to the electron-hole exchange energy in the bulk (Δ_x^{bulk} = 0.23 meV in CdS) and is given by the following expression

$$\Delta_x = A\left(\frac{a}{R}\right)^3 \Delta_x^{bulk}$$

where a is the Bohr radius (~ 30 A^0 in CdS) and A is a constant which depends on the nature of the semiconductor. The 1/ R^3 scaling of Δ_x is a consequence of the effective mass approximation: more elaborate calculations based on empirical pseudopotentials predict exponents between 2 and 3 for InP and CdSe quantum dots (similar trends are obtained in

tight binding for Si nanocrystals; see next section).

The higher exciton state $lS_e \otimes lS_{1/2}$ is also split by the electron-hole exchange interaction into two groups of levels with J = O and J = 1, denoted $\Gamma_0$and Γ_{1u} , respectively.
In the opposite limit of small quantum dots (right side of Fig.1), the electron-hole exchange energy is larger than the spin-orbit interaction. The lowest exciton level, formed by an electron in s-like states and a hole in p-like states, is split by the exchange interaction into a lower triplet state (S = 1), ninefold degenerate, and an upper singlet state (S = 0), threefold degenerate. The introduction of the spin-orbit interaction in perturbation leads to thesplitting of the triplet exciton state into three states with J = 2, J = 1 and J = 0 (Γ_2 , $\Gamma_{11}$and Γ_0, respectively). The singlet state gives another J = 1 state (Γ_{1u}).

The intermediate case, when the electron-hole exchange interaction is comparable with the spin-orbit interaction, can be described by atomistic calculations like tight binding. Inthe simplified model described above, the Hamiltonian including exchange and spin-orbit interactions can be diagonalized in the basis of exciton states formed by the product of the s states for the electron and of the p states for the hole. It leads to the following expressions for the energy splitting's between the exciton states and the lowest state Γ_2.

$$E(\Gamma_{11}) - E(\Gamma_2) = \frac{3\lambda}{4} + \frac{\Delta_x}{2} - \sqrt{\left(\frac{\Delta_x}{6} - \frac{3\lambda}{4}\right)^2 + \frac{2\Delta_x^2}{9}},$$

$$E(\Gamma_{1u}) - E(\Gamma_2) = \frac{3\lambda}{4} + \frac{\Delta_x}{2} + \sqrt{\left(\frac{\Delta_x}{6} - \frac{3\lambda}{4}\right)^2 + \frac{2\Delta_x^2}{9}},$$

$$E(\Gamma_0) - E(\Gamma_2) = \frac{3\lambda}{2},$$

where Δ_x, the exchange term, is a function of the nanocrystal radius. Figure 1 (middle) shows the energy splitting's given by the above equation with respect to Δ_x/λ, i.e. as a function of size. The model explains qualitatively the evolution of the excitonic levels predicted by tight binding calculations that describe the photoluminescence excitation spectra measured on CdS nanocrystals. However, one must note that the excitonic structure is in fact more complex due the presence of hole states with slightly higher energy which are not included in the model.
This simple model also explains the probabilities of optical transitions. Inthe limit of small quantum dots where the exchange interaction is larger thanthe spin-orbit coupling, the optical transitions from the triplet (S = 1) derivedstates, i.e. Γ_2 , Γ_{11} and Γ_0, to the ground state are forbidden in the dipoleapproximation while those from the singlet state Γ_{1u} are allowed

(because thespin must be conserved in the transition). At increasing size, theexchange interaction decreases and the spin-orbit coupling mixes S = 0 andS = 1 states, with the important consequence that the transition from r u becomes optically allowed.

QUANTITATIVE TREATMENT OF QUASI-PARTICLES:

General arguments are developed based on the GW approach which are then substantiated numerically by a tight binding version of this theory. The gap correction is shown to be dominated by the macroscopic surface self-polarization term and exhibits a non-monotonic behaviour versus dimensionality. In the literature, most quantitative calculations deal with the eigenvalue gap ε_g^0determined from the difference in one-particle eigenvalues ε_c^0-$\varepsilon_v^0$for the neutral system. $\varepsilon_g^0$is obtained from empirical techniques (tight binding, pseudopotentials) or from ab initio calculations in LDA and, as we have seen, differs from $\varepsilon_g^{qp}$by large amounts $\delta\sum$ corresponding to self energy corrections. These can be estimated via the GW method derived but the corresponding computations are very time consuming and can be only applied to small systems]. Therefore simpler methods such as one-particle calculations are highly desirable but, as discussed above, their accuracy is a matter of controversies. In principle, the quasi-particle gap ε_g^{qp}can be calculated exactly in density functional theory (DFT) as

$$\varepsilon_g^{qp} = E(n+1) + E(n-1) - 2E(n) \quad \text{---------- (1)}$$

where E(n) is the total energy of the n-electrons neutral system obtained by solving the one-particle Kohn-Sham equations are written in terms of an effective exchange correlation potentialVxc . In LDA, $V_{xc}(r)$ is approximated locally by the corresponding expression of the homogeneous gas of the same electron density n(r). We discuss in the following why the quasi-particle gap ε_g^{qp}LDA obtained from (1) in LDA differs from the true $\varepsilon_g^{qp}$and, in finite systems, from the LDA eigenvalue gapε_g^0LDA. We write

$$\varepsilon_g^{qp} = (\varepsilon_g^{qp})_{LDA} + \Delta = (\varepsilon_g^0)_{LDA} + \delta\Sigma \quad \text{---------- (2)}$$

Here, we want to clarify the dependence of $\delta\sum$and Δ upon the dimensionality of the nanostructure. This is important since Δ reflects a discontinuity of the exact V_{xc} of DFT (not contained in LDA) upon addition of one-electron or hole to the neutral system. We shall find that $\delta\sum$ exhibits a smooth decreasing behaviour with increasing dimensionality. On the

contrary Δ presents a peak between QD and 3D, demonstrating the highly non-local nature of V_{xc}. This behaviour can be explained in terms of general arguments based on the GW approximation in which one can isolate a surface long range (macroscopic) contribution to the self-energy. These arguments are then confirmed via a tight binding GW calculation, well adapted to quantitatively treat this macroscopic part.

QUANTITATIVE TREATMENT OF EXCITONS

Consider numerical calculations of the excitonic gap performed via direct resolution. Again, we consider silicon crystallites as a test case. We start to express the excitonic gap ε_g^{exc} as the difference between the quasi-particle gap ε_g^{qp} and E_{coul}, attractive interaction between these two quasi-particles. We have

$$\varepsilon_g^{exc} = \varepsilon_g^{qp} - E_{coul} = \varepsilon_g^0 + \delta\Sigma - E_{coul}$$

Where $E_{coul} = - < H_{eh} >$ and ε_g^{qp} is written as the sum ofthe independent particle value $\varepsilon_g^0$and the self-energy correction $\delta\sum$.We shall see that there is strong cancellation between the two large quantities $\delta\sum - \delta\sum \text{bulk} = \delta\sum \text{surf}$ and $E_{coul,}$ such that $\varepsilon_g^{exc} \approx \varepsilon_g^0 \delta\sum \text{bulk}$. This justifies why the single particle calculations yield accurate results for ε_g^{exc} We also show that E_{coul}like $\delta\sum$.

isdominated to a large extent by surface polarization charges, and we discuss on this basis the amount of cancellation between $\delta\sum \text{surf}$ and $\delta\sum \text{bulk}$.

CHARGING EFFECT

Single Particle Tunnelling Through Semiconductor Quantum Dots

Consider the tunnelling spectroscopy experiments on InAs nanocrystals performed by Banin et al. Using a scanning tunnelling microscope. They reveal rich features due to the interplay between quantum confinement and charging effects. In this context, we start by describing the calculations which allow a detailed understanding of the experimental data.

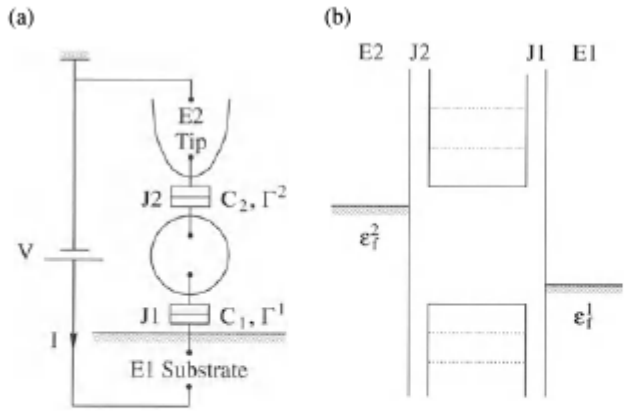

Fig. 1 . Typical double barrier tunnel junction. (**a**) It consists of two metallic electrodes E1 and E2 (e.g. a substrate and the tip of a scanning tunneling microscope) coupled to a nanostructure by tunnel junctions J1 and J2 with capacitances C_1 and C_2 and tunneling rates Γ^1 and Γ^2. (**b**) E1 and E2 are characterized by Fermi energies ε_f^1 and ε_f^2

In, the energy levels ε_i^e and ε_i^h of spherical InAs nanocrystals have been calculated with a Sp^3 tight binding model with second nearest neighbours interactions. The lowest conduction level (lS_e) is s-like, twofold degenerate, and the next level (lP_e) is p-like, a six fold degenerate. The highest two valence levels are found fourfold degenerate. The calculations of the transport properties use an extension of the theory of Averin et al.

The system consists of two metallic electrodes El and E2 weakly coupled to a semiconductor quantum dot by two tunnel junctions J1 and J2 with capacitances C_1 and C_2 . The metallic electrodes El and E2 are characterized by their Fermi energies $\varepsilon_f^1 = \varepsilon_f - e\varphi$ where φ is the bias voltage. The total energy of the quantum dot charged with n electrons and p holes with respect to the neutral state can be approximated by

$$E(\{n_i\},\{p_i\},\varphi) = \sum_i n_i\varepsilon_i^e - \sum_i p_i\varepsilon_i^h + \eta e\varphi q + \frac{1}{2}Uq^2$$

ε_i^e and ε_i^h are the conduction and valence energy levels in the quantum dot, n_i and P_i are electron and hole occupation numbers ($n=\sum_i n_i$, $p = \sum_i p_i$), and q = p-n. In terms of the junction capacitances C_1 and C_2, $U = e^2/(Cl + C2)$ is the charging energy and $\eta = C_1/(Cl + C2)$ is the part of the bias voltage φ that drops across junction J2 in the neutral quantum dot. Tunnelling of an electron via the energy level ε_i^e occurs at transition energy

$$\begin{aligned}\varepsilon_i^e(q|q-1,\varphi) &= E(n_i=1,\{p_j\},\varphi) - E(n_i=0,\{p_j\},\varphi)\ ,\\ &= \varepsilon_i^e - \eta e\varphi + U(-q+\frac{1}{2})\ .\end{aligned}$$

Symmetrically, hole tunnelling occurs at ε_i^h (q + l|q, φ). The current is calculated using the orthodox theory presented. Where one defines tunnelling rates through the junctions (Fig. 1). Both electrons and holes are treated at the same time incorporating the electron-hole recombinant ion rate R(n, p) from the charge state (n, p) to the charge state (n - 1,p - 1) into the master equations. At T $\rightarrow$ 0 K, the I(i φ) curve looks like a staircase. It exhibits a step each time ε_f^1 or ε_f^2 crosses a transition energy. A new charge state then becomes available in the quantum dot (addition step) or a new channel ε_i^e or ε_i^h is opened for tunnelling to a given, already available charge state (excitation step).

This behaviour is apparent in the results of Banin et al. The differential conductance G(φ) = dI(φ)/d φ p is shown in Fig. 2 for an InAs nanocrystal 6.4 nm in diameter. The tip was retracted from the quantum dot so that C1/C2 is maximum and 17 is close to unity. A zero-current gap is observed around φ = 0, followed by a series of conductance peaks for φ< 0
and φ> 0.

To compare with the interpretation of Banin et al, two types of calculations have been performed:

- using the capacitive model of with the calculated tight binding level structure, U and η being considered as fitting parameters chosen to optimize the agreement with the position of the peaks in the G(φ) curve
- a full self-consistent treatment on a system with a realistic geometry describedin Fig. 3. The ground state energy E_0 (n, p, φ) is self-consistently computed for a set of charge states (n,p) and several voltages φ_i. This is done in the Hartree approximation corrected from the unphysical self-interaction term. The electrostatic potential inside the quantum dot is computed with a finite difference method. The tunnelling rates are takenas adjustable parameters but the position of the calculated conductance peaks does not depend on their value.

The calculated G(φ) curves are compared to the experimental one on Fig. 2. The agreement with experiment is extremely good with practically a one to one correspondence between the calculated and experimental peaks over a range of 3.5 V. The negative bias voltages side is clearly improved in the self-consistent calculation.

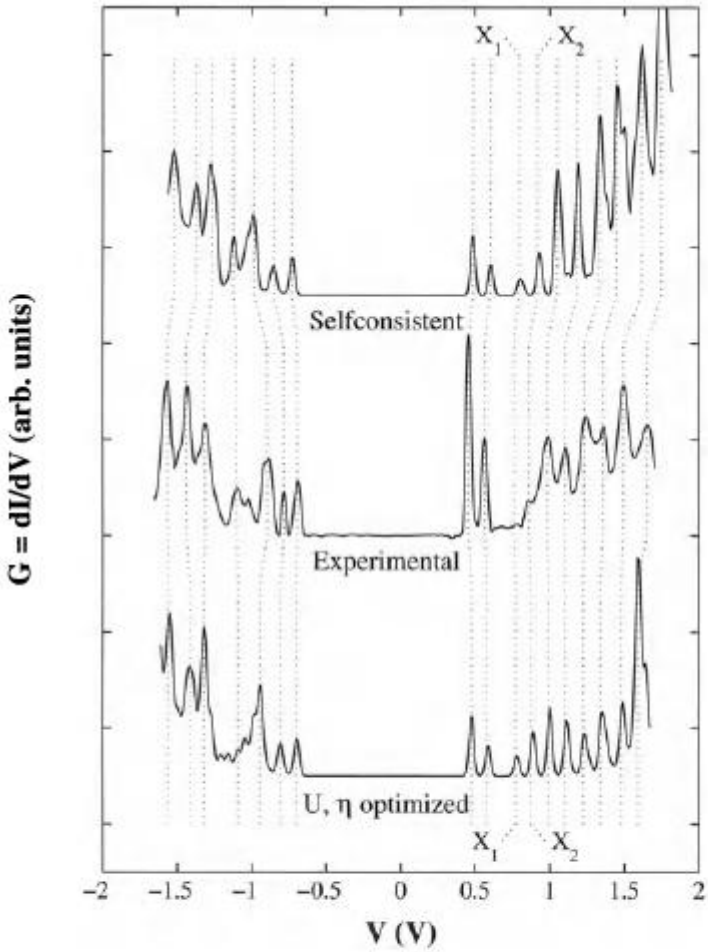

Fig. 2 . Comparison between calculated [138, 173] and experimental [249] differential conductance $G(\varphi)$ curves for a 6.4 nm diameter InAs nanocrystal. The optimized parameters for the capacitive model are $U = 100$ meV and $\eta = 0.9$ ($C_1 = 1.44$ aF, $C_2 = 0.16$ aF). The calculated peaks are broadened with a Gaussian of width $\sigma = 15$ meV

For φ> 0, the first group of two peaks is assigned to the tunnelling of electrons filling the $1S_e$ level, the splitting between the two peaks corresponding to the charging energy. Similarly, the next group of six peaks mainly corresponds to the tunnelling of electrons through the lP_e level, and there is some contributions from the tunnelling of holes. There are also twoexcitation peaks X_1 and X_2 on Fig. 2 (tunnelling through the $1P_e$ level in the charge states n = 0 and n = 1) that are hardly visible on the experimental G(φ) curve.

For φ< 0, the first two peaks can be unambiguously assigned to the tunnelling of holes filling the highest valence level. However, the next group of peaks is a very intricate structure involving single-hole charging peaks and tunnelling of electrons through the lS_e level. This disagrees with the interpretation of Banin et al, based on single-hole transitions. In particular,

the strong increase of the current below -1.25 V is mainly related to the tunnelling of electrons through the $1P_e$ level.

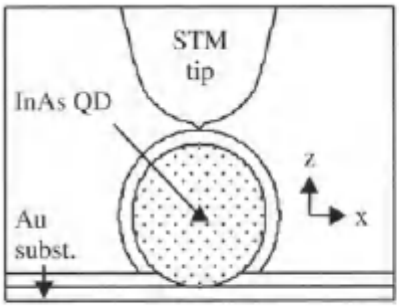

Fig. 3 A scanning tunneling microscope is used to probe the electronic structure of a 6.4 nm InAs nanocrystal. The quantum dot is linked to the gold substrate by a 5 Å thick hexane dithiol layer and is surrounded by a 5 Å thick layer of molecular ligands (dielectric constant = 2.6). The radius of curvature of the Pt-Ir tip is 2.5 nm, and the tip nanocrystal distance is 5 Å

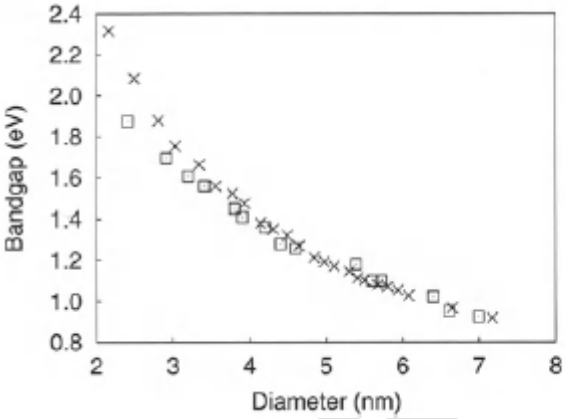

Fig. 4. Comparison between calculated [138, 173] (×) and experimental [249] (□) bandgap energies ε_g^0 of InAs nanocrystals versus size

The experimental spectra have been measured for different nanocrystal sizes allowing to deduce the one-particle bandgap $\varepsilon_g^0 = \varepsilon_1^e - \varepsilon_1^h$ and the charging energy U. Figures 4 and 5 show that the self-consistent tight binding values agree extremely well with experimental ones in the whole range of sizes. This result strongly supports the above interpretation of the tunnelling spectra and validates the predictions of the tight binding calculations even for large confinement energies.

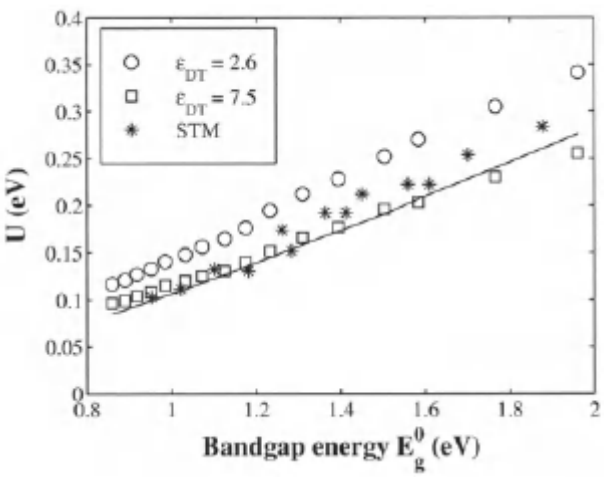

Fig. 5 Comparison between the calculated (tight binding) and experimental (STM = scanning tunneling microscopy results of [249]) charging energies U versus the bandgap energy for the geometry shown in Fig. 4.17. The dielectric constant of the hexane dithiol layer is either $\varepsilon_{DT} = 2.6$ or $\varepsilon_{DT} = 7.5$. Charging energy U given by (3.72) with $\epsilon_{out} = 6$ (*straight line*)

Such calculations point to the importance of the medium surrounding the nanocrystal for an accurate determination of the charging energies. This is dearly apparent in the analytical expressions obtained for spherical nanocrystals of dielectric constant ϵ_{in} embedded in an external medium of dielectric constant ϵ_{out} and calculated with simple effective mass envelope functions. One finds that the self-energy of a carrier directly depends on ϵ_{in} - ϵ_{out} and can thus reverse sign with this quantity. This is not quite the case of the electronic Coulomb repulsion which is always positive but which is proportional to $e^2/(\epsilon_{out}/R)$ which can vary between $0(\epsilon_{out} \rightarrow +\infty)$ and e^2 / R $\epsilon_{out} \rightarrow 0)$. Such conclusions have been confirmed by more refined calculations. In these works, the charging energies was calculated with single particle wave functions obtained from an empirical pseudopotential method. The results are completely in line with the simple formula. As with the tight binding approach just described, the authors have calculated the single particle energies of neutral and chargeddusters for InAs nanocrystals. They have also compared their results with those of Banin et al, and they have shown that the best agreement with experiments occurs for ϵ_{out} = 6. However care should be taken when comparing the predictions of idealized situations (like spherical quantum dots embedded in an homogeneous medium) with the experimental geometry, as done in, which is equivalent to calculating the corresponding capacitances for each particular population of the quantum dot.

LUMINESCENCE

The optical absorption and the stimulated emission are induced by the electromagnetic field. Incontrast, the spontaneous emission occurs even when there is no photon in the system. It is not described in the previous calculation because the electromagnetic field is treated classically. In the following, we shall relate the spontaneous emission to the absorption through the Einstein relationships, which will allow to take into account the local-field effects in a simple manner. Consider the composite material as a system of two levels in thermal equilibrium in an optical cavity of volume V. The number of photons per unit of energy $\hbar\omega$ in the cavity is given by the Planck formula for the black body:

$$N = \frac{8\pi(\hbar\omega)^2 n_{op}^3 V}{h^3 c^3} \frac{1}{\exp\left(\frac{\hbar\omega}{kT}\right) - 1} \quad \text{---------- (1)}$$

The effective rate of transition $|1\rangle \rightarrow |2\rangle$ per photon and per unit time, i.e. the balance between the absorption and the stimulated emission, is given by the product of the absorption coefficient by the velocity of the light

$$P_{12} = \alpha(\omega)\frac{c}{n_{\text{op}}} \quad \text{---------- (2)}$$

The effective number of transitions $|1\rangle \rightarrow |2\rangle$ in the cavity per unit of energy is N P_{12} . At equilibrium, they must be compensated by spontaneous transitions $|2\rangle \rightarrow |1\rangle$ whose number per unit of energy is proportional to the mean occupancy f_2 of the level $|2\rangle$

$$NP_{12} = Af_2 \quad \text{---------- (3)}$$

This relation must be verified at any temperature. At equilibrium, we have $f_2/ f_1 = \exp(-\hbar\omega /kT)$. Using (1) and (2), we obtain

$$A = \frac{8\pi\hbar^2\omega^2 n_{\text{op}}^2 V}{h^3c^2}C(\hbar\omega) \quad \text{---------- (4)}$$

To calculate the spontaneous recombination rate $\Gamma_{sp} = 1/\tau_{sp}$, we must divide A by the number of nanocrystals in the volume V (= pV/Ω) and we must integrate over the energy

$$\Gamma_{\text{sp}} = \frac{1}{\tau_{\text{sp}}} = \frac{\Omega}{pV}\int A\mathrm{d}(\hbar\omega) \quad \text{---------- (5)}$$

leading to

$$\Gamma_{\text{sp}} = \frac{1}{\tau_{\text{sp}}} = \frac{\omega_{21}^3 F^2 e^2 |\langle 1|\boldsymbol{r}\cdot\boldsymbol{e}|2\rangle|^2 n_{\text{op}}}{\pi c^3 \epsilon_0 \hbar} \quad \text{---------- (6)}$$

In this calculation, we have implicitly assumed that the absorption is isotropic. Thus, one usually prefers the following expression

$$\Gamma_{\text{sp}} = \frac{1}{\tau_{\text{sp}}} = \frac{\omega_{21}^3 F^2 e^2 r_{12}^2 n_{\text{op}}}{3\pi c^3 \epsilon_0 \hbar} \quad \text{---------- (7)}$$

Where $r_{12}^2 = |\langle 1|x|2\rangle|^2 + |\langle 1|y|2\rangle|^2 + |\langle 1|z|2\rangle|^2.$

We note the presence of the square of the local-field factor F in the spontaneous emission rate.

OPTICAL PROPERTIES OF HETEROSTRUCTURES AND NANOSTRUCTURES

The optical absorption of systems with reduced dimensionality based on direct gap semiconductors, going from the bulk to quantum wells and quantum dots. We mainly describe the systems in the effective mass approximation for the envelope functions, considering one-particle and excitonic transitions. We only consider the effects of the electronic structure, discarding all the proportionality constants such as the local-field factor. We write the absorption coefficient

$$\alpha(\omega) \propto \frac{1}{\omega} \sum_{i,f} |\langle i|\boldsymbol{e}\cdot\boldsymbol{p}|f\rangle|^2 \delta(\varepsilon_f - \varepsilon_i - \hbar\omega) \quad \text{---------- (1)}$$

where the sum is over the (final) empty states |f> and the (initial) occupied states |i> (T → 0K). Following, the wave function of the initial state has the following form

$$\Psi_i(\boldsymbol{r}) = u_{b_i}(\boldsymbol{r})\phi_i(\boldsymbol{r}) \quad \text{---------- (2)}$$

whereU_{bi} (r) is the periodic part of the Bloch functions at the zone center for the band b_i and ϕ_i (r) is the envelope function. A similar expression holds for the final state. The optical matrix element is

$$\langle i|\boldsymbol{e}\cdot\boldsymbol{p}|f\rangle \approx \boldsymbol{e}\cdot\langle u_{b_i}|\boldsymbol{p}|u_{b_f}\rangle \int_\Omega \phi_i^*\phi_f \mathrm{d}\boldsymbol{r} + \delta_{b_i b_f}\boldsymbol{e}\cdot\int_\Omega \phi_i^*\boldsymbol{p}\phi_f \mathrm{d}\boldsymbol{r} \quad \text{---------- (3)}$$

With

$$\langle u_{b_i}|\boldsymbol{p}|u_{b_f}\rangle = \int_{\Omega_0} u_{b_i}\boldsymbol{p}u_{b_f}\mathrm{d}\boldsymbol{r} \quad \text{---------- (4)}$$

where$\Omega_0$denotes the volume of the elementary cell of the semiconductor. In (3), we have used the fact that the envelope functions are slowly variable functions on the length-scale of the unit cell. In the following, we consider two categories of optical transitions:

- interband transitions that occur between states originating from different bands (b_i == valence, b_J == conduction) where the optical matrix element reduces to the first term in eqn. 2.
- intraband transitions ($b_J = b_i$) involving the dipole matrix elements between envelope functions, the second term in (3).

KARPAGAM ACADEMY OF HIGHER EDUCATION

Coimbatore-641021.

(For the candidates admitted from 2016 onwards)

DEPARTMENT OF PHYSICS

UNIT IV (Objective Type/Multiple choice Questions each Questions carry one Mark)

NANOMATERIALS AND APPLICATIONS

PART –A(Online Examination)

S.No.	QUESTIONS	opt1	opt2	opt3	opt4	ANSWER
1	When the size of the material decreases , the band gap energy _____	increases	decreases	remains constant	zero	increases
2	The Fermi energy of the metal are in the order of _____	5 MeV	5 eV	5 KeV	5 meV	5 eV
3	Quantum effects mainly occurs at _____	conductor	metal	Metal or Semiconductors Nanocrystal	insulator	Metal or Semiconductors Nanocrystal
4	This Coulomb blockade behaviour is also called as _____	maxwell staircase	quantized	ballistic	Coulombic staircase	Coulombic staircase
5	The dimension of the nanomaterials reduced to de-Broglie wavelength, the semiconductor nanomaterials changes to _____	conductor	metal	Metal or Semiconductors Nanocrystal	insulator	insulator
6	The size of the nanocrystal _____ than the de-Broglie wavelength, _____ energy levels formed	Smaller, Discrete	Larger, Discrete	Smaller, continuous	Larger, continuous	Smaller, Discrete
7	How does a semiconductor behave at absolute zero?	conductor	protection device	Semiconductors	insulator	insulator
8	How is the resistance of semiconductor classified?	High resistance	Positive temperature co-efficient	Negative temperature co-efficient	Low resistance	Negative temperature co-efficient

9	The threshold for indirect absorption occurs at wavelength _____	3.01 µm	2.09 µm	0.92 µm	1.09 µm	1.09 µm
10	The semiconductor material for which the lowest energy absorption takes place is :	GaAs	Silicon	GaSb	Germanium	Germanium
11	_____ materials are potentially superior to germanium.	GaAs	Silicon	GaSb	III – V alloys	III – V alloys
12	If the absorption of electromagnetic radiation by matter results in the emission of radiation of same or longer wavelengths for a long or a short time, the phenomenon is termed as which of the following?	Luminescence	Fluorescence	Phosphorescence	Spontaneous emission	Luminescence
13	Prompt emission of X-ray by an atom ionised by a higher energy X-ray is a type of which of the following phenomena?	Luminescence	Fluorescence	Phosphorescence	Spontaneous emission	Fluorescence
14	In X-ray fluorescence spectrometer, the relationship between the excitation intensity and the intensity of fluorescence does not depend on which of the following?	Spectrum of the incident radiation	Angle of radiance	Molecular weight	Incident angle	Incident angle
15	Fluorescence occurs within _____ .	10-5 s	10-5 ms	10-5 µs	10-5ns.	10-5 ms
16	_____ alloys can be fabricated in hetero-junction structures.	InGaSb	III – V alloys	InGaAsP	GaAsSb	III – V alloys
17	The alloys lattice matched to InP responds to wavelengths up to 1.7µm.	InAsSb	III – V alloys	InGaSb	InGaAs	InGaAs
18	Which phenomenon is related to the term radiation?	magnetic phenomenon	gravity	electromagnetic phenomenon	none of the above	
19	Thermal radiation takes place from a body by electromagnetic waves as a result of	the weight of the body	the magnetic power of the body	the temperature of the body	none of the above	electromagnetic phenomenon
20	Rate of transfer of energy by radiation can be increased by	increasing the surface temperature	decreasing the surface area	using shiny white surfaces instead of dull and black surfaces	decreasing the atmospheric pressure	the temperature of the body
21	Thermal energy that reaches surface of earth	Conduction	Convection	Radiation	Conduction and	increasing the

	from sun, is transferred through process of				convection	surface temperature
22	Which of the following is not an example of nanoscience in nature?	Hydrophobic surface of a lotus plant	Hydrophylic surface of a pitcher plant	Sticky pads on the bottom of an ant's foot	Gold that can stretch to form flexibile electronics	Gold that can stretch to form flexibile electronics
23	Which of the following is used to observe the unseen?	Hydrophobocity Microscopes	Magnetos	Atomic Force Tunnelers	Scanning Tunneling Microscopes	Scanning Tunneling Microscopes
24	Nano wires are used in_____	Transistors	Resistors	Capacitors	Transducers	Transistors
25	Nano cones are the predominant structures made with _____	Carbon	Nitrogen	Hydrogen	Silicon	Carbon
26	As per Coulomb's law, force of attraction or repulsion between two point charges is directly proportional to	sum of the magnitude of charges	square of the distance between them	product of the magnitude of charges	cube of the distance	product of the magnitude of charges
27	Electric charges under action of electric forces is called	electrostatic	electric flux	electric field	electric field lines	electrostatic
28	The absorption of photons in a photodiode is dependent on:	Absorption Coefficient α0	Properties of material	Charge carrier at junction	Amount of light	Absorption Coefficient α0
29	The absorption coefficient of semiconductor materials is strongly dependent on	Properties of material	Wavelength	Amount of light	Amplitude	Wavelength
30	In optical fiber communication, the only weakly absorbing material over wavelength band required is:	GaAs	Silicon	GaSb	Germanium	GaSb
31	The threshold for indirect absorption occurs at wavelength _____	3.01 μm	2.09 μm	0.92 μm	1.09 μm	1.09 μm
32	The semiconductor material for which the lowest energy absorption takes place is :	GaAs	Silicon	GaSb	Germanium	Germanium
33	_____ photodiodes have large dark currents.	GaAs	Silicon	GaSb	Germanium	GaSb
34	A photodiode should be chosen with a _____ less than photon energy.	Direct absorption	Band gap energy	Wavelength range	Absorption coefficient	Absorption coefficient
35	_____ materials are potentially superior to germanium.	GaAs	Silicon	GaSb	III – V alloys	III – V alloys

36	_____ alloys can be fabricated in hetero-junction structures.	InGaSb	III – V alloys	InGaAsP	GaAsSb	III – V alloys
37	_____ alloys such as InGaAsP and GaAsSb deposited on InP and GaSb substrate.	Ternary	Quaternary	Gain-guided	III – V alloys	Ternary
38	The alloys lattice matched to InP responds to wavelengths up to 1.7μm.	InAsSb	III – V alloys	InGaSb	InGaAs	InGaAs

Electron Transport: Carrier transport in nanostrcutures. Coulomb blockade effect, thermionic emission, tunneling and hoping conductivity. Defects and impurities: Deep level and surface defects.

APPLICATIONS: Applications of nanoparticles, quantum dots, nanowires and thin films for photonic devices (LED, solar cells). Single electron transfer devices (no derivation). CNT based transistors. Nanomaterial Devices: Quantum dots heterostructure lasers, optical switching and optical data storage. Magnetic quantum well; magnetic dots -magnetic data storage. Micro Electromechanical Systems (MEMS), Nano Electromechanical Systems (NEMS).

CARRIER TRANSPORT IN NANO STRUCTURES

Consider the problem of electron (or hole) transport in networks of nanostructures weakly coupled by tunnel junctions. First, we consider the tunnelling between two neighbouring sites and, second, we present a method to calculate the conductivity of the network.

COULOMB BLOCKADE EFFECT

Materials are often classified as metals, semiconductors and insulators, according to their ability to let current flow through them. Conductivity is defined in terms of the properties of electrons (their number, effective mass, scattering etc.) in the solids and is given by

$$\sigma = \frac{Ne^2\tau}{m^*}$$

where σ is electrical conductivity, N – number of electrons per cm^3, e – electron charge, τ – relaxation time and m* is effective mass of electron.

Resistivity is the inverse of conductivity. Metals are characterized by very low resistivity (~10^{-6} Ωcm). Semiconductors have medium resistivity (few Ωcm) and insulators have large resistance (>10^3 Ωcm). The resistivity (or conductivity) in solids can be measured in principle by connecting electrically conducting wires to solid material of known geometry, applying a voltage difference across it and measuring the current flowing through it.

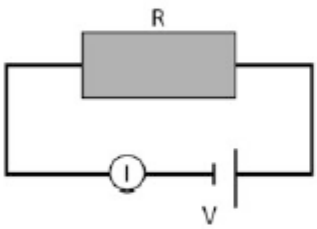

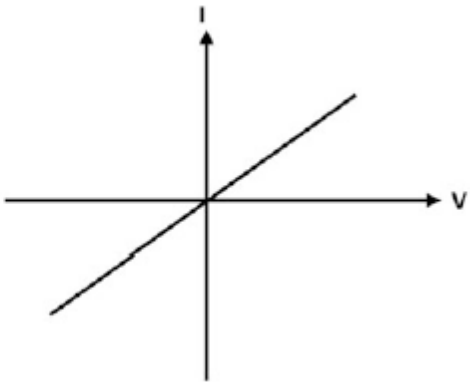

If we reduce now the dimensions of metal piece (or introduce a semiconductor nanoparticles or quantum dot) to ~100 nm or less and wish to measure its conductivity, then it is useful to put metal electrodes (capacitors) on either side so that direct contact between electrodes and metal particle is avoided. This enables to deduce the correct details of electronic structure. There appears then a region around zero voltage for which there is no current flow. This phenomenon is known as Coulomb blockade. This can be understood as follows.

The electrostatic energy E (charging energy) of a parallel plate capacitor having capacitance 'C' is given by

$$E = e^2/2C$$

For small value of the capacitance and low thermal motion of electrons ($kT \ll e^2/2C$) the charging energy E will be significant. The small metal island connected to electron source and drain by tunnel barriers can be charged in such a way that only a single electron is transferred to it when voltage ˙e/2C is applied. Below this voltage electron cannot be transferred. Therefore the region of no current of low bias voltage is known as Coulomb Blockade region. Repeated tunnelling of single electrons produces what is known as Coulomb Staircase.

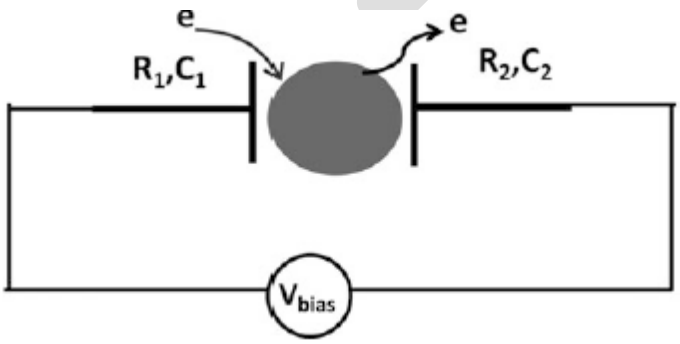

There are many examples now in which phenomenon of Coulomb Staircase has been demonstrated using quantum dots or metal islands. The Coulomb blockade can also be very well understood from Fig.4. When the Fermi levels on both the sides are at the same level, no current flows but the moment one of the electrodes as shown in the figure receives higher potential with respect to the quantum dot, the current can flow between the metal electrodes and the quantum dot. Similarly if the cluster is at higher potential compared to the electrode then the electrons from the cluster tunnel towards the electrode. The single electron transistor is based on the phenomenon of Coulomb blockade.

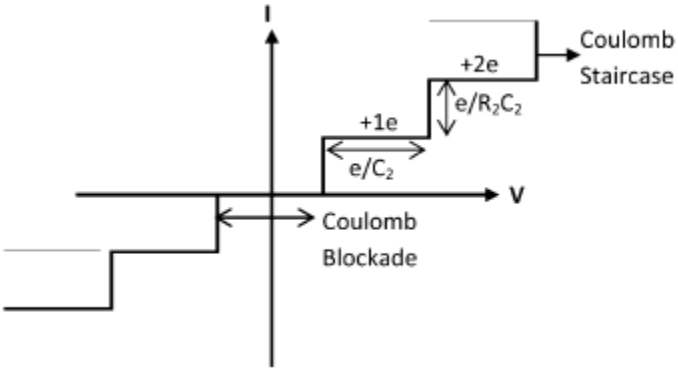

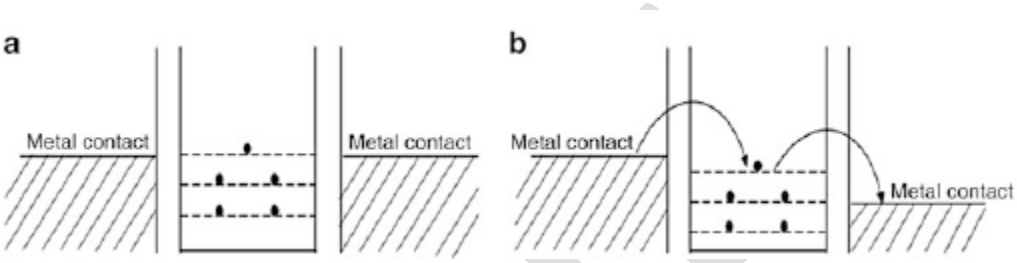

TUNNELLING

In the case of metallic islands in which the density of states is high, Coulomb blockade effects dominate the transport properties of the networks. In the case of semiconductor nanocrystals, the conductivity is also determined by the discretize at ion of the energy levels induced by the quantum confinement. In both cases, the disorder arising for example from the dispersion in size and shape of the nanostructures plays an essential role. Therefore, elastic tunnelling between neighbour nanostructures is rather unlikely and one must consider inelastic tunnelling between non resonant states, which requires to take into account the electron-phonon coupling. We assume that an injected electron only couples to phonons localized in the nanostructure where it resides, which is a reasonable assumption for weakly coupled nanostructures. Atomic vibrations in the barrier may lead to a modulation of the barrier height but we do not consider this effect here. When an electron is transferred from one site to another, there is an emission or an absorption of phonons as required by the conservation of the total energy.

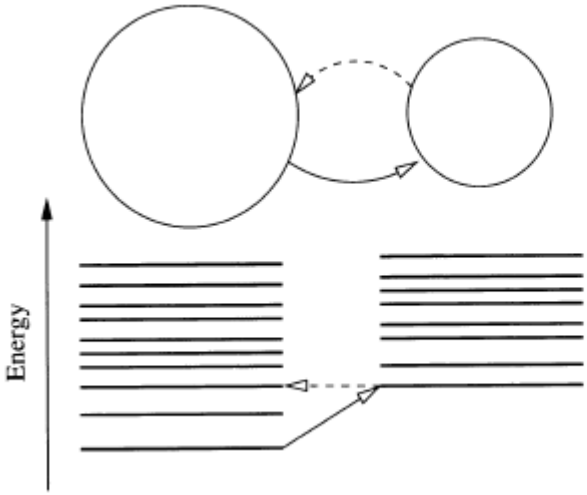

Fig. 1 Tunneling of an electron between two nanostructures. The arrows indicate the most efficient tunnel processes

When an extra carrier is introduced into a nanostructure, there is a relaxation of the atoms toward a new equilibrium situation. The relaxation energy is defined as the Franck-Condon shift (e.g. $df^{(1)}$) for site 1). In order to simplify the problem, we assume as usual that the total energy is a quadratic function of $3N_1 + 3N_2$ configuration coordinates where N_1 and N_2 are the numbers of atoms in the nanostructures 1 and 2, respectively. The probability per unit time for the transfer of an electron from a site 1 to a site 2 is obtained from the Fermi golden rule

$$W_{1\to 2} = \frac{2\pi}{\hbar}\sum_{i,n_1,n_2} p(i,n_1,n_2)\left[\sum_{f,n_1',n_2'} |\langle f,n_1',n_2'|V|i,n_1,n_2\rangle|^2 \delta(E_{f,n_1',n_2'} - E_{i,n_1,n_2})\right] \quad \text{---------- (1)}$$

where $|i, n_1, n_2\rangle$ and $|f, n_1', n_2'\rangle$denote the initial and final states of energy $E_{i,}$ $n_1, n_2$and $E_{f,}$ n_1', n_2' respectively, and p(i, nI, n2) is the probability to find the system in the state $|i, n_1, n_2\rangle$ The integers n_1, n_2 , n_1', n_2' label the vibronic configurations on each site. Since we assume that the vibrations of the two sites are uncoupled, we write

$$|i,n_1,n_2\rangle = |\phi_i^{(1)}\rangle\ |\chi_{n_1}(Q_1 - Q_1^0)\rangle\ |\chi_{n_2}(Q_2)\rangle$$
$$|f,n_1',n_2'\rangle = |\phi_f^{(2)}\rangle\ |\chi_{n_1'}(Q_1)\rangle\ |\chi_{n_2'}(Q_2 - Q_2^0)\rangle \quad \text{---------- (2)}$$

where Q_1^0 denotes the equilibrium configuration of the site 1 with one extra electron, Q_1 = O being the equilibrium configuration for the neutral nanostructure. $|\phi_1^{(1)}\rangle$ and $|\phi_f^{(2)}\rangle$ are the electronic states. The vibronic states χ_{n1} and χ_{n2} are given by the product of $3N_1$ and $3N_2$ harmonic oscillators. We suppose that the matrix element of the tunnelling operator V

between the electronic states does not depend on the phonon quantum numbers. Thus we can factorize in (1) the terms $\langle \chi_{n_1'}(\bar{Q}_1)|\chi_{n_1}(\bar{Q}_1 - Q_1^0)\rangle$ and $\langle \chi_{n_2'}(Q_2 - Q_2^0)|\chi_{n_2}(Q_2)\rangle$ which are given by products of overlaps between displaced harmonic oscillators. Since the coupling to anyone mode is of the order of l/N_1 or $1/N_2$, that one can keep only first-order terms corresponding to change in phonon quantum numbers equal to 0, + 1 and -1, alI the other terms being of higher order. In that case, the probability of the transition can be obtained exactly if all the electron-phonon coupling coefficients are calculated.

Simpler expressions can be obtained when all phonons frequencies in a nanostructure can be approximated by a single one (here $\omega_1$and ω_2) Then one can sum the intensity of all possible transitions corresponding to the same difference in total energies between the final and initial states, for example differing by P_1 phonons of energy $\hbar\omega_1$ and P_2 phonons of energy $\hbar\omega_2$. Then we have

$$E_{f,n_1',n_2'} - E_{i,n_1,n_2} = \varepsilon_f - d_{\mathrm{FC}}^{(2)} - \varepsilon_i + d_{\mathrm{FC}}^{(1)} + p_1\hbar\omega_1 + p_2\hbar\omega_2 \quad \text{---------- (3)}$$

where the Franck-Condon shifts correspond to the relaxation energy when the nanostructure is occupied by one electron. The total intensity of these transitions is equal to WP_1 X WP_2 where W_p is injecting this in (1), we obtain

$$W_{1\to 2} = \frac{2\pi}{\hbar}\sum_{i,f} p(i)|\langle\phi_f^{(2)}|V|\phi_i^{(1)}\rangle|^2 \times \left[\sum_{p_1,p_2} W_{p_1}W_{p_2}\delta(\varepsilon_f - d_{\mathrm{FC}}^{(2)} - \varepsilon_i + d_{\mathrm{FC}}^{(1)} + p_1\hbar\omega_1 + p_2\hbar\omega_2)\right] \quad \text{---------- (4)}$$

which can be written as a convolution of two phonon line-shapes.

In the case of strong electron-phonon coupling ($S_1 = d_{\mathrm{FC}}^{(1)}/\hbar\omega_1 \gg 1$ and $S_2 = d_{\mathrm{FC}}^{(2)}/\hbar\omega_2 \gg 1$), Considering P_1 and P_2 as continuous variables (i.e. $\sum_{p1,p2} \longrightarrow \int dp_1\, dp_2$), the probability per unit time becomes

$$W_{1\to 2} = \frac{2\pi}{\hbar}\sum_{i,f} p(i)|\langle\phi_f^{(2)}|V|\phi_i^{(1)}\rangle|^2 \frac{1}{\pi\mu}\exp\left[-\frac{(\Delta - d_{\mathrm{FC}}^{(1)} - d_{\mathrm{FC}}^{(2)})^2}{\mu^2}\right] \quad \text{---------- (5)}$$

Where

$$\mu = \sqrt{2S_1(\hbar\omega_1)^2\coth\left(\frac{\hbar\omega_1}{2kT}\right) + 2S_2(\hbar\omega_2)^2\coth\left(\frac{\hbar\omega_2}{2kT}\right)} \quad \text{---------- (6)}$$

And $\Delta = \varepsilon_f - d_{FC}^{(2)} - \varepsilon_i + d_{FC}^{(1)}$ is the energy required to transfer the electron from the site 1 to the site 2. An example of variation of $W_{1\to 2}$ with respect to Δ is presented in Fig. 2.

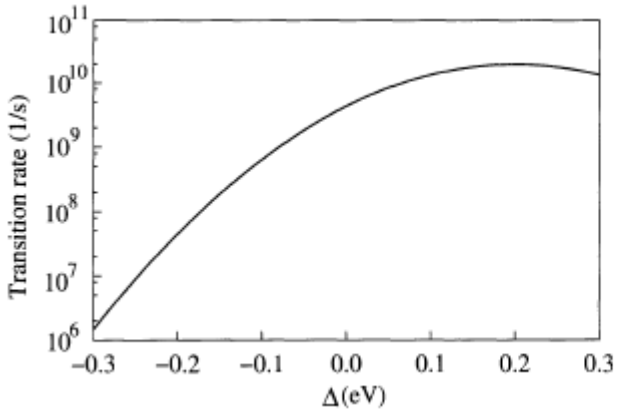

Fig. 2 Probability per unit time for the transition between two nanostructures as a function of the energy Δ ($S_1 = S_2 = 2$, $\hbar\omega_1 = \hbar\omega_2 = 50$ meV, $\langle\phi_f^{(2)}|V|\phi_i^{(1)}\rangle = 1$ meV, $T = 300$K)

As a final remark, we point out that in the limit of strong electron phonon coupling, it is not necessary to assume a single phonon frequency in each nanostructure. It can be shown, using the method of moments, that the expression (5) can be recovered in the general case using the first and second moments of the phonon line-shape, at the condition to write

$$d_{FC}^{(1)} + d_{FC}^{(2)} = \sum_i S_i^{(1)}\hbar\omega_i^{(1)} + \sum_j S_j^{(2)}\hbar\omega_j^{(2)} \quad \text{---------- (7)}$$

where the sums run over all the phonon modes of energy $\hbar\omega_i^{(1)}$ and $\hbar\omega_j^{(2)}$ in nanostructures 1 and 2, respectively, and at the condition to replace (6) by

$$\mu = \sqrt{M^{(1)} + M^{(2)}} \quad \text{---------- (8)}$$

Where

$$M^{(1)} = (d_{FC}^{(1)})^2 + \sum_i (2\bar{n}_i^{(1)} + 1) S_i^1 (\hbar\omega_i^{(1)})^2 \quad \text{---------- (9)}$$

with $\bar{n}_i^{(1)}$ for the phonon frequency $\omega_i^{(1)}$ (a similar expression holds for $M^{(2)}$).

HOPING CONDUCTIVITY

Consider now a network of nanostructures. Our aim is to present a computational method to calculate the conductivity. We consider systems where the degree of randomness is sufficiently large that the transport of carriers takes place by hopping between neighbouring nanostructures. The disorder may arise under different forms such as the topological or cellular

disorder. It was shown that a fixed array of sites can serve as a useful model for topologically disordered systems. Therefore, in the following, we assume a fixed array of sites in which the activated hopping between neighbouring sites i and j is defined by the probability per unit time $W_{i\to j}$ that was calculated in the previous section and from which we want to determine the dynamic conductivity σ(ω).

The combination of the disorder and of a particular topology of the array may dramatically influence the electrical transport, in particular when the system is close to the percolation limit. Due to these constraints, the diffusion of the electron is anomalous at the microscopic scale, in the sense that the diffusion coefficient D depends on time (note that the same theory obviously applies to the holes). However, at the mesoscopic scale, when the mean displacement of the electron becomes larger than the correlation length which characterizes the system, a constant diffusion coefficient can be defined, and the diffusion becomes normal. Here we give a simplified presentation of this theory.

Diffusion Coefficient. The diffusion of electrons of density n(r, t) at a position r and at time t is given by the Fick law and the charge conservation equation

$$\frac{\partial n(\boldsymbol{r},t)}{\partial t} = \frac{1}{e}\boldsymbol{\nabla}\cdot\boldsymbol{J}\ ,$$
$$\boldsymbol{J} = eD\ \boldsymbol{\nabla} n(\boldsymbol{r},t)\ , \qquad \text{---------- (1)}$$

where J is the current density. To solve these equations, we define the following Laplace transform of a function f(t) as

$$F(\omega) = \mathcal{L}\left[f(t)\right] = \int_0^\infty \mathrm{e}^{-(\alpha+\mathrm{i}\omega)t} f(t)\mathrm{d}t\ , \quad \alpha \to 0^+ \qquad \text{---------- (2)}$$

Applying this to (1) in the case of a 1D system, we obtain

$$\mathrm{i}\omega N(x,\omega) = D\frac{\partial^2 N(x,\omega)}{\partial x^2} \qquad \text{---------- (3)}$$

which leads to

$$N(x,\omega) = \frac{1+\mathrm{i}}{2}\sqrt{\frac{\omega}{2D}}\ \frac{n_0}{\mathrm{i}\omega}\exp\left(-\sqrt{\frac{\omega}{2D}}\ |x|\,(1+\mathrm{i})\right) \qquad \text{---------- (4)}$$

The coefficient in front of the exponential has been obtained by the Laplace transform of the normalization condition for n_o electrons in the system

$$\int_{-\infty}^{+\infty} n(x,t)\mathrm{d}x = n_0 \Rightarrow \int_{-\infty}^{+\infty} N(x,\omega)\mathrm{d}x = \frac{n_0}{\mathrm{i}\omega}$$ ---------- (5)

In order to characterize the diffusion of the electrons, we calculate the mean square displacement of the electrons $\overline{x^2(t)}$ at time t defined by

$$\overline{x^2(t)} = \frac{1}{n_0}\int_{-\infty}^{+\infty} x^2 n(x,t)\mathrm{d}x$$ ---------- (6)

Using (4), we obtain that the Laplace transform of $\overline{x^2(t)}$is related to the generalized diffusion coefficient D (ω) by

$$\mathcal{L}\left[\overline{x^2(t)}\right] = \frac{1}{n_0}\int_{-\infty}^{+\infty} x^2 N(x,\omega)\mathrm{d}x = \frac{2D(\omega)}{(\mathrm{i}\omega)^2}$$ ---------- (7)

which can be generalized to a system of dimension d (=1,2,3) as

$$D(\omega) = -\frac{\omega^2}{2d}\int_{0}^{+\infty} \mathrm{e}^{-\mathrm{i}\omega t}\overline{r^2(t)}\mathrm{d}t$$ ---------- (8)

In the case of a normal diffusion, D is a constant and we recover the linear dependence of $\overline{x^2(t)}$ with time t

$$\overline{r^2(t)} = 2dDt$$ ---------- (9)

The expression (8) is particularly interesting in the case of the hopping transport on an array of localized sites defined by vectors s. Let us define the probability $p(s,t|s_o)$ to find an electron on the site s at time t whereas it was on the site s_o at time t = 0. Then we can write

$$\overline{r^2(t)} = \sum_{\boldsymbol{s}} (\boldsymbol{s}-\boldsymbol{s}_0)^2 \langle p(\boldsymbol{s},t|\boldsymbol{s}_0)\rangle$$ ---------- (10)

where the brackets denote the average on the sites S_o. Note that this average is required when the system is disordered. From (8), we deduce the diffusion coefficient

$$D(\omega) = -\frac{\omega^2}{2d}\sum_{\boldsymbol{s}} (\boldsymbol{s}-\boldsymbol{s}_0)^2 \langle P(\boldsymbol{s},\omega|\boldsymbol{s}_0)\rangle$$ ---------- (11)

The conductivity σ(ω)is related to the diffusion coefficient by the Einstein relation

$$\sigma(\omega) = \frac{ne^2}{kT} D(\omega) \quad \text{---------- (12)}$$

where n is the carrier density. We deduce that

$$\sigma(\omega) = -\frac{ne^2}{kT}\frac{\omega^2}{2d}\sum_{\boldsymbol{s}}(\boldsymbol{s}-\boldsymbol{s}_0)^2 \langle P(\boldsymbol{s},\omega|\boldsymbol{s}_0)\rangle \quad \text{---------- (13)}$$

One can wonder if the Einstein relationship holds for hopping transport. Actuality, (13) can be obtained from the Kubo formula

DEEP LEVEL DEFECTS:

Deep level defects are characterized by a strongly localized wave function. One then expects that, a few screening lengths away from the boundary, the wave function of the neutral defect will experience the same local potential as in the corresponding bulk material. This means that the neutral deep level itself remains invariant on an absolute scale at the same position as in the bulk material. It will thus not experience a confinement effect as it is the case for the nanostructure bandgap. Such a property has been extensively used to discuss the Stokes shift of ten observed between luminescence and optical absorption in semiconductor nanocrystals. However this view is too naive and cannot be directly applied to the so-called occupancy or ionization levels E(n + 1, n) where E(n) is the total energy of the system with n electrons on the defect (when the corresponding charge state is stable). These ionization levels are the true observable quantities in capture or emission experiments. To illustrate the situation, we choose the basic example of a non-degenerate level for which one can have n ε {0, 1, 2} with the neutral state corresponding to n = 1. Then one has, if they exist, two ionization levels ε(2, 1) and ε(I, 0) which correspond to the addition of an electron or a hole on the defect, respectively (Fig. 1). Such quantities are naturally obtained via the resolution of the GW equations of Sect. 1.2.4 which also gives information about the distribution of all other excited quasi-particle states and especially the bandgap limits ϵ_c and ϵ_v of the nanostructure which are affected by the confinement effects. To get simple but accurate conclusions we proceed and split the single-particle GW equations into a bulk-like contribution and a surface polarization term due to the finite size of the system. The resolution of this problem should then proceed in three steps:

- solve a set of single particle equations, using ab initio or semi-empirical techniques. This will provide us with the single particle energies and wave functions of the system containing the neutral defect: ϵ_d for the deep level, ϵ_c and ϵ_v for the band limits which will include the confinement effect in the presence of the defect. Note that the presence of the defect is not likely to affect seriously the confinement energies since it is an effect of order 1/N (N being the number of atoms) while the confinement effect is of order (N_s/N)" where N_s is the number of surface atoms and the exponent v is typically between 1 and 2 (the confinement energy in a spherical quantum dot varies like d^{-v} where d is the diameter, and $N_s/N \propto d^{-1}$)
- add to these single particle energies a bulk contribution $\delta\sum b$ calculated in the presence of the defect. This problem has not been solved yet. However one might anticipate some elements of solution. There, one considers that the local density approximation (LDA) for instance correctly treats the short-range part of the self-energy. $\delta\sum b$ is then totally determined by the long range part screened by the bulk dielectric constant. This would end up with the bulk $\delta\sum b$ for the band limits and an intermediate value for the gap state. In any case $\delta\sum b$, even calculated exactly, would be state dependent. As shown for ideal crystallites, this $\delta\sum b$ should not give rise to appreciable confinement effects
- finally add the surface contributions $\delta\sum surf$.

surface contribution $\delta\sum surf$ takes the general form with W_{surf} being the contribution to arising from the surface polarization Now, for a deep defect, we can obtain the shift $(\delta\epsilon_d)_{surf}$ of the level by perturbation theory under the form

SURFACE DEFECTS:

A puzzling problem concerning the optical properties of semiconductor nanostructures is that there is sometimes a large difference between luminescence energies and optical absorption energies. For example, in oxidized porous silicon, there is a huge Stokes shift (≈1 eV for a crystallite diameter ≈ 1.5 nm), much larger than predicted values « 100 me V.In fact, optical absorption energy gaps are in agreement with calculated values for crystallites. Only the luminescence energies differ greatly and, for small crystallites, are practically independent of the size. Such behaviours are more consistent with the existence of deep luminescent centers.

The problem is that little is known regarding their nature and origin. We discuss here the possibility investigated in of the existence of intrinsic localized states which might behave as luminescent systems. Such states correspond to self-trapped excitons and are stabilized because of the widening of the gap induced by the confinement. This possibility is not restricted to the case of silicon crystallites but is likely to be valid for all types of semiconductor crystallites.

To illustrate the physical basis of such self-trapped excitons let us consider an isolated single covalent bond characterized by a σ bonding state filled with two electrons and an empty σ* anti-bonding state. The origin of the binding is the gain in energy resulting from having the two electrons in the lower bonding state. Optical absorption in this system leads to the excitation of One electron in the σ * state. In such a case there is essentially no binding and the repulsive force between the atoms dominates so that the molecule eventually dissociates. If, on the other hand, the molecule is embedded in an elastic medium then it cannot dissociate but One ends up with a large distance between the constituent atoms and a reduced separation between the σ and σ * states. The resulting luminescence energy is thus much smaller than the optical absorption energy, corresponding to a Stokes shift of the order of the binding energy, i.e. ≈ 1 eV.

The applicability of this model to a nanocrystal essentially depends On the possibility of localizing the electron-hole excitation On a particular covalent bond, i.e. of creating a self-trapped exciton. For this, One must be able to draw a configuration coordinate diagram like the One shown in Fig. 1 where the configuration coordinate Q corresponds to the stretching of the covalent bond. For small Q, the ground and first excited states are delocalized over the crystallite and show a normal parabolic behaviour. However, for Q larger than a critical value Q_c, the system localizes the electron-hole pair On One particular single bond, leading to a larger bond length Q_e and a smaller luminescence energy. This self-trapped state can be stable or metastable. An interesting point is that it may exist only for small enough crystallites, in view of the important blue shift as pictured in Fig. 1. Such a self-trapped exciton is likely to be favoured at surfaces of crystallites where the elastic response of the environment is weaker than in the bulk.

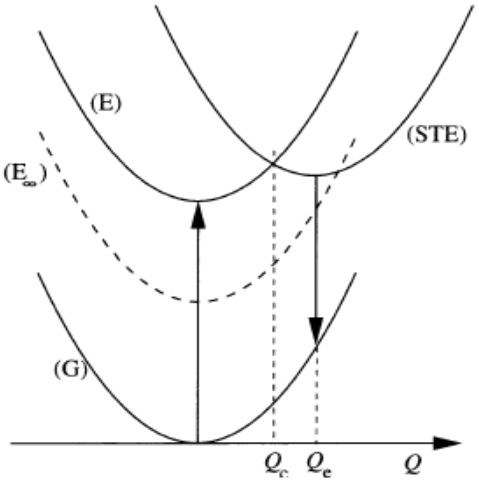

Fig. 1 Schematic configuration coordinate diagram showing the energies of the ground state (G), the free exciton state (E) and the self-trapped exciton state (STE). The curve (E_∞) corresponds to a very large crystallite with no blue shift, showing that the STE state might not exist for very large crystallites

In , two different techniques have been used for the calculations. The first one is a total energy semi-empirical tight binding technique which allows the treatment of relatively large crystallites (≈180 atoms). The second one is based on an ab initio technique in the local density approximation (LDA) which has already been applied to silicon clusters. Because of computation limits, the clusters studied in LDA are restricted to a maximum of ≈30 Si atoms which is not a severe restriction since we are interested in localized surface states. With the two techniques, the total energy is minimized with respect to all the atom positions to get the stable atomic configuration for the ground and first excited states. Only spherical crystallites centered on a silicon atom with the dangling bonds saturated by hydrogen atoms are considered. When needed, one surface dimer is created by removing the two closest hydrogen atoms of the second neighbour silicon atoms at the surface (see schematic side views in Fig. 2). We present here the results for two crystallites: one with 29 silicon and 36 saturating hydrogen atoms (diameter = 1 nm, tight binding energy gap = 3.4 eV, LDA gap = 3.5 e V) where tight binding and LDA techniques predict similar behaviour. Then one can use with confidence tight binding for a much bigger crystallites (123 silicon atoms, 1.7 nm, tight binding gap = 2.63 eV).

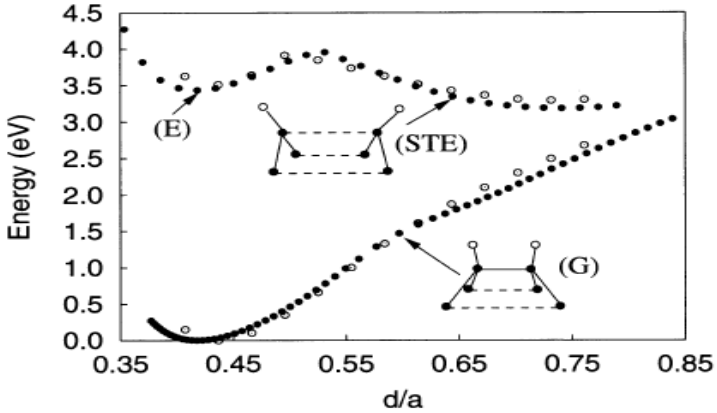

Fig. 2 Total energy (• = tight binding, ○ = LDA) of a spherical crystallite with 29 Si atoms in the ground state and in the excitonic state as a function of the dimer inter-atomic distance d ($a = 0.54$ nm). Schematic side views of the cluster surface dimer in the ground (G) and in the self-trapped state (STE) are also shown

If one first minimizes the total energy of excited crystallites starting from the atomic positions corresponding to the ground state situation, one obtains for very small crystallites <100 atoms) that the system in its excited state relaxes in highly distorted configurations with low symmetry. But, for large enough crystallites, the exciton remains delocalized, and there is a small lattice relaxation. The situation gets different when considering the case of Si-H surface bonds. One finds that it is possible to trap an exciton when these are sufficiently stretched. Then the minimum of energy corresponds to the broken bond, i.e. to hydrogen desorption. In the same spirit, one can get SiH_3 desorption by breaking the Si-Si back-bond in a process similar to polysilanes. A more interesting situation is obtained when stretching the Si-Si bond of a surface dimer. Then the stable atomic configuration for the excited state corresponds to the surface Si atoms returned to their original lattice sites (Fig.2). The electron and the hole are localized on the weakly interacting Si dangling bonds (second nearest neighbours) which form bonding and antibonding states separated by 0.72 e V in the tight binding calculation for the 1 nm crystallite (0.80 eV in LDA). Figure 6.9 fully corresponds to the general schematic picture of Fig. 1. As expected for a localized state, the self trapped exciton bandgap only slightly depends on the crystallite size with a value of 0.52 eV for the 1.7 nm crystallite. We see in Fig. 3 that for this larger crystallite the self-trapped exciton becomes metastable because the free exciton bandgap has decreased in energy. Figure 3 also gives the radiative lifetime in the excited state. In the free exciton state (E), the lifetime is long because of the indirect nature of the silicon bandgap. Increasing the dimer bond length, the lifetime in the self-trapped state first decreases because the localization of the exciton on one bond relaxes the selection rules.

Finally, the lifetime increases because the optical matrix element between the two silicon atoms of the dimer decreases with the bond length. From this, one can conclude that light emission is possible in the self-trapped state. At high temperature, the recombination could be at some intermediate coordinate *Q* with a smaller lifetime and a larger emission energy. More details concerning the calculation can be found.

General statements about the conditions favouring the existence of such self-trapped states for a given bond are the following:

- the elastic response of the environment must be as weak as possible, which is best realized near surfaces
- the size of the nanocrystal must be small, favouring a large blue shift and the stabilization of locally distorted excited states
- the capture of the exciton must allow the release of local stresses. This is the case of the Si-Si dimer where the stresses correspond to the bending of the back-bonds in the free exciton state. Such self-trapped states are likely to be metastable in most cases. The question then arises if and how they can be excited. One answer is provided by the well documented example of the EL_2 defect in GaAIAs which can be optically excited with a long lifetime.

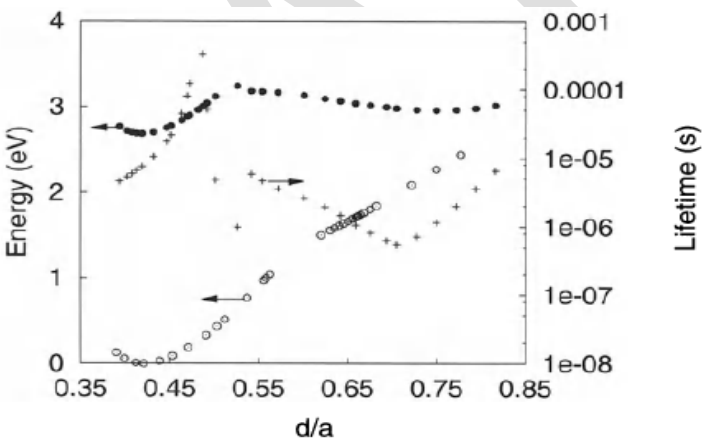

Fig. 3 Total energy of a spherical crystallite with 123 silicon atoms (diameter = 1.67 nm) in the ground state (○) and in the excitonic state (●) as a function of the dimer inter-atomic distance d (a = 0.54 nm). The crosses represent the radiative lifetime in the excitonic state

In conclusion of this section, total energy calculations demonstrate the existence of self-trapped excitons at some surface bonds of Si crystallites. These give a luminescence energy almost independent of size and can explain the Stokes shift observed for small crystallites. On the experimental side, self-trapped excitons have been invoked in Si- $Si0_2$ multi-layers and in

small Si particles . Such self-trapped excitons are not specific to Si nanostructures but should also manifest themselves in crystallites obtained from other semiconductors.

SINGLE ELECTRON TRANSFER DEVICES:

Before analyzing examples of the devices based on single-electron transport, we shall overview briefly a relatively simple technique for the formation ofstructures with low-dimensional electron gas.

The split-gate technique

Having a two-dimensional electron gas on an interface, or in a quantum well, one can further lower the electron-gas dimensionality by various methods. One such method is the so-called split-gate technique. The principles of this technique can be explained as follows. Typically, two-dimensional electrons are separated from the surface of the sample by a wide-bandgap dielectric layer. It can be a SiO2 layer on Si, an AlGaAs barrier layer on GaAs, etc. Figure 1(a) illustrates such a structure. Amodulation-doped barrier layer decreases electron scattering by the donors and results in high electron mobility. A thin GaAs layer grown on the top of this structure is used as additional electrical isolation from the metal gates. Let a metal strip – a gate – be deposited onto the top of this structure. The distribution of the potential energy for the case of a negative applied gate voltage is presented in Fig. 1(b).

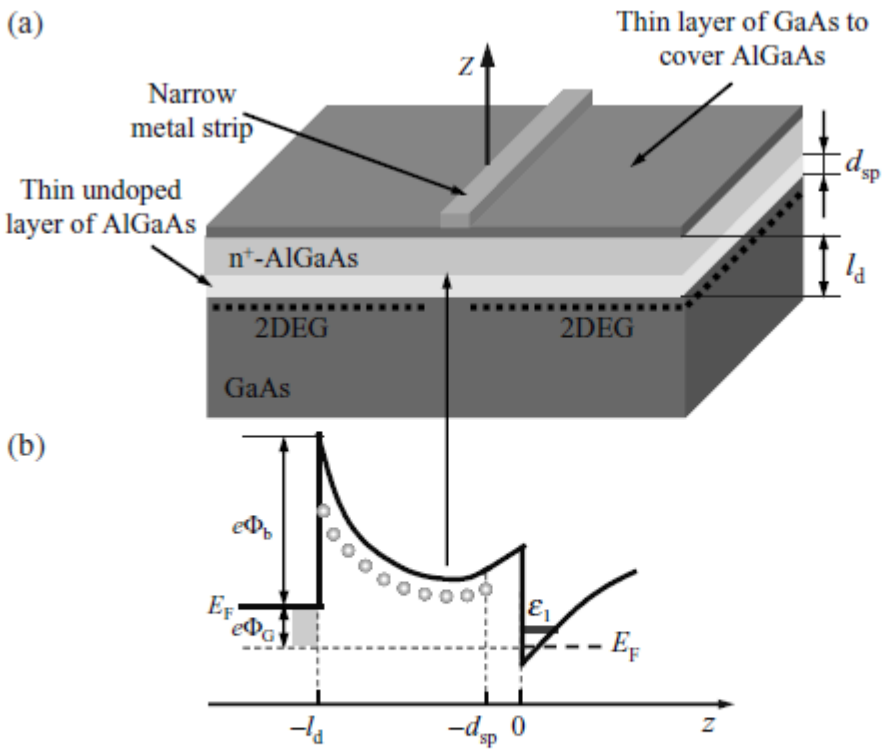

Figure 1 (a) Two-dimensional electron gas (2DEG, denoted by dashed lines) at the interface of a modulation-doped GaAs/AlGaAs heterostructure with a depletion region under the negatively biased narrow metal strip (gate). (b) The band diagram of the AlGaAs/GaAs heterostructure in the gate region. The lowest subband is shown by the ε_1 line. Φ_b is the built-in Schottky voltage and Φ_G is the gate voltage.

According to this energy scheme, two-dimensional electrons are repelled from the region beneath the metal strip; their Fermi energy, E_F, is below the lowest subband energy. As a result, the region under the gate becomes completely depleted, as depicted in Fig. 1. Now it is clear that, by using several gates, possibly of different forms, one can create various configurations of regions occupied by the electrons. It is possible to form wires, dots, rings, cavities, etc. for the two-dimensional electrons. For example, if two closely placed parallel metal strips are fabricated on the top of the heterostructure, then, by applying negative voltage to these two gates, we can form two side barriers for the electrons and confine them into a channel. If the channel is narrow enough, the two-dimensional electrons can be quantized in the second direction and we obtain a quantum wire; such a wire is shown in Fig.2 The confinement of the electrons to the dots, wires, rings, etc. can be accomplished by a heterojunction on one side and electrostatics on all other sides. The split-gate technique has successfully been exploited for measurements of transport regimes in various quantum structures, for example, in quantum point contacts and electron waveguides.

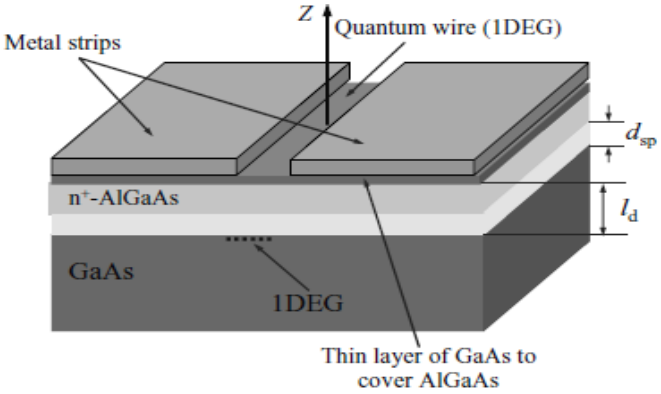

Figure 2 A quantum wire at the interface of a GaAs/AlGaAs heterostructure with two depletion regions under the negatively biased metal strips.

A considerably more sophisticated design of patterning of a two-dimensional gas to a shape desirable for single-electron applications is presented in Fig. 3. The main features of the design shown in Fig. 3(a) are the following: (i) the Ohmic contacts (OC) to the two-dimensional electron gas (contacts to two electron reservoirs (R)) and (ii) a system of gates, which create electrostatic tunnel barriers (TB) and confine electrons into a quantum dot (QD). The tunnel barriers are formed when the voltages applied to the gates are negative with respect to the voltages applied to the contacts. The barriers should be high enough to decouple the quantum dot and the reservoirs. In Fig. 3(b), the resulting potential profile is depicted schematically. Split-gate techniques and resulting structures are used to observe single-electron effects. Indeed, if the quantum-dot-like structure is small enough, it can be considered to be a single-electron box. A voltage applied to the contacts (the source and the drain) induces transfer of electrons through the structure one by one.In general, the flexible split-gate technique is a powerful method to realize single-electron-transport devices.

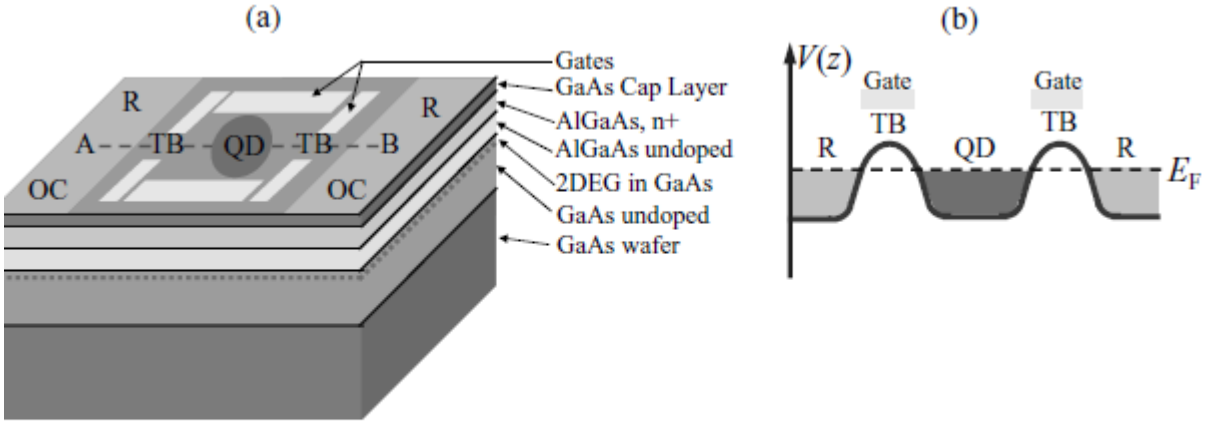

Figure . 3 (a) Design patterning of two-dimensional gas to a shape desirable for single-electron applications: OC, ohmic contacts; R, reservoir of electrons; QD, quantum dot; and TB, tunnel barrier. (b) The potential profile, $V(z)$, along the line A–B. Ohmic contacts, OC, are not shown since they are outside of the depicted region.

MIICRO ELECTROMECHANICAL SYSYTEMS (MEMS):

Although microelectromechanical systems do not technically fall under the subject of nanotechnology, it is useful to briefly discuss them at the beginning of the chapter because they represent a more mature technology, and many of the differences in behaviour observed in the micromechanical world could well apply to the Nano regime, thereby providing a basis for the design of Nano machines.

The extensive fabrication infrastructure developed for the manufacture of silicon integrated circuits has made possible the development of machines and devices having components of micrometre dimensions. Lithographic techniques, described in previous chapters, combined with metal deposition processes, are used to make MEMS devices. Microelectromechanical systems involve a mechanical response to deformation.

The major advantages of MEMS devices are miniaturization, multiplicity, and the ability to directly integrate the devices into microelectronics. *Multiplicity* refers to the large number of devices and designs that can be rapidly manufactured, lowering the price per unit item. For example, *miniaturization* has enabled the development of micrometre-sized accelerometers for activating airbags in cars. Previously an electromechanical device the size of a soda can, weighing several pounds and costing about $15, triggered airbags. Presently used accelerometers based on MEMS devices are the size of a dime, and cost only a few dollars. The size of MEMS devices, which is comparable to electronic chips, allows their integration

directly on the chip. In the following paragraphs we present a few examples of MEMS devices and describe how they work. But before we do this, let us examine what has been learned about the difference between the mechanical behaviour of machines in the macro- and micro worlds.

Figure 1. *Illustration of a MEMS device (a) used to sense impact and initiate expansion of airbags in cars. The automobile is moving from left to right. On impact (b) the horizontal cantilever bar* ***is*** *accelerated to the right and changes the separation of the capacitor plates, thereby triggering a pulse of electric current that activates the bag expansion mechanism.*

In the micro world the ratio of the surface area to the volume of a component is much larger than in conventional-sized devices. This makes friction more important than inertia. In the macroworld a pool ball continues to roll after being struck because friction between the ball and the table is less important than the inertia of its forward motion. In the microregime the surface area : volume ratio is so large that surface effects are very important. In the microworld mechanical behavior can be altered by a thin coating of a material on the surface of a component. We shall describe MEMS sensors that take advantage of this propedy. Another characteristic of the microworld is that molecular attractions between microscale objects can exceed mechanical restoring forces. Thus the elements of a microscale device, such as an array of cantilevers, microsized boards fixed at one end, could become stuck together when deflected. To prevent this, the elements of micromachines may have to be coated with special nonstick coatings. In the case of large motors and machines electromagnetic forces are utilized, and electrostatic forces have little impact. In contrast to this, electromagnetic forces become too small when the elements of the motors have micrometer-range dimensions, while electrostatic forces become large. Electrostatic actuation is often used in micromachines, which means that the elements are charged, and the repulsive electrostatic force between the elements causes them to move. We will describe below an actuator, which uses the electrostatic interaction between charged carbon nanotubes. Many of these differences between micromachines, and macromachines become more pronounced in the nanoregime. There are many devices and machines that have micrometer-sized elements. Since this book is concerned primarily with nanotechnology, we give only a few examples of the microscale analogs.

Figure 1 illustrates the principle behind a MEMS accelerometer used to activate airbags in automobiles. Figure l a shows the device, which consists of a horizontal bar of silicon a few micrometers in length attached to two vertical hollow bars, having flexible inner surfaces. The automobile is moving from left to right in the figure. When the car suddenly comes to a halt because of impact, the horizontal bar is accelerated to the right in the figure, which causes a change in the separation between the plates of the capacitor, as shown in Fig. 1 b. This changes the value of the electrical capacitance of the capacitor, which in turn electronically triggers a pulse of current through a heating coil embedded in sodium azide, NaN_3. The instantaneous heating causes a rapid decomposition of the azide material, thereby
producing nitrogen gas N_2 through the reaction $2NaN_3 \rightarrow 2Na + 3N_2$, which inflates the airbag. Coated cantilever beams are the basis of a number of sensing devices employing MEMS. A cantilever is a small supported beam. The simplest of such devices consist of arrays of singly supported polysilicon cantilevers having various length to width ratios in the micrometer range. The beams can be made to vibrate by electrical or thermal stimuli. Optical reflection techniques are used to measure the vibrational frequency. As shown in Fig. 2, the vibrational frequency is very sensitive to the length of the beam. Thermal sensors have been developed using these supported micrometer-sized cantilevers by depositing on the beams a layer of a material that has a coefficient of thermal expansion different from that of the polysilicon cantilever itself. When the beam is heated, it bends because of the different coefficients of expansion of the coating and the silicon, and the resonant frequency of the beam changes. The sensitivity of the device is in the micro degree range, and it can be used as an infrared (IR) sensor. A similar design can be used to make a sensitive detector of DC magnetic fields.

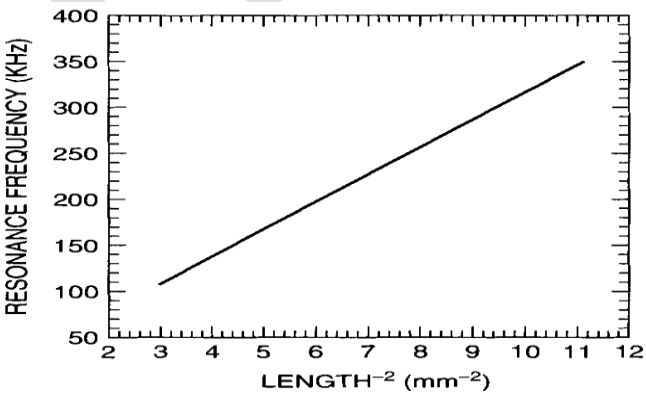

Figure 2 : Plot of the resonance frequency of a MEMS cantilever versus the square ***c*** *the*

reciprocal of the length of the beam

In this case the beam is coated with a material that displays *magnetorestrictive effects*, meaning that the material changes its dimensions when a DC magnetic field is applied. This causes the beam to bend and change its resonance frequency. These devices can detect magnetic fields as small as 10^{-5} G (gauss) [10^{-9}T (tesla)].

NANO ELECTROMECHANICAL SYSTEMS (NEMS):

Nano mechanical machines and devices are in the early stages of development, and many are still in conceptual stages. Numerous computer simulations of possibilities and ideas have been proposed. It turns out that nature is far ahead of us in its ability to produce nano sized machines. Nano motors exist in biological systems such as the flagellar motor of bacteria. Flagellae are long, thin, blade-like structures that extend from the bacteria. The motion of these flagellae propel the bacteria through water. These whip-like structures are made to move by a biological Nano motor consisting of a highly structured conglomerate of protein molecules anchored in the membrane of the bacterium. The motor has a shaft and a structure about the shaft resembling an armature. However, the motor is not driven by electromagnetic forces, but rather by the breakdown of adenosine triphosphate (ATP) energy-rich molecules, which causes a change in the shape of the molecules. Applying the energy gained from ATP to a molecular ratchet enables the protein shaft to rotate. Perhaps the study of biological nanomachines will provide insights that will enable us to improve the design of mechanical nanomachines.

Optical lithography is an important manufacturing tool in the semiconductor industry. However, to fabricate semiconductor devices smaller than 100 nm, ultraviolet light of short wavelengths (193 nm) is required, but this will not work because the materials are not transparent at these wavelengths. Electron-beam and X-ray lithography, discussed in earlier chapters, can be used to make nanostructures, but these processes are not amenable to the high rate of production that is necessary for large-scale manufacturing. Electron-beam lithography uses a finely focused beam of electrons, which is scanned in a specific pattern over the surface of a material. It can produce a patterned structure on a surface having 10-nm resolution. Because it requires the beam to hit the surface point by point in a serial manner, it cannot produce structures at sufficiently high rates to be used in assembly-line manufacturing

processes. X-ray lithography can produce patterns on surfaces having 20-nm resolution, but its mask technology and exposure systems are complex and expensive for practical applications.

More recently, a technique called ***nanoimprint lithography*** has been developed that may provide a low-cost, high-production rate manufacturing technology. Nanoimprint lithography patterns a resist by physically deforming the resist shape with a mold having a nanostructure pattern on it, rather than by modifying the resist surface by radiation, as in conventional lithography. A resist is a coating material that is sufficiently soft that an impression can be made on it by a harder material. A schematic of the process is illustrated in Fig. 1. A mold having a nanoscale structured pattern on it is pressed into a thin resist coating on a substrate (Fig. 1 a), creating a contrast pattern in the resist. After the mold is lifted off (Fig. 1 b), an etching process is used to remove the remaining resist material in the compressed regions (Fig. 1 c). The resist is a thermoplastic polymer, which is a material that softens on heating. It is heated during the molding process to soften the polymer relative to the mold. The polymer is generally heated above its glass transition temperature, thereby allowing it to flow and conform to the mold pattern. The mold can be a metal, insulator, or semiconductor fabricated by conventional lithographic methods. Nanoimprint lithography can produce patterns on a surface having 10-nm resolution at low cost and high rates because it does not require the use of a sophisticated radiation beam generating patterns for the production of each structure.

The scanning tunnelling microscope (STM), uses a narrow tip to scan across the surface of the material about a nanometer above it. When a voltage is applied to the tip, electrons tunnel from the surface of the material and a current can be detected. If the tip is kept at a constant distance above the surface, then the current will vary as the tip scans the surface. The amount of detected current depends on the electron density at the surface of the material, and this will be higher were the atoms are located. Thus, mapping the current by scanning the tip over the surface produces an image of the atomic or molecular structure of the surface.

An alternate mode of operation of the STM is to keep the current constant, and monitor the deflection of the cantilever on which the tip is held. In this mode the recorded cantilever deflections provide a map the atomic structure of the surface.

The scanning tunnelling microscope has been used to build nanosized structures atom by atom on the surface of materials. An adsorbed atom is held on the surface by chemical bonds with the atoms of the surface. When such an atom is imaged in an STM, the tip has a trajectory of the type shown in Fig. 2 a. The separation between the tip and the adsorbed atom is such that

any forces between them are small compared to the forces binding the atom to the surface, and the adsorbed atom will not be disturbed by the passage of the tip over it. If the tip is moved closer to the adsorbed atom (Fig. 2 b) such that the interaction of the tip and the atom is greater than that between the atom and the surface, the atom can be dragged along by the tip. At any point in the scan the atom can be reattached to the surface by increasing the separation between the tip and the surface. In this way adsorbed atoms can be rearranged on the surfaces of materials, and structures can be built on the surfaces atom by atom. The surface of the material has to be cooled to liquid helium temperatures in order to reduce thermal vibrations, which may cause the atoms to diffuse thermally, thereby disturbing the arrangement of atoms being assembled. Thermal diffusion is a problem because this method of construction can be carried out only on materials in which the lateral or in-plane interaction between the adsorbed atom and the atoms of the surface is not excessive. The manipulation also has to be done under ultra-high-vacuum conditions in order to keep the surface of the material clean.

Figure 3 depicts a circular array of iron atoms on a copper surface, called a “quantum corral”, assembled by STM manipulation. The wavelike structure inside the corral is the surface electron density distribution inside the well corresponding to three quantum states of this two-dimensional circular potential well, in effect providing a visual affirmation of the electron density predicted by quantum theory. This image is taken using an STM with the tip at such a separation that it does not move any of the atoms. The adsorbed atoms in this structure are not bonded to each other. The atoms will have to be assembled in three-dimensional arrays and be bonded to each other to use this technique to build nanostructures. Because the building of three-dimensional structures has not yet been achieved, the slowness of the technique together with the need for liquid helium cooling and high vacuum all indicate that STM manipulation is a long way from becoming a large-scale fabrication technique for nanostructures. It is important, however, in that it demonstrates that building nanostructures atom by atom is feasible, and it can be used to build interesting structures such as the quantum corral in order to study their physics.

KARPAGAM ACADEMY OF HIGHER EDUCATION

Coimbatore-641021.

(For the candidates admitted from 2016 onwards)

DEPARTMENT OF PHYSICS

UNIT V (Objective Type/Multiple choice Questions each Questions carry one Mark)

NANOMATERIALS AND APPLICATIONS

PART –A(Online Examination)

S.No.	QUESTIONS	opt1	opt2	opt3	opt4	ANSWER
1	Process of emission of electrons from hot metal surfaces is called	plastic emission	thermionic emission	static emission	current emission	thermionic emission
2	At room temperature, electron cannot escape metal surface due to	attractive forces of nucleus	repulsive forces of electrons	repulsive forces of nucleus	pulling force of protons	attractive forces of nucleus
3	One of the applications of Bulk micromachining is :	SAW sensor	Resonant sensor	Temperature sensor	Pressure sensor	Resonant sensor
4	.....method removes material through erosive action:	Diamond milling	Soft lithography	Micro-electro discharge machining	Powder blasting	Micro-electro discharge machining
5	Which of the following are the three most widely used micromachining processes	Bulk, surface, PMMA	Surface, bulk, LIGA	PMMA, LIGA, surface	LIGA, CMP, surface	Surface, bulk, LIGA
6	Which of the following MEMS components would LEAST likely be fabricated using bulk micromachining processes?	Cantilevers	Microfluidic channels	Probes	Gear trains	Gear trains
7	Photoresist is to surface micromachining as _____ is to LIGA.	Beryllium	Gold	KOH	Plexiglas or PMMA	Plexiglas or PMMA
8	Which choice below best describes the goal for nanotechnology advances in medicine?	To improve technology for finding cures	Aid the FBI for investigative methods	Improve the application of cosmetics	Increase food production	To improve technology for finding cures

9	What can nanotechnology best help with for consumer products?	Produce floating devices	Reduce the size of devices	Make stuff light up	Larger and stronger materials	Reduce the size of devices
10	Why are nanoelectronic devices a less expensive alternative to the design of current electronic devices?	They are slower operating	They require less parts and materials	They are less reliable	They are more vulnerable to viral software	They require less parts and materials
11	The components fabricated using surface micromachining are _____ aspect ratio components relative to other micromachining processes.	Low	medium	high	ultra high	Low
12	Particles emitted from hot cathode surface are	negative ions	positive ions	protons	electrons	electrons
13	One of the most used kinds of lasers in microfabrication is:	Excimer	Diamond milling	Bulk micromachining	Pressure sensor	Excimer
14	Which of then following is example of direct access?	magnetic disc	floppy disc	program tape	plain disc	magnetic disc
15	Interest of increasing wafer diameter from 200 mm to 300 mm	The price of a 300 mm wafer is lower	It is easier to fabricate	To produce more silicon devices from a single wafer	To increase the size of a die	To produce more silicon devices from a single wafer
16	If a single walled CNT is semiconducting, the bandgap scales with ----------	the value of diameter, d	the square value of diameter, d2	the reciprocal value of diameter, 1/d	the reciprocal square value of diameter, 1/d2	the reciprocal value of diameter, 1/d
17	The term photo voltaic comes from _____	spanish	greek	german	english	greek
18	The term photo voltaic is in use since _____	1840	1844	1849	1850	1849
19	When the source of light is not sun light then the photo voltaic cell is used as _____	Photo diode	Photo voltaic cell	Photo detector	Photo transmitter	Photo detector
20	Solar cells are made from bulk materials that are cut into wafer of _____ thickness	120-180µm	120-220µm	180-220µm	180-240µm	180-240µm
21	_____ photo voltaic devices in the form of thin films.	Cadmium Telluroide	Cadmium oxide	Cadmium sulphide	Cadmium sulphate	Cadmium Telluroide
22	_____ is a direct band gap material	Copper Indium Gallium Selenide	Copper Selenide	Copper Gallium Telluride	Copper Indium Gallium Diselenide	Copper Indium Gallium Selenide

23	Dye-sensitized solar cells are made from _____ organic dye.	Ruthium melallo	Aniline	Safranine	Induline	Ruthium melallo
24	Quantum dot solar cells are based on _____	Gratzel cell	Solar cell	Voltaic cell	Galvanic cell	Gratzel cell
25	The quantum dot used are _____	CdS	CdTe	PbO	GaAs	CdTe
26	the cathode and the anode of the diode are referred to as	emitter and collector	electrode	terminals	connections	emitter and collector
27	_____ entering the structure from the emitter is described by the wavefunction	proton	electron	neutron	photon	electron
28	the lifetime of an electron in the well equals	5 x 10-12s	5 x 10-12μs	5 x 10-12ms	5 x 10-12ns	5 x 10-12s
29	The widths of the quantum wells are equal to	36 Å	46 Å	56 Å	66 Å	46 Å
30	The heights of the barriers vary from _____	0.3 eV to 1.2 V	0.3 eV to 1.2 eV	0.3 eV to 1.2 mV	0.3 eV to 1.2 MeV	0.3 eV to 1.2 eV
31	For asymmetric barriers, the maximum transmission at E⊥ = εn is _____	positive	unity	less than unity	negative	less than unity
32	The process responsible for the resonant-tunneling effect is the so-called	sequential tunneling process	quantum tunneling process	tunneling process	differential process	sequential tunneling process
33	For the lower temperature, there is _____ current at finite voltage biases	positive	negative	unit	almost zero	almost zero
34	As of public record at the end of 2002, which country was making the greatest annual investment in molecular nanotechnology research?	Russia	Japan	China	India	Japan
35	What is the term used in the field of nanotechnology to describe an as-yet theoretical device that "will be able to bond atoms together in virtually any stable pattern?"	Stacker	Replicator	Assembler	Constructor	Assembler
36	What is the general name for the class of structures made of rolled up carbon lattices?	Nanorods	Nanotubes	Nanosheets	Fullerrods	Nanotubes
37	The efficiency of the solar cell is about	25%	15%	40%	60%	15%
38	The output of the solar cell is of the order	0.1W	1W	10W	100W	1W
39	What is the maximum possible output of a solar array?	300 W/m2	100 W/m2	250 W/m2	500 W/m2	250 W/m2

40	The current density of a photo voltaic cell ranges from	10 – 20 mA/cm2	40 – 50 mA/cm2	20 – 40 mA/cm2	60 – 100 mA/cm2	40 – 50 mA/cm2
41	Optical switching can be classified into _____ categories.	Two	Three	Four	One	Two
42	_____ are the array of switches which forms circuit switching fabrics.	Packet arrays	Optical cross connects	Circuit arrays	Optical networks	Optical cross connects
43	What is the main disadvantage of OCS?	Regenerating mechanism	Optical session	Time permit	Disability to handle burst traffic	Disability to handle burst traffic
44	How many functions are performed by an optical packet switch?	4	3	2	1	4
45	_____ provides data storage for packets to resolve contention problems.	Switching	Routing	Buffering	Reversing	Buffering
46	_____ provides efficient designation, routing, forwarding, switching of traffic through an optical packet-switched network.	Label correlation	Multiprotocol label switching	Optical correlation	Routing	Multiprotocol label switching
47	_____ mode is temporary, selective and continuous.	Cell switching	Buffer switching	Cache	Circuit switching	Circuit switching
48	_____ refers to the process whereby a node finds one or more paths to possible destinations in a network.	Routing	Framing	Lightning	Cloning	Routing